République Algérienne Démocratique et Populaire

Ministère de l'Enseignement Supérieur et de la Recherche Scientifique

Université Hadj Lakhdar - Batna 1

Faculté des Sciences de la Matière

Département de Physique

Thèse

Présentée en vue de l'obtention du

Diplôme de Doctorat

par:

Benslama Hana

Thème:

Phénoménologie du rayonnement des gluons de basse énergie dans les collisionneurs des particules

Domaine:	Sciences de la Matière
Filière:	Physique
Specialité:	Physique des Rayonnements et Astrophysique
Intitulé de la Formation:	Physique des Rayonnements et Astrophysique

Soutenue le: 06/07/2023

Devant le jury:

Président:	Bouldjedri Abdelhamid	Prof.	Université de Batna 1
Rapporteur:	Delenda Yazid	Prof.	Université de Batna 1
Examinateurs:	Aouachria Mekki	Prof.	Université de Batna 1
	Redouane-Salah Essma	Prof.	Université de M'sila

People's Democratic Republic of Algeria
Ministry of Higher Education and Scientific Research

Hadj Lakhdar University - Batna 1
Faculty of Matter Sciences
Department of Physics

Thesis

Submitted in fulfillment of the requirement
for the degree of Doctorate

by:
Hana Benslama

Title:

Phenomenology of soft gluon radiation at particle colliders

Domain:	Matter Sciences
Branch:	Physics
Option:	Physics of Radiation and Astrophysics
Title of the formation:	Physics of Radiation and Astrophysics

Defended on: 06/07/2023

In front of the jury:

Chairperson:	Abdelhamid Bouldjedri	Prof.	University of Batna 1
Supervisor:	Yazid Delenda	Prof.	University of Batna 1
Examiners:	Mekki Aouachria	Prof.	University of Batna 1
	Essma Redouane-Salah	Prof.	University of M'sila

Table of Contents

List of Figures

List of Tables

Acknowledgements

First and foremost, I would like to thank Allah for giving me courage, patience, and strength throughout all these years of study.

I would like to take this opportunity to convey my sincere thanks and gratitude to my supervisor, professor Yazid Delenda, for teaching me the foundation of this field and for all the hard work he made to ensure the success of this thesis. Thank you for sharing your ideas, your incredible physical intuition, understanding of physics and helping me to understand them. It was a great chance to work with someone I respect and appreciate as a scientist, who always has the patience to answer my questions and has such a remarkable interest in physics, as well as being such a role model for me. It has been a privilege being your student. My thanks extend to professor Kamel Khelifa-Kerfa for collaborating on the work presented herein and in particular for providing the numerical program EVENT2.

I would like to convey my heartfelt gratitude and love to my parents, my dear sisters, my dear brothers and all their dear children for their unconditional love, immense support and encouragement. You are and always will be my strongest source of encouragement, inspiration and motivation

Dedication

I dedicate this thesis to my dear parents, my sisters, my brothers especially to my dear niece Mariam.

List of Publications

H. Benslama, Y. Delenda, K. Khelifa-Kerfa and A. M. Ibrahim,*" Eikonal Amplitudes and Non-global Logarithms from the BMS Equation,"* Phys. Part. Nucl. Lett.18 (2021) [arXiv:2006.06738 [hepph]].

Chapter 1

Introduction

The underlying theory which addresses the question of what makes up the universe and seeks to understand the elementary building blocks of matter and how they interact, is firmly established. The theory is known as the Standard Model of particle physics "SM". Currently, the largest and highest energy machine in the world that is aimed at testing whether the theory is fully relevant for describing nature, is the CERN's Large Hadron Collider experiment (LHC). Many aspects of the SM have been already probed (7 and 8 TeV for Run I, and 13 TeV for Run II), and a series of tests have failed to find any significant discrepancy between experiment and the predictions of this model [1]. With the discovery of the only missing SM particle the Higgs boson [2],[1] announced by ATLAS [3] and CMS [4] in July 2012, the SM explains the majority of the experimental results with extraordinary precision and has now achieved its full glory [5, 6].

Although the SM is our current best tested theory of all time, is nevertheless far from being a closed field and cannot represent a complete description of nature. Many open questions and unexplained problems are still unanswered by the SM, such as neutrino masses and mixing [8],[2] Baryon asymmetry of the universe [9],[3] and perhaps most significantly the absence of an accurate description of the gravitational force using quantum field theory. Furthermore, the SM does not provide any clues about the nature of dark matter [10]. In order to explain these puzzles and finding answers to these questions, some yet unknown particles or interactions would be needed, that clearly indicate new physics beyond the Standard Model (BSM). Currently, numerous imaginative theories for new physics have been proposed, notably several Super-Symmetric (SUSY) models [11] that seemed to provide an elegant solution, but experiments have yet to provide guidance pointing to the existence of SUSY particles.

[1] The discovery of the Higgs boson (spin-0 neutral particle with parity of +1 and mass of approximately 125 GeV) gave a sound justification for the origin of mass for massive gauge bosons as well as fermions.

[2] Contrary to the results of neutrino oscillation experiments, which imply that the neutrinos have non-vanishing masses, in the SM, the neutrinos are assumed to be massless [7].

[3] When the laws of physics appear to be almost symmetric for matter and anti-matter, the universe is abundant in matter.

Presently, collisions at the LHC occur at such high energies (13.6 TeV) that even massive particles such as electroweak bosons ($W^{\pm}$, Z^0, Higgs boson), the top quark and any new particles whose masses fall close to the electroweak scale will often exhibit transverse momentum (p_t) far exceeding their rest mass (m). When these particles decay hadronically, the decay products are more likely to get clustered into a single energetic fat jet [13]. The abundant presence of highly boosted ($p_t \gg m$) SM particles may indicate the existence of new physics. For instance, in specific extensions of the SM, they emerge as decay products of TeV-scale BSM particles. QCD jets in the background generated from high-energy quarks and gluons, on the other hand, may acquire a mass through radiation, frequently in the same mass range as the boosted jets. Identifying the origin of the signal jets and distinguishing them from the overwhelming QCD background is an important challenge at the LHC.

To overcome these challenges, several techniques relying on jet substructure have been developed to extract the internal dynamical properties of high p_t jets [14,15] in order to determine whether they are signals or background jets. Over the past few years, a variety of tools have been introduced, and they can often be grouped into three broad classes: Groomers [16, 17], Triggers (Prong finders) [18, 20], and Jet shapes observables (radiation constraints) [21–24]. Most recently, another avenue that can be employed to study jet substructure problems, is that of neural networks and machine learning techniques [25]. The calculation of QCD background events in the LHC poses a formidable challenge. Future electron-positron colliders such as the International Linear Collider (ILC) and the Circular Collider in electron mode (FCC-ee), on the other hand, provide a cleaner experimental environment with lower radiation levels. A key advantage of these experiments over the LHC is their low background and well-defined initial states, which should significantly improve precision measurements and offer a convenient environment for observations of new physics. Establishing a better understanding and achieving precision calculation of QCD event and jet shapes observables created in e^+e^- collisions, which will potentially be allowing for an efficient background subtraction, is rather the aim of this thesis.

Infrared and collinear (IRC) safe measures of the geometrical characteristics of the energy/momentum flow in a hadronic final state are provided by event-shape variables [26–29]. In order to better understand the dynamics of quark and gluon scattering, it became mandatory to go beyond event shapes, and define the final state in terms of clusters of jets (jet shapes) rather than individual hadrons. For this to be possible, only recently many jet definitions have been developed [32, 33]. In this thesis we study two observables: single-hemisphere mass distribution, which is an event shape observable, and azimuthal decorrelation between jets which is a typical jet shape observable whereby final states are clustered using several infrared and collinear (IRC) safe jet algorithms. More details on IRC safe jet algorithms will be discussed in Chapter 3.

In order to interpret the experimental results, one must first establish as thorough understanding of the underlying theory as possible. Establishing a connection between the theoretical predictions and experimental data is the goal of particle physics phenomenology.[4] To make this connection, theoretical tools to study shape distributions may be divided into two complementary broad classes. The first is the numerical simulations that employ Monte-Carlo (MC) event generators to model most of the physics that happens in particle collisions. The generation of the hard process takes place using perturbation theory (PT). Additional partonic activity is generated, including initial state radiation (ISR) and final state radiation (FSR).[5] Non-perturbative physics (the underlying event (UE), pile-up (PU), and hadronisation) are also handled. Herwig [34,35], Pythia [36,37], and Sherpa [38] are currently amongst the widely used MC event generators. However these different event generators use various models for both perturbative and non-perturbative effects. Consequently, very different predictions were pointed out between them and the intrinsic theoretical uncertainty is large making the level of precision they provide may be regarded a problem that has yet to be solved. Furthermore, the typical accuracy of event generators is usually leading logarithm (LL). As one of the perturbative issues that MC generators handel, is that of the resummation of large logarithms present in the distributions of most observables, which are mainly caused by the miscancellation of infrared and/or collinear singularities at the matrix-element level. For more accurate predictions and to check the validity of the MC tools, in this thesis we rather focus on the second theoretical approach, i.e., analytical calculations, both at fixed-order and all-orders (resummation) of event and jet shape distributions, based on the traditional perturbative QCD (pQCD) approach. The latter said procedure investigates factorizations and exponentiation properties of QCD matrix elements. Comparisons of the analytical findings to the output of MC programs are provided as well. Another avenue that can be performed in terms of analytical tools is an effective field theory for soft and collinear parton emissions, a so-called Soft Collinear Effective Theory (SCET) [39,40], but it is beyond the scope of this thesis.

For global observables of sufficiently inclusive shape which are sensitive to radiation every where in phase space, the resummation of the said large logarithms is relatively simple and has even been successfully done analytically to NNNLL accuracy [44]. NLL accuracy in a large number of QCD observables that are referred to as non-global, i.e., those sensitive to emissions in restricted regions of the angular phase space, has proven difficult to reach due to their cumbersome resummation. Emissions outside the "forbidden" region which themselves subsequently emit a single gluon back into the "measured" region lead to a tower of large single logarithms $\alpha_s^n L^n$ [52,94]. The treatment of these non-global logarithms (NGLs) relies on multiple gluon branchings that increasingly become complicated at higher orders in PT. Their

[4] This implies that one collects information from experimental studies, creates new models or hypotheses, and creates techniques to calculate quantities that can be compared to current or forthcoming data.

[5] More on ISR, FSR, UE, PU, and MPI will be in chapter 3.

resummation, contrary to that of global observables mentioned above, cannot be performed by a consideration of a fixed number of gluon emissions since an iterative pattern could not thus far be spotted.

NGLs were first spotted and numerically resummed in the large-N_c limit (N_c is the number of quark colors) by Dasgupta and Salam in Refs. [52, 94]. Banfi, Marchesini and Smye derived a non-linear integro-differential equation, the BMS equation [95], whose solution resums NGLs at large N_c for emissions off a given dipole. A numerical solution of this equation was provided in the same reference for away-from-jets energy flow. An analytic solution to the BMS equation was also achieved by means of a perturbative expansion in the strong coupling up to fifth order by Schwartz and Zhu in Ref. [96]. An analogous integro-differential equation was also proposed by Weigert [97] that resums NGLs to all orders at finite N_c, and was solved numerically in Ref. [98] in the context of away-from-jets energy flow, and in Ref. [99] for the hemisphere mass distribution in $e^+e^- \to q\bar{q}$ events. Additionally, in Refs. [100, 101] an evolution algorithm that deals with NGLs at finite N_c to all orders was developed. Ref. [102], evaluated NGLs at finite N_c up to fifth order in the coupling by computing Eikonal amplitudes of soft gluon emissions (as in Ref. [93]) and using phase space considerations. NGLs have also been considered in the context of groomed multi-prong jet shape observables in Ref. [103].

Another point that we would like to address concerning the significant impact that one inevitably faces when applying jet algorithms other than the anti-k_t algorithm [121] (such as the k_t [120], Cambridge-Aachen C/A [48] as well as the SISCone algorithm [19]) to non-global observables, is twofold. Firstly, the said observables receive a tower of extra large single logarithms in the independent emission terms relative to global observables. We refer to these large logarithms as " clustering logarithms" (CLs). They were first pointed out in [49] for energy flow into gaps-between-jets distribution. At NLL accuracy, the said extra single logarithms have a non-trivial impact on the global part (primary emissions) which deviates from naive single gluon exponentiation, that was first pointed out in [49, 50]. Secondly, a significant reduction in the NGLs contribution was observed in the same observable (energy flow into gaps between jets distribution) [50, 51] due to the soft clustering inherent in such algorithms. The all-orders resummation can currently only be obtained via the MC program of [52]. Despite the fact that analytical resummation of CLs has proven to be highly intricate, it has, however, been shown for both gaps-between jets [50] and jet mass [53] in e^+e^- annihilation, through explicit fixed-order calculations of the first few orders up to $\mathcal{O}(\alpha_s^4)$ in the perturbative expansion that CLs exhibit a pattern of exponentiation. We carry out analogous calculations for the dijet azimuthal deccorolation in Chapter. 4.

This thesis is organized as follows. In Chapter 2 we begin by outlining some of the principles of pQCD, emphasizing on features that will be relevant to this thesis, such as Infrared and Collinear (IRC) safety which is mandatory for the perturbative calculation of the observables

under consideration. In chapter 3 we provide a brief overview of QCD phenomenology and jets. Furthermore, to define jets using different jet algorithms, the class of sequential-recombination jet algorithms is reviewed in this chapter. Chapter 4 is concerned with the study of the non-global jet shape distribution, the azimuthal decorrelation between jets in e^+e^- annihilation, and its resummed calculation which includes both non-global and clustering logarithms which are of fundamental importance for this work. In chapter 5 which is similar in content to Ref. [54], we approximate the analytical solution to the BMS equation by proposing an exponential of a series in the coupling α_s, and we perform analytical calculations for the non-global logarithms up to fourth order in the exponent for the specific hemisphere mass distribution in e^+e^- collisions. Finally, we conclude in chapter 6 and summarise the finding of our work in this thesis. Additionally, we also discuss prospects for future works on the topic.

Chapter 2

SM review and QCD generalities

The Standard Model (SM) of particle physics has viewed the universe as having a limited number of foundational constituents, known as elementary particles. With higher energies the structure of matter can be probed and what has been thought to be the most basic elementary objects has changed over time. In the 19^{th} century, atoms were considered as elementary particles but they are today considered to be composed of nuclei surrounded by electrons.[1] While the electron is still thought to be one of the elementary particles of nature, the nucleus appears to consist of nucleons (protons and neutrons) that have since been discovered to be build out of more fundamental objects, the quarks and gluons.

Charge	**Gen I**	**Gen II**	**Gen III**
$\frac{2}{3}$	u up	c charm	t top
$-\frac{1}{3}$	d down	s strange	b bottom

Table 2.1: The six quarks of the Standard Model.

There are six different quarks in nature with fractional electric charges, which are divided into three generations (see Table 2.1), and can exist in three different color states, say, red, green and blue. Till this time, the other particles, the electron and its heavier versions, i.e., the muon and tau as well as their corresponding neutrinos that are thought to be elementary, are all members of another group of six particles with integer charges known as *leptons*, see Table 2.2. The "matter" particles consist therefore of three generations of leptons and quarks. They all come with spin half 1/2, and hence called fermions, and by charge conjugation, one can associate an anti-fermion to each fermion.

The SM of particle physics is a quantum field theory (QFT) that describes three of the four fundamental forces of nature affecting the fermionic quark and lepton (matter) fields, known to us: the electromagnetic, weak and strong forces. Unlike quantum electrodynamics (QED) in

[1]For more detailed narrative of the history of particle physics, see [55]

Charge	Gen I	Gen II	Gen III
-1	e^- electron	μ^- muon	τ^- tau
0	ν_e electron neutrino	ν_μ muon neutrino	ν_τ tau neutrino

Table 2.2: The six leptons of the Standard Model.

which the behaviour of the force has been well understood from its classical theory of Maxwell and Lorentz,[2] the form of the interaction for both weak and strong forces were not available. The dynamics (the behaviour of the force) of QED is hardly constrained by renormalizibility and a symmetry principal called local gauge invariance. In regards to the former, QED is a renormalizible QFT in the sense that ultraviolet (UV) divergences are absorbed into a redefinition of the Lagrangian parameters (mass and coupling constant) that become measurable scale dependent and are taken from experiment. The latter indicates that the electromagnetic force arises as a result of the QED Lagrangian's invariance under local phase transformations of the unitary group U(1). Consequently, gauge invariance restricts the terms of the Lagrangian and establishes the types of interactions that can exist. The quanta of the gauge field come with integer spin and hence belong to bosons and are referred to as gauge bosons. The electromagnetic interactions between charged particles are indeed mediated by the exchange of a force carrying particle, called the photon (γ). By analogy to QED, the theories of weak and strong interactions were also established using the local gauge invariance, and hence are all examples of gauge theories.

The weak interaction of quarks and leptons which all have the weak isospin charge, is based on the local special unitary SU(2) symmetry group (called weak isospin), and mediated by three gauge bosons (Z^0, W^+, W^-) that also carry the weak isospin charge and thus interact with each others as well. Glashow, Salam and Weinberg were the first who unified electromagnetic and weak interactions, constituting the electroweak (EW) theory described by the spontaneously broken gauge symmetry SU(2) $\times$ U(1) [59]. The spin-1 three gauge bosons together with the photon γ are the force carriers of the EW interaction. The dynamics of the strong interaction between quarks, binding them into hadrons, is described by the theory of Quantum Chromodynamics (QCD), in which the underlying symmetry group is the exact non-Abelian color gauge group SU(3) acting on the color degree of freedom. The quantization of QCD had been achieved by Faddeev and Popov [60] and its renormalizibility had been proved by 't Hooft and Veltman [61]. QCD is the subject of this thesis and any further discussion beyond its scope will be ignored. The invariance of the QCD Lagrangian under local phase transformations of $SU(3)_c$ results in the formation of eight massless gauge boson fields referred to as gluons which

[2]QED is the quantum field theory that describes the electromagnetic force holding together atoms and affecting everything that carry electric charge or magnetic moments.

are quite similar to photons and effect anything that has color charge. While the gauge field in QED (γ) is electrically neutral, in QCD the gluons carry color charge, which means they interact not only with quarks and anti-quarks, but also amongst themselves.

In this chapter we will present a short description of the particular features of QCD which will play an important role in the development of subsequent chapters. In order to do this, we start with the SU(3) color gauge symmetry underlying the structure of QCD. Subsequently, we will briefly describe the corresponding QCD Lagrangian, then explore the Feynman rules that can be derived from it, and finally apply these rules to compute scattering amplitudes and cross sections. In subsect. 2.1.3, a special attention will be given to renormalization issues that leads to the running of the strong coupling constant and that gives rise to the concepts of asymptotic freedom and confinement. Further discussion on the latter will be given in subsect. 2.1.4. Finally, we consider the properties of the scattering amplitude in the soft and collinear limits in subsect. 2.1.5.

2.1 Quantum chromodynamics

In this section we briefly introduce the theory of strong interactions, QCD, providing only some general concepts needed in later chapters of this thesis. For more details, the following textbooks [62–69] are recommended.

2.1.1 $\mathrm{SU(N_c)}$ and color algebra

It is worthwhile to begin by briefly recalling some basic characteristics of the gauge group $\mathrm{SU(N_c)}$, on which QCD is based. For more details one can see [74, 75]. The special unitary ($\mathrm{UU^\dagger} = 1$) Lie group $\mathrm{SU(N_c)}$ consists of a set of $\mathrm{N_c} \times \mathrm{N_c}$ complex matrices with determinant one. The $\mathrm{SU(N_c)}$ transformations are just rotations in the color space through an angle θ and has the general form

$$\mathrm{U} = e^{i\,\theta^a\,T^a} \quad , \quad a = 1, ..., \mathrm{N_c}^2 - 1\,. \tag{2.1}$$

The color matrices $T^a_{ij} \equiv t^a_{ij}$ which have dimension $\mathrm{N_c} \times \mathrm{N_c}$ are the $\mathrm{N_c}^2 - 1$ generators of the rotation in the fundamental (F) representation (R) of $\mathrm{SU(N_c)}$. These generators are hermitian and traceless, close under commutation relations and satisfy a Lie algebra such that

$$\left[t^a, t^b\right] = i\, f^{abc}\, t^c, \tag{2.2}$$

and the Jacobi identity

$$\left[t^a, \left[t^b, t^c\right]\right] + \left[t^b, \left[t^c, t^a\right]\right] + \left[t^c, \left[t^a, t^b\right]\right] = 0\,, \tag{2.3}$$

which leads to

$$f^{bcd}f^{ade} + f^{abd}f^{cde} + f^{cad}f^{bde} = 0\,. \tag{2.4}$$

The set of real f^{abc} is known as the structure constants of the algebra, which are completely antisymmetric when their indices are interchanged, $f^{abc} = -f^{bac}$, $f^{abc} = -f^{acb}$. They are given by

$$f^{abc} = -2i\left(\left[t^a, t^b\right] t^c\right). \tag{2.5}$$

The non-Abelian nature of the group emerges clearly in the presence of non-zero f^{abc}s. The structure constants themselves also satisfy the same algebra given in Eq. (2.2), and hence being the generators of SU($\mathrm{N_c}$) in the adjoint (A) representation whose dimension is $(\mathrm{N_c}^2-1)\times(\mathrm{N_c}^2-1)$

$$(T^a)_{bc} \equiv -i\,f^{abc}\,, \tag{2.6}$$

$$\left[T^a, T^b\right] = i\,f^{abc}\,T^c\,. \tag{2.7}$$

For both representations, the generators are usually normalized so that

$$\mathrm{Tr}(t^a\,t^b) = \mathrm{T_F}\,\delta^{ab} \quad , \quad \mathrm{T_F} = \frac{1}{2}\,, \tag{2.8}$$

$$\mathrm{Tr}(T^a\,T^b) = \mathrm{T_A}\,\delta^{ab} \quad , \quad \mathrm{T_A} = \mathrm{N_c}\,, \tag{2.9}$$

where $\mathrm{T_R}$ denotes the Dynkin index for the representation R. Let us now take the product of two generators

$$(t^a_{ij})^2 = \sum_{a=1}^{\mathrm{N_c}^2-1}\sum_{k=1}^{\mathrm{N_c}} t^a_{ik}\,t^a_{kj} = \mathrm{C_F}\,.\,\mathbb{1}\,\delta_{ij}\,, \tag{2.10}$$

$$(T^a_{bc})^2 = \sum_{a=1}^{\mathrm{N_c}^2-1}\sum_{d=1}^{\mathrm{N_c}^2-1} T^a_{bd}\,T^a_{dc} = \mathrm{C_A}\,.\,\mathbb{1}\,\delta_{bc}\,. \tag{2.11}$$

Such a product is called the quadratic Casimir operator (or color charge) $\mathrm{C_R}$, which commutes with all the generators of the representation, and because of its invariance under SU($\mathrm{N_c}$) transformations, is therefore proportional to the identity matrix. In Eq. (2.8), if we put $a = b$ and sum over a, we get

$$\mathrm{Tr}(t^a\,t^a) = \frac{1}{2}(\mathrm{N_c}^2 - 1)\,. \tag{2.12}$$

On the other hand

$$\mathrm{Tr}(t^a\,t^a) = \mathrm{C_F}\mathrm{Tr}(\mathbb{1}) = \mathrm{C_F}\,\dim(\mathrm{F}) = \mathrm{C_F}\,\mathrm{N_c}\,, \tag{2.13}$$

and hence

$$\mathrm{C_F} = \frac{\mathrm{N_c}^2 - 1}{2\mathrm{N_c}}. \tag{2.14}$$

C_F is the color charge associated with a quark splitting into a quark and a gluon. In a similar fashion, the calculation of the Casimir operator in the adjoint representation C_A which is the color charge associated with a gluon splitting into gluons, gives $C_A = N_c$. The anti-commutation relations of the generators are given by

$$\left\{t^a, t^b\right\} = \frac{\delta^{ab}}{N_c}.\mathbb{1} + d^{abc}\, t^c\,. \tag{2.15}$$

Unlike f^{abc}, d^{abc} are totally symmetric under the interchange of any of their indices, and are given by

$$d^{abc} = 2\mathrm{Tr}\left(\left\{t^a, t^b\right\} t^c\right). \tag{2.16}$$

2.1.2 The QCD Lagrangian and Feynman rules

The QCD Lagrangian density is given by [62]

$$\mathcal{L}_{\mathrm{QCD}} = \mathcal{L}_{\mathrm{classical}} + \mathcal{L}_{\mathrm{gauge-fixing}} + \mathcal{L}_{\mathrm{ghost}}. \tag{2.17}$$

The classical QCD Lagrangian density is the Dirac Lagrangian density coupled to the Yang-Milles Lagrangian density

$$\mathcal{L}_{\mathrm{classical}} = \sum_f \overline{q}_f^k \left(i\not{D} - m_f\,\delta_{kl}\right)_{kl} q_f^l \; - \frac{1}{4}\, F^a_{\mu\nu}\, F_a^{\mu\nu}\,, \tag{2.18}$$

where the sum is over all quark flavors. We identify the Dirac fields q_f as being quark fields of flavor f and mass m_f, and their conjugates $\overline{q}_f = q^\dagger\,\gamma^0$. The quark fields transform in the fundamental representation of $SU(N_c)$ which is a three dimensional color space. The number of colors is therefore $N_c = 3$, with k, l running from 1 to N_c, or $k, l = \{\mathrm{red}, \mathrm{green}, \mathrm{blue}\}$, hence the quark field is represented by a triplet $q^l = \left(q^r, q^g, q^b\right)$, with q^l being Dirac spinor fields.[3] $\not{D} = \gamma^\mu\, D_\mu$ where γ^μ are the traceless Dirac matrices satisfying the Clifford algebra

$$\{\gamma^\mu, \gamma^\nu\} = 2\, g^{\mu\nu}\,,$$

with $g^{\mu\nu} = \{1, -1, -1, -1\}$ is the Minkowski metric tensor [76]. The covariant derivative for QCD which encoded the interaction between quarks and gluons is given by

$$D_\mu = \partial_\mu \delta_{ij} - i\, g_s \sum_{a=1}^{8} A^a_\mu\, t^a_{ij}\,, \tag{2.19}$$

[3] We have suppressed spinor indices. The sum over repeated indices is assumed.

where the index a spans the gluon's eight color degrees of freedom, t^a are the generators of $\mathrm{SU(N_c)}$ in the fundamental representation ($\mathrm{N_c} \times \mathrm{N_c}$ matrices). The strong coupling $g_s = \sqrt{4\pi\alpha_s}$ determines the strength of the strong interaction between colored particles. The second term of the classical Lagrangian contains the dynamics of the gluon gauge fields A^a_μ. The field strength tensor $F^a_{\mu\nu}$ is given by

$$F^a_{\mu\nu} = \partial_\mu A^a_\nu - \partial_\nu A^a_\mu - g_s f^{abc} A^b_\mu A^c_\nu \,, \tag{2.20}$$

where $f^{abc} = i T^a_{bc}$ are the generators of $\mathrm{SU(3)_c}$ in the adjoint representation. Unlike the Abelian gauge bosons of QED, in QCD the gluons undergo self-interactions. The non-Abelian last term in Eq. (2.20) is the most important difference between QED and QCD, when expanded, it involves terms describing the three and four gluon self-interactions. The property of asymptotic freedom is ultimately caused by these new terms.

In constructing our field theory, QCD, the local invariance of the classical Lagrangian under $\mathrm{SU(3)_c}$ transformations, is required. These transformations result in quark fields being transformed in the fundamental representation, while gluon fields being transformed in the adjoint representation of $\mathrm{SU(3)_c}$ so that

$$\begin{aligned} q^i(x) \to q'(x) \equiv q^j(x) &= \exp\left(i\,\theta^a(x)\,t^a_{ij}\right) q^i(x), \\ A_\mu(x) \to A'_\mu(x) &= \exp\left(i\,\theta^a(x)\,T^a\right) \left[A_\mu(x) + \frac{i}{g_s}\partial_\mu\right] \exp\left(-i\,\theta^b(x)\,T^b\right) \,, \end{aligned} \tag{2.21}$$

where $A_\mu = \sum_{a=1}^{8} A^a_\mu T^a$, and so

$$T^a F^a_{\mu\nu} \to T^a F'^a_{\mu\nu} = \exp\left(i\,\theta^a(x)\,T^a\right) t^a F^a_{\mu\nu} \exp\left(-i\,\theta^b(x)\,T^b\right) \,.$$

Because of the self interaction term, $F^a_{\mu\nu}$ is no longer invariant under gauge transformations, however, $F^a_{\mu\nu}F^{\mu\nu}_a$ is invariant. On the other hand, the local symmetry requirement forbids the corresponding mass term for the gauge field, so they are massless.

The classical Lagrangian contains parts which represent free quarks and free gluons and also contains parts representing the interactions between them, and hence can be written as

$$\mathcal{L}_{\text{classical}} = \mathcal{L}_0 + \mathcal{L}_{\text{int}} \,. \tag{2.22}$$

Because of the interaction term $\mathcal{L}_{\text{int}}$, exact solutions become no longer possible. In fact the only other standard procedure for calculating experimentally measurable quantities like decay rates and interaction cross sections, is by resorting to perturbation theory. Assuming the interaction term to be sufficiently small, it can be considered as a small perturbation of the free theory described by $\mathcal{L}_0$. The basic quantity to consider is the amplitude (the invariant matrix elements) $\mathcal{M}_{if}$ of the interacting theory which is then squared and summed (averaged) over final (initial)

state spin, polarisation and color, to give the required probability $\mathcal{P}$ for the occurrence of the interaction, i.e., transformation between initial and final states

$$\mathcal{P} = |\overline{\mathcal{M}_{if}}|^2 \,. \tag{2.23}$$

For reactions involving two incoming beams of particles $\mathcal{A}$ and $\mathcal{B}$, e.g., at LEP or LHC, the total cross section for the reaction $\mathcal{A} + \mathcal{B} \to f$ is given by

$$\begin{aligned}\sigma_{tot} &= \int \mathcal{F}\, |\overline{\mathcal{M}_{if}}|^2 \, \mathrm{d}\Pi_f \\ &= \int \frac{1}{2E_{\mathcal{A}} 2E_{\mathcal{B}} |v_{\mathcal{A}} - v_{\mathcal{B}}|} \, |\overline{\mathcal{M}_{if}}|^2 \, (2\pi)^4 \, \delta^{(4)} \left(P_{\mathcal{A}} + P_{\mathcal{B}} - \sum_f P_f \right) \prod_f \frac{\mathrm{d}^3 P_f}{(2\pi)^3 \, 2E_f} \, \frac{1}{n!} \,,\end{aligned} \tag{2.24}$$

with $\mathcal{F}$ being the flux of the initial particles, $\mathrm{d}\Pi_f$ is the final state phase space, E and v stand for energy and speed of particles and n is the number of identical particles in the final state. One can expand the amplitude $\mathcal{M}$ in a power series of the strength coupling g_s ($g_s \ll 1$)

$$\mathcal{M} = M^{(0)} + g_s \, \mathcal{M}^{(1)} + g_s^2 \, \mathcal{M}^{(2)} + g_s^3 \, \mathcal{M}^{(3)} + ... \tag{2.25}$$

It turns out that the calculation of σ_{tot} at each order in the strength coupling g_s, might be feasible using Feynman diagrams and assigning them factors for each vertex (describing the local interaction of quantized fields), propagator (corresponding to virtual intermediate states) and external legs (describing the incoming and outgoing real particles), and hence interactions are depicted in terms of diagrams. These Feynman rules can be derived from the classical Lagrangian. $\mathcal{L}_{int}$ generates the vertices while $\mathcal{L}_0$ produces the propagators. For example, the quark propagator can therefore be obtained using $\mathcal{L}_0$, by simply replacing $\partial\mu \to -i\, P^\mu$ and taking the inverse of the term between the quark field and its conjugate. On the other hand, the gluon propagator is constructed from the inverse of the bilinear term $A^a_\mu \, A^b_\nu$ which is however not invertible and hence it is not possible to construct the gluon propagator. The interpretation is that our definition of the gauge field A^a_μ is not unique, due to the fact of the freedom to make gauge transformations. This problem can therefore be controlled by introducing the gauge-fixing term $\mathcal{L}_{\text{gauge}-\text{fixing}}$ [69], and there exist several classes of gauge fixing to this problem. In practice, the commonly useful one which respects Lorentz invariance is the covariant gauge parameterized by ξ

$$\mathcal{L}_{\text{gauge}-\text{fixing}} = -\frac{1}{2\xi} \left(\partial^\mu A^a_\mu \right)^2 \,. \tag{2.26}$$

The physical predictions are actually invariant under the choice of ξ. Some widespread choices include: the Landau gauge ($\xi \to 0$) and the Feynman gauge $\xi \to 1$. We work within this latter that greatly simplifies our calculations. A spin-1 massless gluon should only have two physical degrees of freedom (the transverse gluon polarizations). However when using the

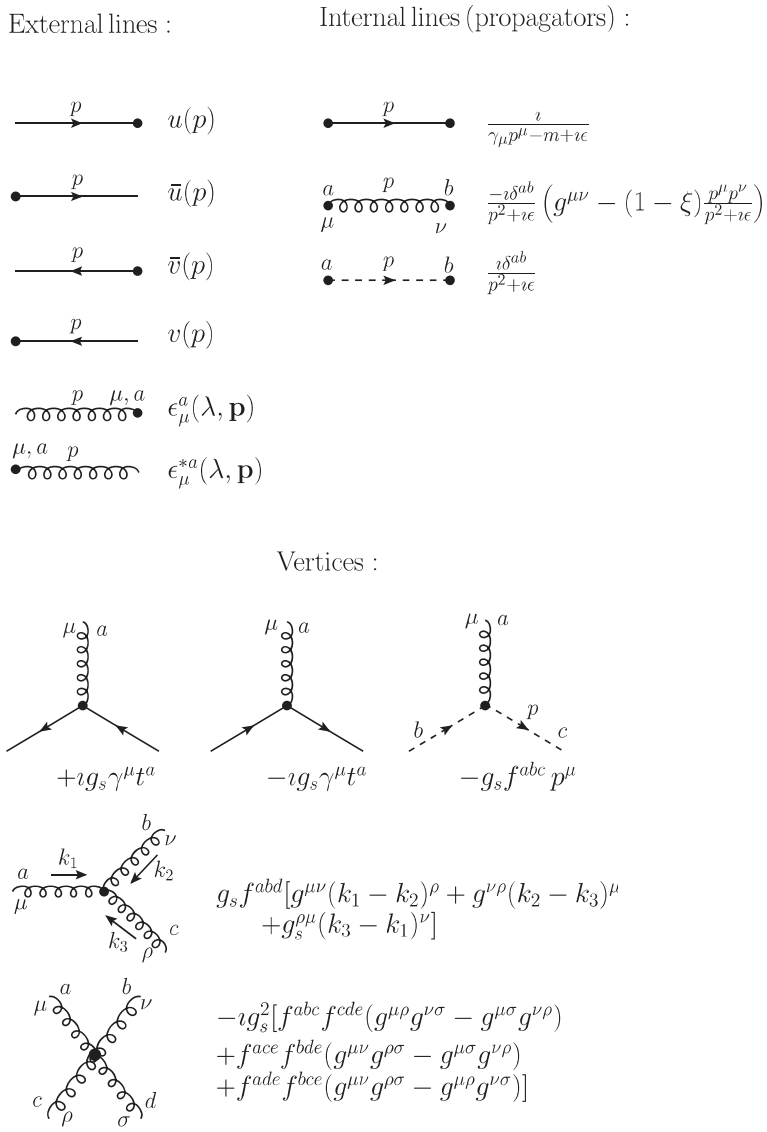

Figure 2.1: Feynman rules for QCD in a covariant gauge, solid lines represent quarks, curly lines represent gluons, and dashed lines represent ghosts.

covariant gauge, the unphysical time-like and longitudinal polirazations of the gluons could also propagate within loops. To eliminate the unphysical degrees of freedom, the fourth term in Eq. (2.17) must be added to the covariant gauge fixing term,[4] the kinetic term for the unphysical ghosts

$$\mathcal{L}_{\text{ghost}} = \partial_\mu \eta^{a\dagger} D^\mu_{ab} \eta^b \,, \tag{2.27}$$

where the η^a are anti-commuting scalar fields known as Fadeev-Popov ghosts [77]. Conventionally, quarks are represented by solid lines, gluons by curly lines, and ghosts are represented by dotted lines. The Feynman diagrams along with Feynman rules for QCD are depicted in Fig. 2.1.

[4]The ghost Lagrangian term depends on the gauge-fixing term chosen where there are gauges whereby the ghosts are not needed. For example, the axial gauge does not require ghost accounting.

2.1.3 Renormalization and ultraviolet divergences

It is often straightforward to apply Feynman rules to compute scattering amplitudes for a given process at leading order (LO) in the strong coupling. However, LO results are generally not precise enough to much the current experimental precision and therefore to obtain an accurate theoretical predictions of an observable in QCD, one must calculate its higher orders perturbative corrections. In fact, when advancing beyond LO to next to leading order (NLO) and beyond, there will be Feynman diagrams involving loops. Fig. 2.2 depicted one such diagram. However, the loop diagrams produce ultraviolet (UV) divergent integrals over arbitrary large momentum ($k \to \infty$) which present a problem in perturbation approach.

The Lagrangian is actually expressed in terms of unmeasurable bare parameters such as the strong coupling constant g_s^0 and the fermion masses m^0. It is well established that the UV divergences may be absorbed into redefinitions of these bare parameters that will become scale dependent. Consequently, the Lagrangian will be expressed in terms of physically measurable quantities, rendering the theory under consideration UV finite. This procedure is known as renormalization and the measurable parameters are typically taken to be renormalized.

In order to accomplish this the divergent integrals must first be regularized and there exist several approaches to this problem. In practice, the commonly useful method which respects Lorentz invariance and unitarity as well as maintains the gauge symmetry of the theory is called dimensional regularization [78–80]. This technique will change the number of space-time dimensions to $d = 4 - 2\epsilon$ instead of $d = 4$ dimensions, where ϵ is a small parameter. The loop integrals in this dimension are convergent. When taking the limit $\epsilon \to 0$, the result will then include a term proportional to $1/\epsilon$, which is obviously a singularity.

For the purpose of removing these kind of divergences, the basic idea of renormalization should be applied. This is achieved by introducing infinite renormalization factors Z_i to absorb the UV divergences. The renormalization then amounts to the replacement

$$g_s^0 = Z_g(\mu) g_s(\mu)\,, \tag{2.28}$$

$$m^0 = Z_m(\mu) m(\mu)\,, \tag{2.29}$$

$$\chi^0 = Z_\chi(\mu)\chi(\mu), \quad \chi \equiv A, \psi\,, \tag{2.30}$$

where the superscript (0) stands for bare fields and parameters. The Z_i are given by

$$Z_i = 1 - \delta_i\,.$$

The δ_i are the counterterms that precisely cancel the UV divergent terms to all orders. This procedure introduces a scale dependence, the renormalization scale (μ). In addition to the poles in the Z_i, the freedom in absorbing a finite part is determined by the scheme of renormalization

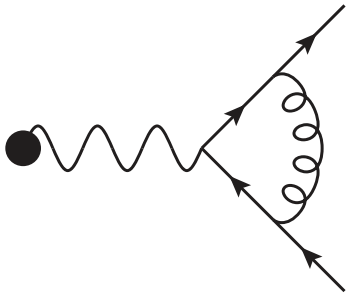

Figure 2.2: A typical Feynman diagram showing the next-to-leading order virtual corrections to the process $e^-e^+ \to q\bar{q}$.

and there are different schemes of renormalisation within the dimensional regularisation scheme. It is often convenient to use the modified minimal substraction ($\overline{MS}$) scheme [81] which removes the UV poles plus a fixed finite contribution, $\ln 4\pi - \gamma_E$, where $\gamma_E = 0.5772$ is the numerical value for the Euler constant.

2.1.4 Running of the strong coupling constant

As a consequence of renormalization, the strong coupling constant becomes scale dependent $\alpha_s(\mu) \equiv g_s^2(\mu)/4\pi$ and this is in turn the reason for the paradoxial term "the running of strong coupling constant", which is not really a constant. Let us now see how pQCD describes the energy scale dependence of the strong coupling. Since the perturbative calculation of any physical observable should be renormalization scheme and scale independent, hence the variation of the renormalized running coupling is governed by the renormalization group equation (RGE) [62, 85], which can be written as

$$\mu^2 \frac{\partial \alpha_s}{\partial \mu^2} = \beta(\alpha_s)\,, \tag{2.31}$$

and therefore the running of the coupling is determined by the $\beta(\alpha_s)$ function which has the perturbative expansion

$$\beta(\alpha_s) = -\alpha_s^2\left(\beta_0 + \beta_1\alpha_s + ...\right)\,, \tag{2.32}$$

where the β_i coefficients are contributions extracted from different higher loop orders. Some of the Feynman diagrams giving the one loop contribution β_0 are shown in Fig. 2.3. β_0 and β_1 are given by

$$\beta_0 = \frac{(11\,\mathrm{C_A} - 2\,n_f)}{12\pi}\,, \tag{2.33a}$$

$$\beta_1 = \frac{\left(17\,{\mathrm{C_A}}^2 - 5\,\mathrm{C_A}\,n_f - 3\,\mathrm{C_F}\,n_f\right)}{24\pi^2}\,, \tag{2.33b}$$

where $n_f = 5$ is the number of active quark flavours. As long as $n_f < 17$, then the coefficient β_0 is always positive, and so far max (n_f)=6 in nature, hence this result is always satisfied. Eq. (2.31) can be re-expressed as

$$\int_{\alpha_s(\mu^2)}^{\alpha_s(Q^2)} \frac{d\alpha_s}{\beta(\alpha_s)} = \int_{\alpha_s(\mu^2)}^{\alpha_s(Q^2)} \frac{d\mu^2}{\mu^2} = \ln \frac{Q^2}{\mu^2} . \tag{2.34}$$

Neglecting β_1 and higher coefficients of the $\beta(\alpha_s)$ function to only include the one loop β_0 contribution, then its solution is given by

$$\alpha_s(Q^2) = \frac{\alpha_s(\mu^2)}{1 + \beta_0 \alpha_s(\mu^2) \ln(Q^2/\mu^2)} , \tag{2.35}$$

which means that once the strong coupling $\alpha_s(\mu)$ is determined at a given scale μ that should be in the perturbative domain, then its value at any other large scale Q^2 can be achieved using the above equation. [5] In QED with Abelian (non-interacting) photons, only the electron loop contributed to the 1-loop order giving an overall positive β, and consequently at high energies the QED coupling increases ($\alpha \sim 1/128$). At low energies it gets small ($\alpha \sim 1/137$). However in QCD, besides the quark loop which gives a negative contribution to the expression of β_0 (Eq. (2.33a)), there are other contributions coming from the non-abelian self interactions amongst gluons (see Fig. 2.3) which provide a positive term proportional to C_A, leading to a positive β_0 and an overall negative β function. Hence, the self-interaction of the gluons is precisely what leads to asymptotic freedom. Because of this sign, in the high energy limit ($\mu^2 \to \infty$), the strength of the strong coupling decreases to approach zero. In fact collisions between hadrons at very high energy (short distance) are dominated by the interactions among essentially free quarks and gluons where pQCD can be correctly applied. On the contrary, when the energy gets smaller (long distance), if we ignore this fact and compute the perturbative solution of the RGE equation even at low energies, we will find that there exists a scale at which the running coupling barge into a singularity when $\mu^2 \to \Lambda_{QCD}$. This is called the Landau pole. In fact Eq. (2.35) can be re-expressed in terms of Λ_{QCD} as

$$\alpha_s(Q^2) = \frac{1}{\beta_0(\mu^2) \ln(Q^2/\Lambda^2_{QCD})} . \tag{2.36}$$

This scale characterizes the region in which the running coupling increases and hence pQCD is no longer usable. Using $\overline{MS}$ scheme and $n_f = 5$, it was found that Λ_{QCD} is typically of the order of ~ 200 Mev which is the order of magnitude of the mass of the lightest hadrons [71]. In this non-perturbative region the running coupling grows and the color interactions become stronger confining quarks and gluons inside hadrons, which in turn provide the reason why partons (quarks and gluons) have never been seen in isolation as free particles. This phenomenon is

[5] Usually the magnitude of α_s in QCD is given at the mass of the Z boson: $\alpha_s(\mu = m_Z) \sim 0.118$ [70].

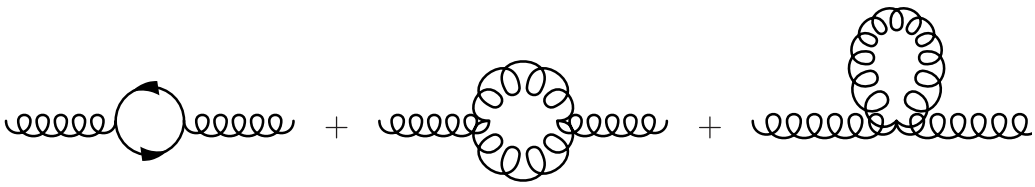

Figure 2.3: The Feynman diagrams giving the one loop β_0 contribution to the β function; the first is the quark loop and the next two are the gluon loops.

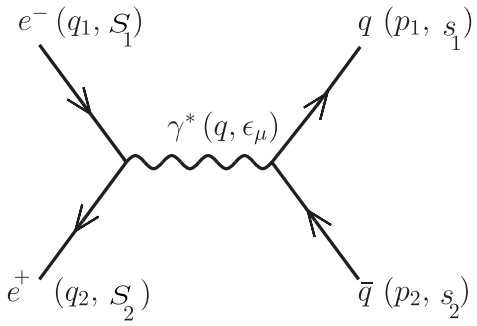

Figure 2.4: A schematic picture showing the leading order Feynman diagram for the process $e^+e^- \to q\bar{q}$.

known as *color confinement* which is in fact beyond the scope of pQCD. Furthermore, in such region, one will be interested in the calculation of non-perturbative inputs like PDFs (see next chapter).

2.1.5 e^+e^- annihilation and infrared divergences

In the previous section, we have discussed the UV divergences associated with the high momentum limit and hence short distance physics. We will now assume that UV renormalization has been carried out and as a starting point we will discuss the infrared and collinear (IRC) singularities which are the topic of this thesis. Despite the fact that the structure of IRC singularities in QCD is universal, we will look at how they appear in the perturbative QCD calculations for the process e^+e^- annihilation into hadrons that can proceed through an intermediate photon or a Z boson. The perturbative expansion of this process can be written as

$$\sigma_{tot}(e^+e^- \to hadrons) = \sigma_0 + \sigma_1 + \sigma_2 + \sigma_3 + ... \tag{2.37}$$

The basic Feynman diagram representing the born (σ_0) cross section is depicted in Fig. 2.4. Using Feynman rules shown in Fig. 2.1, the born matrix element (amplitude) M_0 is given by

$$\begin{aligned} iM_0 &= \bar{u}(p_1, s_1, i)\,(i\,e\,e_{q_f}\,\gamma^\mu)\,v(p_2, s_2, j)\,\frac{(-i\,g_{\mu\nu})}{q^2}\,\bar{v}(q_1, S_1)\,(-i\,e\,\gamma^\nu)\,u(q_2, S_2) \\ &= (-e^2\,e_{q_f})\,\frac{i}{q^2}\left[\bar{u}(p_1, s_1, i)\,\gamma_\mu\,v(p_2, s_2, j)\right]\left[\bar{v}(q_1, S_1)\,\gamma^\mu\,u(q_2, S_2)\right], \end{aligned} \tag{2.38}$$

where u and v are the Dirac spinors. The final state quark and anti-quark have momenta p_1 and p_2 and spins s_1 and s_2 whilst the incoming electron and positron have momenta q_1 and q_2 and spins S_1 and S_2, with i, j being the colour indices of the quark and anti-quark, and e_{q_f} is the quark electric charge. For simplicity, we choose to work in the center of mass frame and it is useful to take the squared center of mass energy $s < M_Z^2$, so that only photon exchange is important. Defining

$$q = (\sqrt{s}, 0, 0, 0)\,, \tag{2.39}$$

$$s = (q_1 + q_2)^2 = (p_1 + p_2)^2\,. \tag{2.40}$$

The squared amplitude (averaged and summed over initial and final state quantum numbers) reads

$$|\overline{M_0}|^2 = \frac{1}{s^2}\, J^{\mu}_{(e)}\, J^{(q)}_{\mu}\,, \tag{2.41}$$

where the initial spin averaged electron tensor is given by

$$\begin{aligned} J^{\mu}_{(e)} &= \frac{e^2}{4} \sum_{S,S'} \left[\bar{v}(q_1, S_1)\, \gamma^{\mu}\, u(q_2, S_2)\right] \left[\bar{u}(q_2, S_2')\, \gamma^{\nu}\, v(q_1, S_1')\right] \\ &= \frac{e^2}{4} \mathrm{Tr}\left(\not{q}_1 \gamma^{\mu} \not{q}_2 \gamma^{\nu}\right) \\ &= e^2\, \left(q_1^{\mu}\, q_2^{\nu} + q_1^{\nu}\, q_2^{\mu} - g^{\mu\nu}\, q_1.q_2\right)\,, \end{aligned} \tag{2.42}$$

and the hadronic tensor is given by

$$\begin{aligned} J^{(q)}_{\mu} &= \sum_{i,j,k,l} \sum_{s,s'} e^2\, e_{q_f}^2 \left[\bar{u}(p_1, s_1, i)\, \gamma_{\mu}\, v(p_2, s_2, j)\right] \left[\bar{v}(p_2, s_2', k)\, \gamma_{\nu}\, u(p_1, s_1', l)\right] \\ &= \sum_{f=1}^{n_f} e^2\, e_{q_f}^2\, \delta_{jk}\delta_{il}\, \left(p_{1\mu}\, p_{2\nu} + p_{1\nu}\, p_{2\mu} - g_{\mu\nu}\, p_1.p_2\right) \\ &= \mathrm{N_c} \sum_{f=1}^{n_f} e^2\, e_{q_f}^2\, \left(p_{1\mu}\, p_{2\nu} + p_{1\nu}\, p_{2\mu} - g_{\mu\nu}\, p_1.p_2\right)\,. \end{aligned} \tag{2.43}$$

The spin sums are easily performed using the spinors completeness relations

$$\sum_{s,s'} u(p)\bar{u}(p) = \not{p} \quad , \quad \sum_{s,s'} v(p)\bar{v}(p) = \not{p}\,. \tag{2.44}$$

To carry out the Dirac traces we have used some useful trace technology relations which follow from the fundamental commutation relations of the Dirac matrices. We note that $\sum_{i,j,k,l} \delta_{jk}\, \delta_{il} = \sum_{i,j} \delta_{ij}\delta_{ji} = \mathrm{N_c}$. Substituting Eqs. (2.42) and (2.43) into Eq. (2.41), the

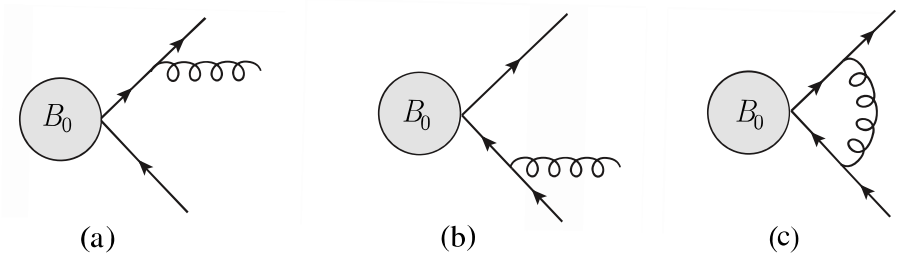

Figure 2.5: Real soft gluon emission and virtual gluon exchange contributing to the cross section $e^-e^+ \to q\bar{q}g$ at next-to-leading order. B_0 stands for the leptonic part of the process.

born crosse section reads

$$\begin{aligned}\sigma_0 &= \frac{1}{2s}\int \frac{\mathrm{d}^3\vec{p_1}}{(2\pi)^3}\frac{1}{2E_1}\frac{\mathrm{d}^3\vec{p_2}}{(2\pi)^3}\frac{1}{2E_2}(2\pi)^4\,\delta^4\left(q_1+q_2-p_1-p_2\right)\,|\overline{M_0}|^2 \\ &= \mathrm{N_c}\,\frac{4\pi\,\alpha^2}{3s}\sum_{f=1}^{n_f} e_{q_f}^2\,,\end{aligned} \tag{2.45}$$

where $\alpha = e^2/4\pi$ is the fine structure constant (the QED coupling constant).

As a next step, let us examine the first-order soft corrections to the born (hard) cross-section, namely the corrections of order α_s. At next to leading order (NLO), the Feynman diagrams representing the real emission of a soft gluon off either of the external hard partons legs (tree level diagrams) and virtual corrections to the interaction vertex, are depicted in Fig. 2.5. Gluons emitted from final state particles are known as final state radiation (FSR). Let us first compute the contribution from the real diagrams. Implementing Feynman rules, the amplitude for real emission corresponding to the sum of the two diagrams a and b is given by

$$\begin{aligned}iM_1 = \bar{u}(p_1,s_1,i)\,\Big[(-ig_s t^a_{ij})\,\gamma^\mu\,\epsilon^{a*}_\mu(k,\lambda)\,\frac{i(\not{p}_1+\not{k})}{(p_1+k)^2}\,B_0 \\ + B_0\,\frac{i(\not{p}_2+\not{k})}{(p_2+k)^2}\,(ig_s t^a_{ij})\,\gamma^\mu\,\epsilon^{a*}_\mu(k,\lambda)\Big]\,v(p_2,s_2,j)\,,\end{aligned} \tag{2.46}$$

where B_0 stands for the leptonic part of the process, and $\epsilon^{a*}_\mu(k,\lambda)$ is the gluon polarization vector which has momentum k, with indices a and λ denoting the gluon color and polarization; g_s is the strong coupling. The quark, antiquark and gluon are all on mass shell, in the sense that $p_1^2 = p_2^2 = k^2 = 0$. Taking the Eikonal approximation in which the gluon momentum is small with respect to that of the hard quark and anti-quark, i.e., $|k| \ll |p_1 - p_2|$ (or equivalently $k \to 0$ and $p_1 \sim p_2$) and hence allows us to neglect $\not{k}$ in the numerator of the quark and anti-quark propagators. The corresponding eikonal Feynman rules are shown in Fig. 2.6, and the color matrices in the fundamental and adjoint representations are represented by

- $+t^a$ if the radiating parton is an outgoing quark (incoming antiquark).
- $-t^a$ if the radiating parton is an incoming quark (outgoing antiquark).

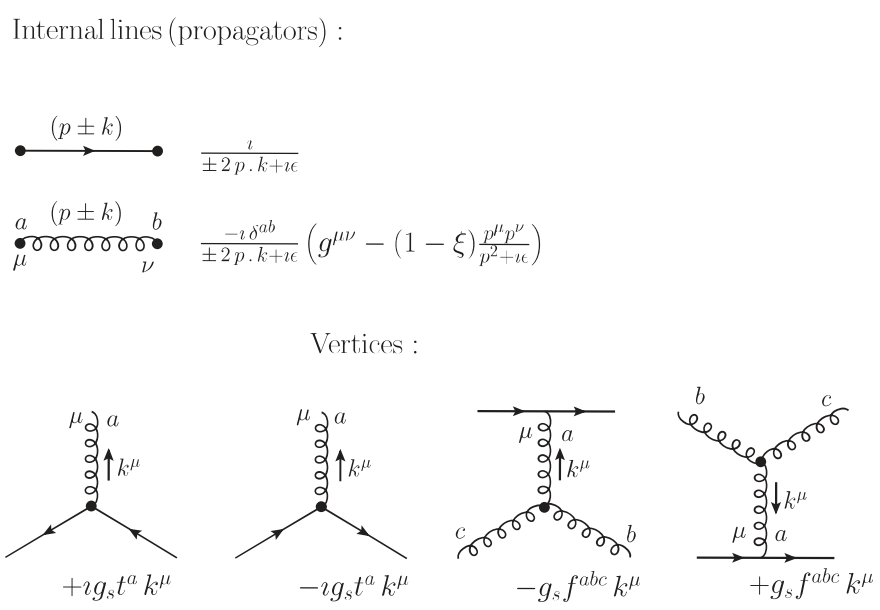

Figure 2.6: Eikonal Feynman rules for QCD.

- $+(-)if^{abc}$ if the radiating parton is an outgoing (incoming) gluon.

We use the equations of motion for massless (anti) spinor $\bar{u}(p_1)\, \not{p}_1 = 0$ and $\not{p}_2\, v(p_2) = 0$, and the Dirac algebra

$$\begin{aligned} \bar{u}(p_1)\, \gamma^\mu\, \not{p}_1 &= \bar{u}(p_1) \gamma^\mu\, \gamma^\nu = 2\bar{u}(p_1)\, p_1^\mu\,, \\ \not{p}_2\, \gamma^\mu\, v(p_2) &= p_{2\nu}\, \gamma^\nu\, \gamma^\mu\, v(p_2) = 2v(p_2)\, p_2^\mu\,. \end{aligned} \tag{2.47}$$

The amplitude should thus be simplified to

$$\begin{aligned} iM_1 &= g_s t^a_{ij}\, \epsilon^{a*}_\mu(k,\lambda)\, \left[\bar{u}(p_1, s_1, i)\, B_0 v(p_2, s_2, j)\right]\, \left[\frac{p_1^\mu}{p_1.k} - \frac{p_2^\mu}{p_2.k}\right] \\ &= g_s t^a_{ij}\, \epsilon^{a*}_\mu(k,\lambda)\, (iM_0)\, \left[\frac{p_1^\mu}{p_1.k} - \frac{p_2^\mu}{p_2.k}\right]\,. \end{aligned} \tag{2.48}$$

Multiplying by the conjugate transpose, summing over final state spins, polarization and colors and averaging over initial state spins, the amplitude squared is therefore given by

$$\begin{aligned} |\overline{M_1}|^2 &= g_s^2\, \mathrm{Tr}(t^a_{ij}\, t^b_{kl})\, \delta_{jk}\, \delta_{il}\, \delta_{ab}\, \frac{|\overline{M_0}|^2}{\mathrm{N_c}}\, \frac{2\, p_1.p_2}{(p_1.k)(p_2.k)} \\ &= g_s^2\, \mathrm{Tr}(t^a_{ij}\, t^a_{ji})\, \frac{|\overline{M_0}|^2}{\mathrm{N_c}}\, \frac{2\, p_1.p_2}{(p_1.k)(p_2.k)} \\ &= g_s^2\, \mathrm{C_F}\, |\overline{M_0}|^2\, \frac{2\, p_1.p_2}{(p_1.k)(p_2.k)}\,, \end{aligned} \tag{2.49}$$

where the sum over gluon polarizations is given by $\sum_{\lambda,\lambda'} \epsilon^{a*}_\mu(k,\lambda)\, \epsilon^b_\nu(k,\lambda') = -g_{\mu\nu}\, \delta^{ab}$, and the $\mathrm{Tr}(t^a_{ij}\, t^a_{ji}) = \mathrm{C_F}\, \mathrm{N_c}$. In the Eikonal approximation (soft limit) we note that the amplitude factorizes out into a product of a hard Born amplitude and an Eikonal factor involving all the

IRC singularities (see below). Consequently the real cross section for the process $e^-e^+ \to q\bar{q}g$ is given by

$$\sigma_1^{real} = 2\,\mathrm{C_F}\,g_s^2\,\sigma_0 \int \frac{\mathrm{d}^3k}{(2\pi)^3\,2E_g}\,\frac{(p_1.p_2)}{(p_1.k)\,(p_2.k)} \tag{2.50}$$

$$= \mathrm{C_F}\,\frac{\alpha_s}{\pi}\,\sigma_0 \int \frac{\mathrm{d}E_g}{E_g}\,\frac{\mathrm{d}\phi}{(2\pi)}\,\mathrm{d}\cos\theta\,w_{12}^k\,, \tag{2.51}$$

where $\alpha_s = g_s^2/4\pi$, and E_g is the gluon energy. Here θ and ϕ are the polar and azimuthal angles of the emitted gluon. The antenna function, which corresponds to a soft gluon k stretching between the two Eikonal (color-connected) legs 1 and 2, is defined as follows

$$w_{12}^k = E_g^2\,\frac{(p_1.p_2)}{(p_1.k)\,(p_2.k)}\,. \tag{2.52}$$

In the center of mass frame, The four-momenta of the outgoing quark, anti-quark and gluon are given by

$$\begin{aligned} p_1 &= \frac{\sqrt{s}}{2}\,(1,0,0,1)\,,\\ p_2 &= \frac{\sqrt{s}}{2}\,(1,0,0,-1)\,,\\ k &= E_g\,(1,\sin\theta\,\cos\phi,\sin\theta\,\sin\phi,\cos\theta)\,. \end{aligned} \tag{2.53}$$

Evaluating the 4-momenta products and substituting the result into Eq. (2.51) we get

$$\sigma_1^{real} = \mathrm{C_F}\,\frac{\alpha_s}{\pi}\,\sigma_0 \int \frac{\mathrm{d}E_g}{E_g}\,\mathrm{d}\cos\theta\,\frac{2}{(1-\cos\theta)(1+\cos\theta)}\,. \tag{2.54}$$

We clearly note that the cross section may be infinite (divergent) either as $(E_g \to 0)$ which is known as soft or infrared singularity, or as $(\theta \to 0,\pi)$ implying that the 4-momentum of the gluon is parallel to that of either the quark or the ant-quark; this is referred to as a collinear divergence. Unlike UV divergences, IRC divergences are concerned with long distance behaviour (like hadronisation). The key point is that from an experimental viewpoint the soft and collinear gluons could not be distinguished from the process without gluon emission. This in turn would therefore be reflected in the corresponding theoretical calculation. The condition of the cancellation of these divergences is given by the Bloch-Nordsieck (BN) [82] and Kinoshita-Lee-Nauenberg (KLN) [83, 84] theorems which state that in a theory with massless fields, transition rates are free of IRC singularities that should actually cancel out when contributions from both virtual and real emission diagrams are added, living a finite result. The virtual cross section turns out to include exactly the same soft and collinear divergences and we can see this explicitly at order α_s in Appendix A. To perform the phase space integral for both real and virtual contributions in a well defined manner, we need first to introduce a regulator, and

use dimensional regularization. The singularities then appear as poles in the regulator ϵ when taking the limit $\epsilon \to 0$. Each of these singularities gives rise to a single pole $1/\epsilon$. Whenever the gluon becomes both collinear and soft a double pole arises, $1/\epsilon^2$.

Chapter 3

Phenomenology of QCD and jets

As we are entering the era of hadron and lepton colliders, an emergent structure consisting of collimated bunches of hadrons, referred to as jets, is typically the most frequent object observed. They can be viewed as proxies for hard quarks or gluons produced during the collision. Their evolution is completely controlled by the strong force, which is described by QCD in the SM. Jets not only exhibit the QCD behaviour across a wide range of energy scales, but also serve as signatures of new physics when constructed from the decays of heavy BSM particles. However, jets are not basically well-defined objects, and in order to accomplish this, one needs to establish a strictly defined procedure that allows the reconstruction of jets from the set of hadrons in the final state and we do so in Sec. 3.2.

Unlike electrons which are still considered to be elementary particles, protons are made up of partons (quarks and gluons), which severely complicates the observed final state and limits our understanding of the underlying processes. For instance, which parton participates in the collision or which fraction of each proton's energy is carried by the colliding partons is formerly unknown. In this step, the relative probability to find the scattering partons is given by the parton distribution functions (PDFs), which depend on the factorisation scale μ_f and the parton's momentum fraction x.[1] More on this will be discussed in Sec. 3.1. A typical jet event at the LHC consisting of several parts, in which a 2 hard partons scattering carrying fraction momenta x_1 and x_2 of the incoming protons has occurred, is illustrated in Fig. 3.1. Since the incoming partons' energy scale greatly differs from the hard scattering scale, gluon radiation will fill up the phase space, allowing hard partons to radiate gluons before entering the era of the hard process, a so-called initial state radiation (ISR). The hard scattering of colored partons which occurs at a much short timescale $(1/Q)$, produces a few hard partons or other BSM particles. These new partons then shower soft and collinear/wide-angle QCD radiation at ever lower energies and this phenomena is referred to as final state radiation (FSR), which results in large logarithmic contributions to the final cross section. The resummation of these

[1]The variable x represents the momentum fraction of the struck parton relative to the proton, known as Bjorken-x.

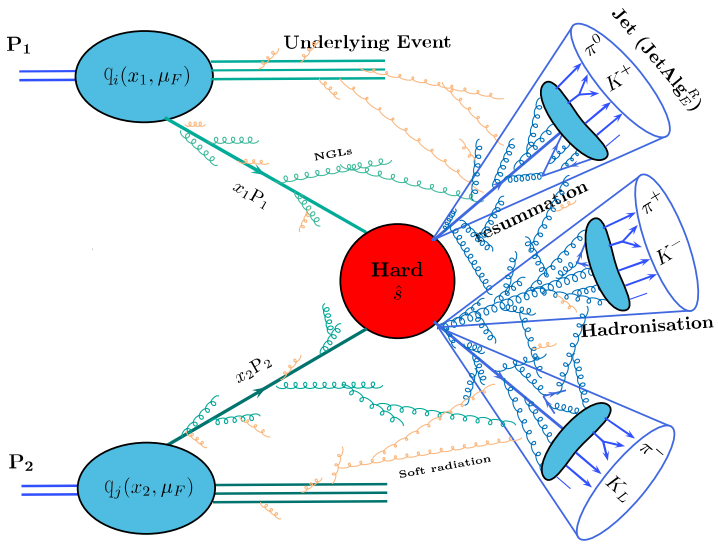

Figure 3.1: A theoretical representation of a typical jet event at the LHC involves perturbative and non-perturbative effects. Former effects include: hard scattering subprocess, soft and collinear radiation (resummation), soft and wide-angle radiation, non-global logs (NGLs), effects of jet algorithms with jet radius R and recombination scheme E. Latter effects include: underlying event (UE), pile up interactions, and hadronization. This figure is taken from Ref [12].

large logarithms which is the key issue of this thesis, will be investigated in Sec. 3.3.

The resulting event may be viewed as a central hard partonic scattering surrounded by the so-called underlying event (UE). The UE receives contributions not only from the breakup of the proton, (beam-beam remnants (BBR)),[2] but also from multiple parton interactions (MPI), which originate from semi-hard parton-parton scattering inside the same proton-proton collision. Furthermore, several proton-proton collisions, known as pile-up (PU), may take place almost simultaneously within the experimental interaction region due to the intense environment that the LHC's high liminosity creates. Finally, at the lowest scale ($\Lambda_{\rm QCD}$), the dynamical hadronisation process which actually happens at a much longer timescale ($1/\Lambda_{QCD}$), turns partonic degrees of freedom (the colored partons resulting from the showering as well as those coming from softer interactions, both from UE and PU) to hadronic degrees of freedom (color singlet hadrons) that we actually observe in the detector.[3] This final step of the jet components interacting in the detector is represented in Fig. 3.4

In e^+e^- collisions, both incoming particles are elementary, without substructure, and thus colliding particles and collision energy can be precisely defined. Furthermore, the complications in analyzing LHC events due to ISR, UE, MPI and PU are essentially removed. With these advantages, both linear (ILC) and circular (FCC-ee) e^+e^- future colliders offer an excellent potential for precision physics as well as discovering and studying new physics signals as they hit their designed energy (1-3 TeV) .

[2]BBR are what are left after a parton is removed from each of the first two beam hadrons.
[3]The hadronisation process has not been fully understood and remains the holy grail of QCD.

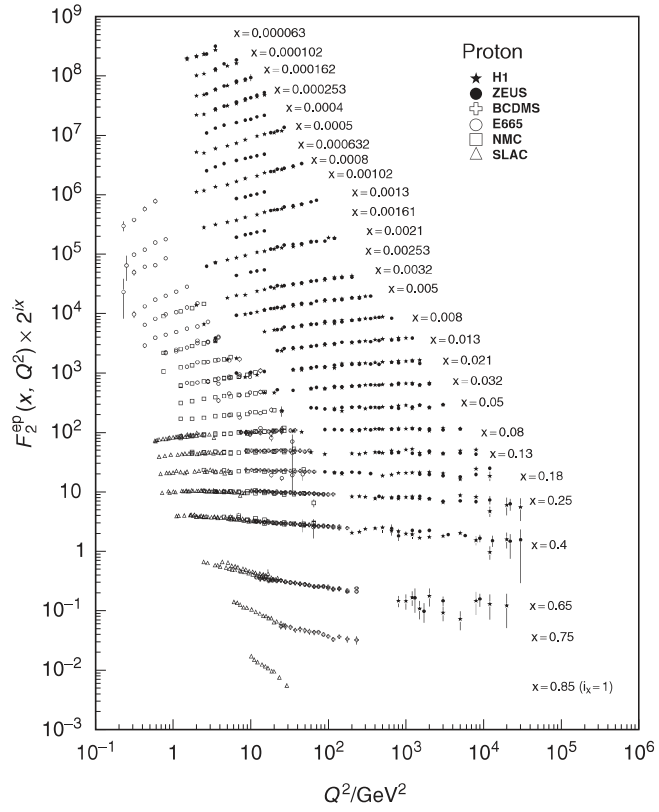

Figure 3.2: Measurements of $F_2(x, Q^2)$ at HERA. Results from both the H1 and ZEUS experiments are shown. Bjorken scaling is confirmed in deep inelastic scattering data where for $0.01 < x < 0.5$, only a weak Q^2 dependence of $F_2^{ep}(x, Q^2)$ is observed. Scaling violations are evident at both very low and very high x values. For instance, the proton structure function is noted to decrease (increase) with increasing Q^2 at high (low) x values. [Particle Data Group (Beringer et al.) 2012].

3.1 Scaling violations and factorization

We will now embody the effect of gluon radiation by partons. In the naive parton model [57,58], it was supposed that parton's transverse momentum is constrained to be very small in comparison to the longitudinal one, and hence one could neglect it. For instance, in deep inelastic scattering (DIS), the parton that is struck by the photon can however acquire large transverse momentum via the emission of gluons prior to the hard interaction (ISR). The real emitted partons will either tend to be collinear to the original incoming parton or soft, resulting in soft and collinear divergences. In the same way as final state soft and collinear divergences present in e^+e^- annihilation that are indeed all cancelled upon adding real and virtual contributions, initial state soft divergences do cancel out. Consequently the final expression's left over divergences are initial state collinear divergences.

Here we will just review some results, but for a complete review see for example [62]. The naive parton model predicts at the lowest order that PDFs which describes the distribution and

dynamics of partons in the colliding hadrons, depend only on the Bjorken-x

$$F_2(x,Q^2) = \sum_{q,\bar{q}} e_q^2\, x\, q_0(x)\,,$$

thus confirming Bjorken scaling, $F_2(x,Q^2) \to F_2(x)$. [4] But when taking gluon radiation into account, i.e., when $\mathcal{O}(\alpha_s)$ QCD corrections are added, the F_2 structure function is found to be

$$F_2(x,Q^2) = x\sum_{q,\bar{q}} e_q^2\left[q_0(x) + \frac{\alpha_s}{2\pi}\int_x^1 \frac{\mathrm{d}\xi}{\xi} q_0(\xi)\left\{P_{qq}\left(\frac{x}{\xi}\right)\ln\left(\frac{Q^2}{m^2}\right) + C\left(\frac{x}{\xi}\right)\right\}\right], \tag{3.1}$$

where C is a finite function, Q is the hard scale of the process, and (x/ξ) is the momentum fraction of the incoming parton relative to the proton. We now note that beyond leading order, the structure function is Q^2 dependent and the Bjorken scaling is then broken by logarithms of Q^2. The logarithmic scale violations that were beyond the scope of the parton model (see Fig. 3.2), were therefore found to be in excellent agreement with the QCD predictions, firmly establishing the QCD as the correct theory of the strong interactions. In the above equation P_{qq} is the Altareli-Parisi splitting function which represents the probability that the daughter quark keep a fraction z of the parent quark momentum $q \to qg$ (see Fig. 3.3). The leading order $P^0_{qq}(z)$ is defined by

$$P^0_{qq}(z) = C_F\left[\frac{(1+z^2)}{(1-z)_+} + \frac{3}{2}\delta(1-z)\right]. \tag{3.2}$$

For any smooth function $f(z)$ the plus prescription is defined so that

$$\int_0^1 \mathrm{d}z\,\frac{f(z)}{[1-z]_+} \equiv \int_0^1 \mathrm{d}z\,\frac{f(z)-f(1)}{1-z}\,, \tag{3.3}$$

to exclude the soft divergences at $z=1$ due to the full cancellation of soft-real divergences with the corresponding virtual ones. On the other hand, the logarithmic term involves collinear singularities as $m^2 \to 0$. These singularities which are a sign of non-perturbative effects, are removed by renormalization of the non-perturbative PDFs, the so-called collinear factorization procedure. In clear similarity with ultraviolet renormalization, factorization theorem introduces a new factorization scale (μ_f) that can be considered as the scale which separates the short and long distance physics. Roughly speaking, a parton with high transverse momentum larger than (μ_f) participate in the hard scattering partonic cross section $\hat{\sigma}$ (see Eq. (3.8)), which is infrared safe and calculable in PT. While a parton with transverse momentum less than (μ_f) is

[4] $F_1(x,Q^2)$ and $F_2(x,Q^2)$ are structure functions which define the structure of the proton as viewed by the virtual photon in DIS. Bjorken had estimated that in the limit of $Q^2 \to \infty$, at fixed x, the structure functions depend only on x. This means that no matter how hard it is struck, the proton structure appears the same to any electromagnetic probe [56].

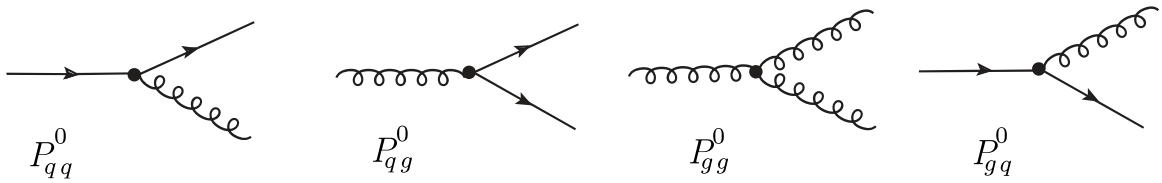

Figure 3.3: A diagrammatic representation of the leading order QCD splitting functions.

then absorbed into the non-perturbative PDFs. The renormalized quark distribution function is

$$q(x,\mu^2) = q_0(x) + \frac{\alpha_s}{2\pi}\int_x^1 \frac{\mathrm{d}\xi}{\xi}\, q_0(\xi)\left\{P_{qq}\left(\frac{x}{\xi}\right)\ln\left(\frac{\mu_f^2}{m^2}\right) + C_q\left(\frac{x}{\xi}\right)\right\}. \tag{3.4}$$

We can regard $q_0(x)$ as an unmeasurable bare distribution. We have used

$$\ln(Q^2/m^2) = \ln(Q^2/\mu_f^2) + \ln(\mu_f^2/m^2)\,. \tag{3.5}$$

Note that the singular term $\ln(\mu_f^2/m^2)$ as well as the non-singular term $C\,(x/z)$ are absorbed into $q(x,\mu_f^2)$.[5] Then we have

$$\begin{aligned} F_2(x,Q^2) &\equiv \sum_{q,\bar{q}} e_q^2\, x\, q(x,Q^2) \\ &= \sum_{q,\bar{q}} e_q^2\, x \int_x^1 \frac{\mathrm{d}\xi}{\xi}\, q(\xi,\mu_f^2)\left\{\delta\,(1-\xi) + \frac{\alpha_s(\mu_f^2)}{2\pi}\,P\left(\frac{x}{\xi}\right)\ln\left(\frac{Q^2}{\mu_f^2}\right)\right\}. \end{aligned} \tag{3.6}$$

Now the integral in Eq. (3.6) is finite. Furthermore, we have to introduce the gluon contribution where gluons can split into quarks $g \to q\bar{q}$ (see Fig. 3.3). In a similar fashion to the analysis made above, the calculation of the gluon contribution may be computed, leading to an extra term in the quark distribution

$$\begin{aligned} q(x,\mu_f^2) = q_0(x) &+ \frac{\alpha_s}{2\pi}\int_x^1 \frac{\mathrm{d}\xi}{\xi}\, q_0(\xi)\left\{P_{qq}\left(\frac{x}{\xi}\right)\ln\left(\frac{\mu_f^2}{m^2}\right) + C_q\left(\frac{x}{\xi}\right)\right\} + \\ &+ \frac{\alpha_s}{2\pi}\int_x^1 \frac{\mathrm{d}\xi}{\xi} g_0(\xi)\left\{P_{qg}\left(\frac{x}{\xi}\right)\ln\left(\frac{\mu_f^2}{m^2}\right) + C_g\left(\frac{x}{\xi}\right)\right\}. \end{aligned} \tag{3.7}$$

Even though the calculation of PDFs which involve small distance effects where the strong coupling is large, is indeed beyond the scope of pQCD, their Q^2 evolution is calculable. They should therefore be extracted from experimental measurements of the structure functions in DIS, $F_2(x,Q^2) = \sum_{q,\bar{q}} e_q^2\, x\, q(x,Q^2)$. PDFs are universal (process independent) in the sense that once they are computed in a given process, they could be used in any other hard reaction. In practice, DIS experiments are commonly intended to measure the distribution functions (PDFs),

[5] The exact definition of the parton density and the non-singular piece depends on the renormalization and factorization schemes. For example, in the DIS scheme the C(z) contribution is absorbed into the renormalized parton density and we have $F_2(x,Q^2) = \sum_{q,\bar{q}} e_q^2\, x\, q(x,Q^2)$.

which are then performed to calculate cross sections for hadron-hadron collision experiments. A typical factorised physical cross section for a process initiated by two protons with momenta P_1 and P_2 takes the form [72, 73]

$$\sigma(P_1, P_2) = \sum_{ij} \int \mathrm{d}x_1 \, \mathrm{d}x_2 \, q_i(x_1, \mu_f) \, q_j(x_2, \mu_f) \, \hat{\sigma}(p_1, p_2, \alpha_s(\mu_f), Q/\mu_f) + \mathcal{O}(1/Q^p) \,, \tag{3.8}$$

where $p_i = x_i \, P_i$ is the momentum of parton i participating in the hard scattering, as schematically depicted in Fig. 3.1. The last term means that factorization is not an exact result, but it often stands up to corrections that behave as inverse powers of the hard scale Q, with p being a real number.

The μ_f^2 independence of any physical quantity implies that $F_2(x, Q^2)$ should satisfy the following renormalization group equation

$$\frac{\mathrm{d}F_2(x, Q^2)}{\mathrm{d}\ln \mu_f^2} = 0 \,, \tag{3.9}$$

allowing us to extract an evolution equation for the quark and gluon distributions, called the Dokshitzer-Gribov-Lipatov-Altarelli-Parisi (DGLAP) evolution equation [90–92]

$$\begin{aligned}
\frac{\mathrm{d}q(x, Q^2)}{\mathrm{d}\ln \mu_f^2} &= \frac{\alpha_s(\mu_f^2)}{2\pi} \int_x^1 \frac{\mathrm{d}\xi}{\xi} \left[q(\xi, \mu_f^2) \, P_{qq}\left(\frac{x}{\xi}\right) + g(\xi, \mu_f^2) \, P_{qg}\left(\frac{x}{\xi}\right) \right] , \\
\frac{\mathrm{d}g(x, Q^2)}{\mathrm{d}\ln \mu_f^2} &= \frac{\alpha_s(\mu_f^2)}{2\pi} \int_x^1 \frac{\mathrm{d}\xi}{\xi} \left[\sum_{q\bar{q}} q(\xi, \mu_f^2) \, P_{gq}\left(\frac{x}{\xi}\right) + g(\xi, \mu_f^2) \, P_{gg}\left(\frac{x}{\xi}\right) \right] .
\end{aligned} \tag{3.10}$$

The splitting function P_{ij} has an expansion in the running coupling of the form

$$P_{ij}(z, \alpha_s) = P_{ij}^0(z) + \frac{\alpha_s}{2\pi} P_{ij}^1(z) + \dots \,. \tag{3.11}$$

Examples of Feynman diagrams for the leading order (LO) splitting functions are shown in Fig. 3.3 and the LO splitting functions are given by

$$\begin{aligned}
P_{qq}^0(z) &= \mathrm{C_F} \left[\frac{1+z^2}{(1-z)_+} + \frac{3}{2}\delta(1-z) \right] , \\
P_{qg}^0(z) &= \mathrm{T_R} \left[z^2 + (1-z^2) \right] , \quad \mathrm{T_R} = \frac{1}{2} , \\
P_{gq}^0(z) &= \mathrm{C_F} \left[\frac{1+(1-z)^2}{z} \right] , \\
P_{gg}^0(z) &= 2\,\mathrm{C_A} \left[\frac{z}{(1-z)_+} + \frac{1-z}{z} + z(1-z) \right] + \delta(1-z) \, \frac{(11\,\mathrm{C_A} - 4\,n_f\,\mathrm{T_R})}{6} ,
\end{aligned} \tag{3.12}$$

where $\mathrm{C_A} = \mathrm{N_c}$, and n_f is the number of quark flavours. This equation can be solved numerically. Once the x dependence of the PDFs is known as an input at some low scale μ_0^2

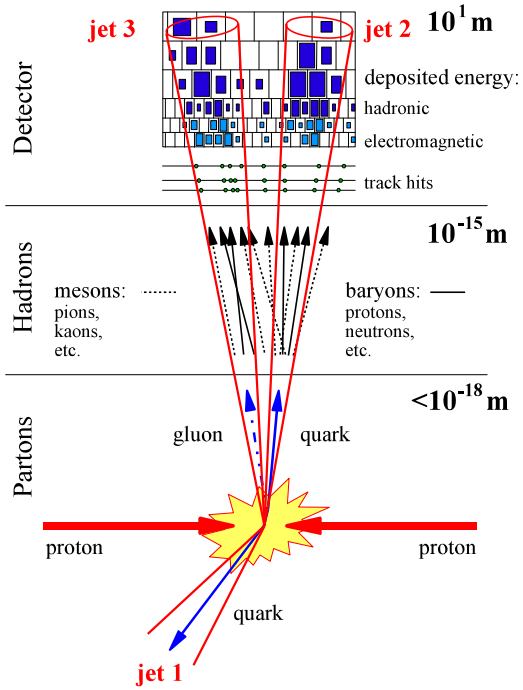

Figure 3.4: This diagram represents the steps involved in producing and measuring a jet. This figure is taken from Ref [130].

bellow which perturbation theory can not be applied, i.e., derived from experimental data and fitted to a simple functional form, then the x dependence at any other higher Q^2 values can be calculated using the DGLAP equation. The distribution functions' characteristic decrease at large x and increase at small x depicted in Fig. 3.2, are indeed quite well described by this equation.

3.2 Jet definitions and algorithms

As a first step towards understanding the long-distance hadrons detected in calorimeter cells in terms of short-distance physics, partons (see Fig. 3.4) and/or decaying massive particles (boosted), an accurate definition of the jet is necessary. To actually reconstruct a jet, various "jet definitions" have been introduced in the literature [45, 46]. A typical jet definition is composed of two essential elements: a *jet algorithm* which can be seen as a set of mathematical rules to combine objects which are, in some way close to one another, into jets. Moreover, a jet definition employs a *recombination scheme* which describes the way kinematic properties of the resulting jet are determined from its constituents. Many recombination schemes have been used, such as the winner-take-all (WTA), the massless p_t or E_t schemes. The widely used one, the *E-scheme* which works by adding the components of the four-vectors, will be performed in this work. The IRC safety and other characteristics that should be fulfilled in jet algorithms, were set out by the "Snowmass accord" [47]. Jet algorithms are broadly classified into two types: cone algorithms and sequential-recombination algorithms. Unlike sequential-

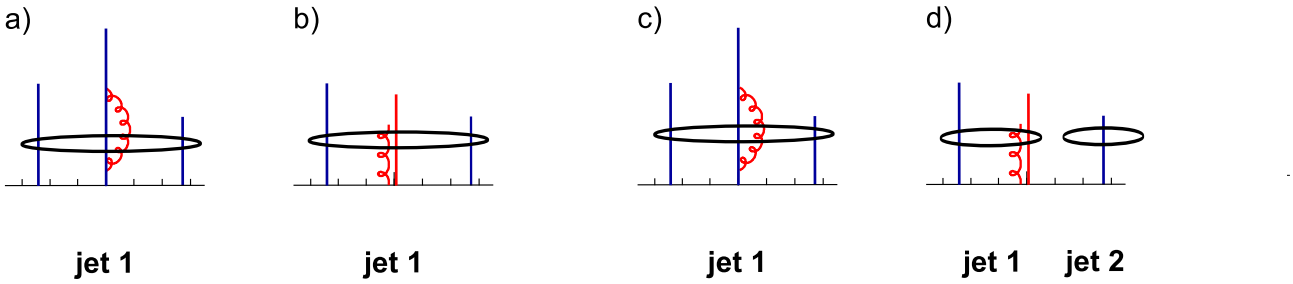

Figure 3.5: Figures (a), (b) illustrate collinear safe jet algorithms and figures (c), (d) illustrate collinear unsafe jet algorithms.

recombination algorithms which are all IRC safe, most of the cone algorithms which, are beyond the scope of this work, are not.

3.2.1 IRC safety of jet algorithms

In order to be able to compute jet cross sections and properties using pQCD, the definition of jets should be IRC safe. This property implicitly means that if the final state particles are modified by a soft emission or collinear splitting, the set of hard jets should remain unchanged. Once this property is fulfilled, in fixed-orer pQCD calculations, IRC singularities should cancel out when contributions from both virtual and real emission diagrams are added. Additionally, when the hard scale Q increases, some inverse power of Q suppresses non-perturbative phenomena, such as those caused by hadronization, which can be made small by sufficiently increasing Q. However, IRC unsafe jet algorithms, may change the number of final jets, and thus a jet definition will produce infinite results at some point in the perturbative expansion because of the lack of cancellation of infrared divergences. For instance, tree-level splittings may produce one set of jets, while loop diagrams may produce another, breaking the cancellation and leading to infinite cross-sections as illustrated in Fig. 3.5. Furthermore, a perturbative unsafe jet definition does not exhibit the power suppression of non-perturbative phenomena. Consequently, only perturbative safe definitions will be performed in this thesis

3.2.2 Sequential recombination algorithms

Sequential recombination algorithms (SR) typically determine the closest pair of particles based on some distance metric and merging them together to form new pseudo particles. The algorithm define two distance metrics, the former determines when particles are combined and the latter decides when jets are constructed. This continues iteratively until the well separated pseudo particles, which are the output jets, are formed. There is no unique SR algorithm and various definitions of closeness in phase-space define different algorithms with different strengths and weaknesses.

Generalised kt algorithm for pp collisions

Currently, the following algorithm is the most frequently used in studies including jets at the LHC [120]. In order to examine its role in clustering jets, let us first provide a remainder that explains how it works:

1. Set the particles in the event as our starting list of objects.

2. For each pair of objects (i, j), one computes the inter-particle distances (the first distance metric) in the rapidity-azimuth plane, defined by

$$d_{ij} = \min\left(k_{ti}^{2p}, k_{tj}^{2p}\right) \frac{\Delta_{ij}^2}{R^2}, \tag{3.13}$$

   where p is a free parameter that parameterises the type of the algorithm, k_{ti} is the transverse momentum of particle i, R is the jet-radius and Δ_{ij}^2 is given by

$$\Delta_{ij}^2 = \left[(\eta_i - \eta_j)^2 + (\phi_i - \phi_j)^2\right] .$$

   The distance to the beam (the second distance metric) is defined by

$$d_i = k_{ti}^{2p} . \tag{3.14}$$

3. Then iteratively search for the minimum $d_{\min}$ of all distances d_{ij} and d_i.

   (a) If $d_{\min} = d_{ij}$, then particle i is clustered into its nearest neighbour j, producing a single protojet using a recombination scheme, and add (remove) the protojet (objects i and j) to (from) the current list of objects.

   (b) If $d_{\min} = d_i$, particle i is classified as a jet and excluded from the further clustering.

   Return back to step 2 until the final state is entirely composed of jets.

According to the value of p, SR algorithms may be divided into three broad classes:

- *k_t algorithm* [120]: corresponds to $p = 1$ in Eq. (3.13). It clusters soft and collinear particles first, and consequently tends to construct jets more sensitive to extra soft radiation in the event, such as the UE or PU.

- *Cambridge/Aachen (C/A) algorithm* [48]: corresponds to $p = 0$ in Eq. (3.13). It is energy-independent and clusters particles based only on their angular separation. Thus it is less sensitive to soft radiation than k_t algorithm.

- *Anti-k_t algorithm* [121]: corresponds to $p = -1$ in Eq. (3.13). It combines the hardest particles first, giving circular hard jets unsensitive to soft radiation, making it an appealing

alternative to certain cone-type algorithms. As a result, the anti-k_t algorithm is the widely used one at the LHC.

It is worth mentioning that to leading order, perturbative computations of jet shapes distributions such as the azimuthal deccorelation between jets are identical between all three SR algorithms.

Generalised kt algorithm for e^+e^- collisions

In this work we adopt the generalised k_t or anti-kt algorithms, suited for e^+e^- annihilation, where the algorithms works with the distances

$$d_{ij} = \min\left(E_i^{2p}, E_j^{2p}\right) \frac{\left(1-\cos\theta_{ij}\right)}{\left(1-\cos R\right)}\,, \tag{3.15}$$

$$d_{ij} = E_i^{2p}\,, \tag{3.16}$$

where E_i is the energy of the i^{th} emission, and θ_{ij} is the angle between k_i and k_j such that $\cos\theta_{ij} = \cos\theta_i\cos\theta_j + \sin\theta_i\sin\theta_j\cos(\phi_i - \phi_j)$.

3.3 Jet shape distributions

Event shapes, like sphericity and thrust [30,31] provide quantitative statements about data. For instance, the value of the transverse sphericity gives an idea on whether an event is pencil-like, planar, spherical, or anything in between, where each of these topologies yields a different value for the event shape.[6] Jet shapes, formed by taking a weighted sum over the four-momenta, transverse momenta, energies, etc of all particles comprising the jet, are event-shape-like observables defined using clusters of jets instead of individual hadrons. They confine soft-gluon radiation within jets, where QCD jets exhibit different radiation patterns from those of highly-boosted heavy particle decay products. They are anticipated to be larger for QCD jets than for an electro-weak boson jet decays. Likewise, gluon-initiated jets that are characterised by high radiation activity (due to the large color charge of gluons), are expected to radiate more soft gluons than quark-initiated jets.

Now we consider the dijet azimuthal deccorelation as an example of a jet shape distribution, which will be discussed with more detail in the next chapter. We study the integrated azimuthal deccorelation distribution (cross section) normalised to the born crosse section (σ_0) given by the general expression

$$\Sigma(\Delta) = \frac{1}{\sigma_0}\int_0^{\Delta}\frac{\mathrm{d}\sigma}{\mathrm{d}\Delta'}\,\mathrm{d}\Delta'\,. \tag{3.17}$$

[6] Sphere-like events are often connected to multi-jet structures, while pencil-like events are typically connected to events with two collimated back-to-back jets (di-jet structure).

The perturbative expansion of the shape distribution (3.17) in terms of the coupling α_s may be cast in the form

$$\Sigma(\Delta) = 1 + \Sigma_1(\Delta) + \Sigma_2(\Delta) + \Sigma_3(\Delta) + ... \tag{3.18}$$

3.3.1 The one-loop calculation

We start by considering the contribution of a real soft emission k to the shape distribution (3.17). The integral to be considered related to the probability for the azimuthal deccorelation to be less than a given value Δ, is then

$$\Sigma_1^r(\Delta) = \int \mathrm{d}\Phi_1 \, |\mathcal{M}_1|^2 \, \Theta\left(\Delta - \frac{2k_t}{\sqrt{s}}\right) \, \Theta_{\mathrm{out}}(k) \,, \tag{3.19}$$

where the superscript r denotes the real emission case and $\mathrm{d}\Phi_1$ is the one gluon phase space. The constraint $\Theta_{\mathrm{out}}(k) = \Theta\left(\cos R - |c|\right)$ ensures that gluon 1 is emitted outside both jets. To find the total correction we now have to consider virtual emissions whose matrix element has exactly the same form as that in the real emission case with an overall minus sign, as discussed in Appendix A, but no constraint is present. Thus putting together real and virtual contributions, the first order correction reads

$$\Sigma_1(\Delta) = \int \mathrm{d}\Phi_1 \, |\mathcal{M}_1|^2 \, \Theta\left[(\Delta - \frac{2k_t}{\sqrt{s}}) - 1\right] \, \Theta_{\mathrm{out}}(k) \,. \tag{3.20}$$

The -1 term stands for the virtual correction that completely cancel the real emissions which contribute only in the region $(\Delta > 2k_t/\sqrt{s})$, while the total correction is fully determined by the virtual contributions with $(2k_t/\sqrt{s} > \Delta)$ which are not vetoed

$$\Sigma_1(\Delta) = -\int \mathrm{d}\Phi_1 \, |\mathcal{M}_1|^2 \, \Theta\left(\frac{2k_t}{\sqrt{s}} - \Delta\right) \, \Theta_{\mathrm{out}}(k) \,. \tag{3.21}$$

Notice that the detailed evaluation of the phase space integrals both at one and two-loops will be postponed to Chapter 4.

3.3.2 Non-global logarithms

Having established that the observable at hand is non-global i.e., sensitive to emissions in a limited region of the phase-space (outside both jets). Consequently, in addition to the inclusion of the non-global component, the analysis of the resummed result at LL accuracy, [7] implies also taking into account the impact of the k_t clustering algorithm on the resummation.

[7] For the dijet azimuthal deccorelation, collinear singularities do not contribute (double logarithms are absent) and all leading terms arising from large angle soft emission i.e., single logarithms are leading logs (LL).

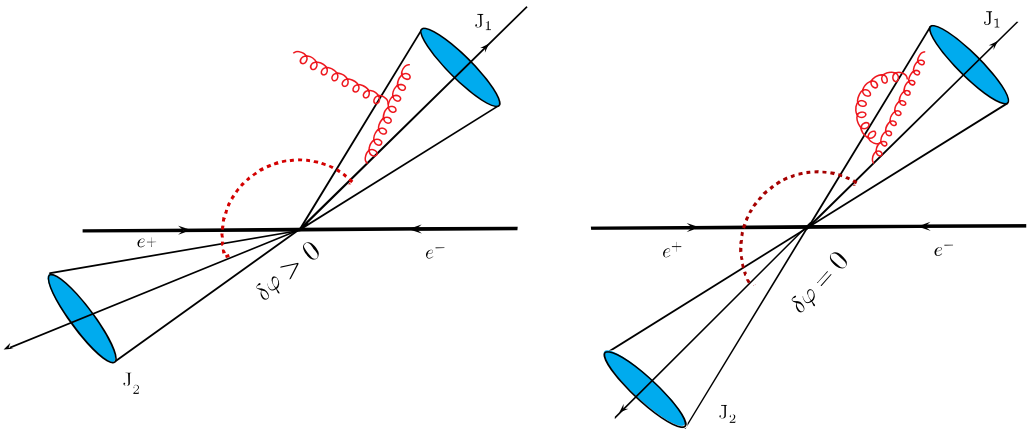

Figure 3.6: A schematic representation showing gluon configurations (correlated emissions) that produce non-global logs at leading-order in dijet events at fixed-order $\mathcal{O}(\alpha_s^2)$.

NGLs with anti-k_t calculation

Besides to the single Sudakov logarithms associated with primary soft wide angle emissions, our specific dijet azimuthal decorrelation example starts receiving a new set of large single logarithms of the type $(\alpha_s \ln 1/\Delta)^n$. These large logarithms are known as non-global logarithms (NGLs), which by definition start appearing at $\mathcal{O}(\alpha_s^2)$ in the perturbative expansion. The said new contributions are essentially associated with energy ordered large angle secondary branching (correlated) soft gluon emissions originating from the complementary region of phase space i.e., inside jet regions, as illustrated in Fig. 3.6. To obtain the structure of NGLs, we now carry out an explicit two gluons calculation k_1 and k_2, considering the eikonal approximation, i.e., strong energy ordering ($k_{t1} \gg k_{t2}$). In the said approximation we shall only focus on the irreducible term of the factorised two-loops amplitude squared for the emission of two real gluons off the initiating hard $q\bar{q}$ pair, which is given by

$$\overline{\mathcal{W}}_{12}^{RR} = 2\mathrm{C_F}\,\mathrm{C_A}\,\mathcal{A}_{ab}^{12}\,, \tag{3.22}$$

with

$$\mathcal{A}_{ab}^{12} = \omega_{ab}^{1}\left(\omega_{a1}^{2} + \omega_{1b}^{2} - \omega_{ab}^{2}\right)\,. \tag{3.23}$$

The latter term which accounts for correlated emissions $\propto \mathrm{C_F C_A}$, missed by the single gluon exponentiation that we will discuss later, will generate NGLs we aim to study and resum. The NGLs are completely produced by the soft emission k_2 emitted outside both jets that is coherently radiated by the soft, but harder emission k_1 emitted inside the jet. While the real gluon k_2 produces small deviation of the recoil azimuthal angle from zero, its corresponding virtual correction does not (see Fig. 3.6). This causes real-virtual mis-cancellation in the jet-shape fraction and thus ultimately leading to NGLs.

NGLs with k_t

We now highlight the fact that the use of the k_t clustering algorithm has proved useful in reducing the NGLs involved in the integrated distribution due to the soft clustering inherent in such algorithm. When the real soft gluon emitted outside both jets from the harder one that is emitted inside the jet is closest to its parent emitter in rapidity and azimuth, it gets clustered back to the jet. This case entirely cancels against virtual corrections and therefore makes no contribution to NGLs. By employing this clustering procedure, NGLs significantly diminish because their dominant contribution is only when the two gluons are unaffected by the clustering. As a result, a real-virtual mismatch occurs, and NGLs are produced.

3.3.3 CLustering logarithms

While the use of the k_t clustering algorithm can significantly reduce the non-global logarithm component, we shall now argue that it gives rise to yet another type of large single logarithms in the independent emission part. We refer to these large logs "clustering logs" (CLs) that first appear at two-loops $\mathcal{O}(\alpha_s^2)$ from the regions which are cancelled in the ant-k_t case. For a resummation aiming at LL accuracy in the azimuthal deccorolation, such miscancelling contributions must thus be investigated. While the leading double-logarithms which are absent for the observable at hand, remain exactly unchanged as for the anti-k_t case, at single logarithmic accuracy, soft gluon clustering modifies the global term which distinguishes from a single gluon's naive exponentiation. There are four distinct diagrams contributing to the independent emission of two soft gluons in the energy ordered regime $k_{t1} \gg k_{t2}$. These diagrams which are illustrated in Fig. 3.7, all share the same contribution to the squared matrix element for ordered two-gluon emission, up to a sign. One can write the contributions for both double real (1) and double virtual (4) diagrams as follows

$$\mathcal{W}(k_1, k_2) = 4\,{\mathrm{C_F}}^2\, g_s^4\, \omega_{ab}^1\, \omega_{ab}^2\,. \tag{3.24}$$

The one-real one-virtual terms (2) and (3) in Fig. 3.7 both hold the same result as well, with opposite sign. In this picture, we can have four different regions based on the position of the gluons k_1 and k_2: k_1, k_2 outside the jet, k_1, k_2 inside the jet or either of the gluons inside and the other outside the jet. The distance measures to consider are : $d_{12}, d_{2j}, d_{1j}, d_2, d_1$. The smallest of these distances will always be those containing particle 2 because they have k_{t2}^2. Since we always consider particle 2 to be outside the jet then $d_2 < d_{2j}$, and hence d_{2j} becomes irrelevant and we do not compare with it. The aforementioned regions all yield the same results as the anti-k_t algorithm, except the case when the hardest gluon k_1 is inside the jet ($d_{1j} < d_1$) and the softest gluon k_2 is outside both jets ($d_{2j} > d_2$), will give a non zero contribution. We first start with diagram (3), where k_1 is virtual, and thus cannot pull k_2 inside the jet. This diagram

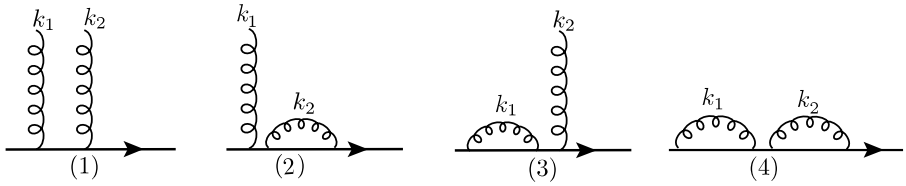

Figure 3.7: Feynman diagrams that give rise to independent two-gluon emission from a hard parton line.

will be vetoed (since real emissions with $\delta\phi > \Delta$ are not permitted), and consequently have no contribution to the azimuthal deccorolation distribution. Then we consider diagrams (2) and (4), where both of them will contribute but with a relative minus sign ($\delta\phi < \Delta$ is always fulfilled for virtual contributions), and thus cancel each others, living only diagram (1). When $d_{12} < d_2$, the real gluon k_1 gets cluster k_2 back to the jet and so diagram (1) will contribute to the azimuthal deccorolation as a virtual diagram with a plus sign, making large CLs take place.

3.3.4 Resummation

IRC safe QCD observables are defined to be unaffected by the emission of soft momenta and by the splitting of a final state momentum into collinear momenta [41, 62].[8] Once this property is fulfilled, event/jet shapes distributions can be systematically computed in PT. The fixed order description expands the experimentally measured event/jet shape distribution (y) of high p_t QCD jets in powers of the strong coupling α_s into leading order (LO), next to leading order (NLO), next to next to leading order (NNLO), and so on. These power series are in fact assumed to be finite order by order in PT. However, the soft and collinear region in phase space results in infrared divergences in QCD matrix elements. By adding real and virtual contributions, these divergences are cancelled for IRC safe observables. This is strictly true and the fixed order calculation is reliable and convergent only far away from the two-jet region, say, in regions of phase space where radiation of hard and large angle gluons dominates and the event/jet shape rather have large values ($y \sim 1$). Fixed-order calculations are usually carried out with the help of Fixed-order Monte Carlos (FOMCs) such as EVENT2 [42], and EERAD3 [43], for e^+e^- annihilation. While the typical accuracy of EVENT2 is next-to-leading order (NLO), it reaches next-to-next-to-leading order (NNLO) with EERAD3.

On the other hand, in the exclusive boundary of phase space, say, in regions of small y ($y \ll 1$) with any additional partons being soft and/or collinear to the original event partons, the events resemble the born event and are dominated by the two-jet configurations. It turns out that they even satisfy the Sterman Weinberg criteria but nevertheless the perturbative expansion can be divergent order by order in PT. This divergence follows primarily from the

[8] Infrared and collinear safety has long been used as key criteria by Sterman Weinberg to determine which observables can be calculated with pQCD.

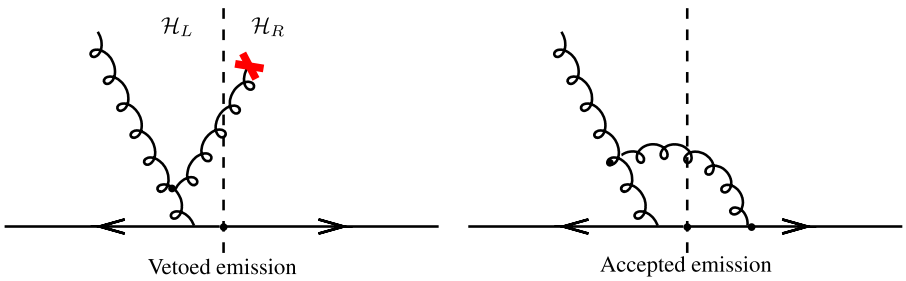

Figure 3.8: Left: vetoed emission. Right: accepted emission.

miscancellation of infrared and/or collinear singularities at the matrix-element level. This is due to the fact that the suppression of real emissions (vetoed) without any corresponding restriction on virtual ones producing the loss of balance between theme (see Fig. 3.8). The said mismatch between real and virtual emissions which results in the manifestation of large logarithmic corrections in ratios of the energy scales present in the process involving jet p_t, jet radius R, and the measured value of the jet shape, spoil the convergence of the perturbative expansion in α_s. So to restore this convergence, it is necessary to resort to the summation of these large logarithms to all orders in α_s. Such a task which is a completely satisfactory solution within the context of PT is what one refers to as "*resummation*". In general for global observables, one can show that these large logarithms exponentiate, which allows one to write the normalised integrated cross-section for the event/jet shape to be smaller than some value y as follows:

$$\Sigma(y) = C(\alpha_s) \exp\left[Lg_1(\alpha_s L) + g_2(\alpha_s L) + \alpha_s g_3(\alpha_s L) + ...\right] + D(\alpha_s, y)\,, \tag{3.25}$$

with $L = \ln(1/y)$, $C(\alpha_s)$ sums the loop constants and the remainder function $D(\alpha_s, y)$ vanishes in the limit $y \to 0$. The function $g_1(\alpha_s L)$ resums leading logarithms (double logarithms (LL)), $\alpha_s^n L^{n+1}$, $g_2(\alpha_s L)$ resums next-to-leading logarithms (single logarithms (NLL)), $\alpha_s^n L^n$, $g_3(\alpha_s L)$ resums next-to-next-to-leading logarithms (NNLL), $\alpha_s^n L^{n-1}$, and so on. This exponentiation originates essentially from the factorisation property fulfilled for global observables both for the n-particle QCD matrix elements (in the eikonal limit) as well as for the phase space that may be divided into hard and soft pieces after employing an integral transform conjugate to the kinematical variable y [62]. The all-orders perturbative expansion of $\Sigma(y)$ may be cast in the form

$$\Sigma(y) = 1 + \sum_{n=1} \left(\frac{\alpha_s}{2\pi}\right)^n \left(\sum_{m=0}^{2n} R_{nm} L^m + \mathcal{O}(y)\right). \tag{3.26}$$

One convention is to refer to all terms $\alpha_s^n L^{2n}$,[9] as leading logarithms (LL), terms $\alpha_s^n L^{2n-1}$, as next-to-leading logarithms (NLL), terms $\alpha_s^n L^{2n-2}$, as next-to-next-to-leading logarithms (NNLL), etc.

[9]Note that the accuracy of the resummation in the exponent is distinct from that in the expansion.

Global Resummation

To calculate the resummed distribution of primary global logarithms, we first consider the factorisation of the real emission contribution to the integrated shape distribution. The integral to be considered related to the probability for events with $|\pi - \Delta\phi|$ to be less than a given value Δ, may be written explicitly to all orders in the following factorised form

$$\Sigma^r(\Delta) = \sum_{n=0}^{\infty} \frac{1}{n!} \prod_{i=1}^{n} \int \frac{\mathrm{d}k_{ti}}{k_{ti}} \frac{\mathrm{d}\cos\theta_i}{\sin^2\theta_i} \frac{\mathrm{d}\phi_i}{2\pi} \frac{\alpha_s(k_{ti})}{\pi} 2\mathrm{C_F}\, \omega^i_{ab} \Theta\left(\Delta - \sum_{i\notin jets} \frac{2k_{t,i}}{Q} |\sin\phi_i|\right) , \quad (3.27)$$

where the superscript r denotes the real emission case. The symmetry factor which allows for the permutation of n identical gluons does drop off when a specific ordering of the partons transverse momenta (e.g., $k_{tn} \ll \cdots \ll k_{t2} \ll k_{t1} \ll Q$) is assumed. Notice that the coupling being runing at a renormalisation scale k_{ti} for the i^{th} emission. What remains is the factorization of the shape fraction step function which is only feasible in a conjugate space using the following transformation

$$\Theta\left(\Delta - \sum_{i\notin jets} \frac{2k_{t,i}}{\sqrt{s}} |\sin\phi_i|\right) = \frac{1}{\pi} \int_{-\infty}^{+\infty} \frac{\mathrm{d}b}{b} \sin(b\,\Delta) \prod_{i\notin jets}^{n} \exp\left(ib \frac{2k_{t,i}}{\sqrt{s}} |\sin\phi_i|\right) , \quad (3.28)$$

where b is the conjugate of Δ. To figure out the total correction, we must now account for virtual emissions whose matrix element corresponds exactly to that in the real emission case with an overall minus sign. The resummed result is given by

$$\Sigma(\Delta) = \frac{1}{\pi} \int_{-\infty}^{+\infty} \frac{\mathrm{d}b}{b} \sin(b\,\Delta) \exp\left(-\Sigma_1(b)\right) , \quad (3.29)$$

where

$$\Sigma_1(b) = -\,2\mathrm{C_F} \int \frac{\mathrm{d}k_t}{k_t} \frac{\mathrm{d}\phi}{2\pi} \frac{\alpha_s(k_t)}{2\pi} \frac{\mathrm{d}\cos\theta}{\sin^2\theta} \omega^1_{ab} \left[\exp\left(i\,b\,\frac{2k_t}{\sqrt{s}}\,|\sin\phi|\right) - 1\right] . \quad (3.30)$$

The -1 term stands for the virtual correction. Taking account of secondary gluon branching the running coupling should be evaluated in the Catani-Marchesini-Webber (CMW) scheme often considered

$$\alpha_s = \alpha_s^{\overline{MS}} \left(1 + \frac{\alpha_s^{\overline{MS}}}{2\pi} K\right) , \quad (3.31)$$

with

$$K = \mathrm{C_A}\left(\frac{67}{18} - \frac{\pi^2}{6}\right) - \frac{5}{9}\, n_f\,. \quad (3.32)$$

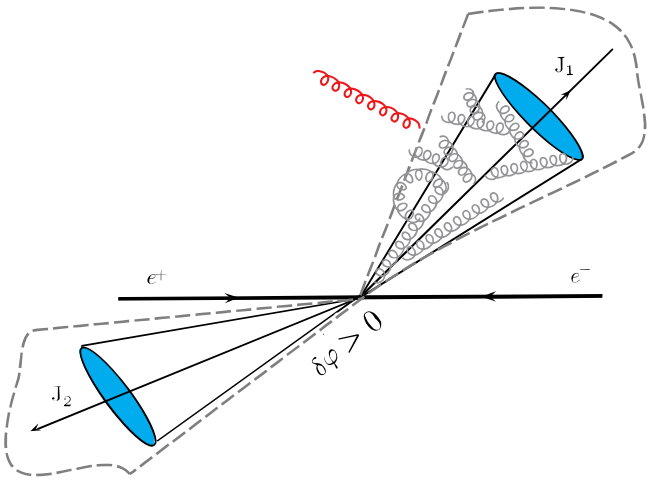

Figure 3.9: A set of energy-ordered soft and collinear gluons emitted inside jet regions with complex geometrical structure will coherently emit a single softest gluon outside both jets. Such configurations give rise to non-global logs at higher orders.

To compute the above resummed exponent to NLL accuracy we are considering, we can make the following substitution

$$\exp\left(i\,b\,\frac{2k_t}{\sqrt{s}}\,|\sin\phi|\right)-1\to-\Theta\left(k_t-\frac{\sqrt{s}}{2\bar{b}}\right)\,, \tag{3.33}$$

where $\bar{b}=\gamma_E\,b$ with $\gamma_E=0.577$ being the Euler-Mascheroni constant. Thus we arrive at the following result

$$\Sigma_1(\bar{b})=\,2\mathrm{C_F}\int\frac{\mathrm{d}k_t}{k_t}\,\frac{\mathrm{d}\phi}{2\pi}\,\frac{\alpha_s(k_t)}{2\pi}\,\frac{\mathrm{d}\cos\theta}{\sin^2\theta}\,\omega^1_{ab}\,\Theta\left(k_t-\frac{\sqrt{s}}{2\bar{b}}\right)\,. \tag{3.34}$$

The evolution parameter t is given by

$$t(\bar{b})\equiv\int^{\sqrt{s}/2}\frac{\alpha_s(k_t)}{\pi}\,\frac{\mathrm{d}k_t}{k_t}\,\Theta\left(k_t-\frac{\sqrt{s}}{2\bar{b}}\right)=-\frac{1}{2\pi\beta_0}\ln(1-2\lambda_{\bar{b}})\,, \tag{3.35}$$

with $\lambda_{\bar{b}}=\alpha_s\beta_0\ln\bar{b}$. The global resummed shape distribution in the b space is merely the exponentiation of the single parton emission shape fraction. After resummation is achieved, in order to perform the b integral in Eq. (3.29), we use the saddle point method. It may be shown that the saddle point in the b integral to SL accuracy is simply given by $1/\Delta$. The global resummed shape distribution in the Δ space is

$$\Sigma_{\mathrm{global}}(\Delta)=\exp\left[\Sigma_1(\Delta)\right]\,. \tag{3.36}$$

LL and NLL resummation

For the observable at hand, azimuthal deccorelation, which is non-global, the all order calculation described above is not sufficient to achieve full LL accuracy. In order to do so, non global contributions must be resummed to all orders and we must consider configurations of many soft gluons. At the n^{th} order of this configuration, a complex geometrical structure can be produced with the $(n-1)$ soft and collinear energy-ordered particles emitted inside the jet, that will coherently emit a single softest gluon outside both jets as shown in Fig. 3.9. While the resummation of the aforementioned primary global logs to all orders is feasible and relatively straightforward, this complicated geometry makes the analytical resummation of NGLs to all orders highly cumbersome. Moreover, the color algebra is complicated because of color correlations. NGLs were first analyzed using the large $\mathrm{N_c}$ limit whereby the color correlations become trivial. Furthermore, Monte Carlo (MC) provides an easy way to handle the complicated geometry numerically either using a dipole evolution code [52] or resorting to the BMS equation [95]. A key point to notice is that the resummation of NGLs is expressed as a factor $\mathcal{S}(t)$ multiplying the single gluon Sudakov form factor

$$\Sigma(\Delta) = \exp\left[\Sigma_1(\Delta)\right]\, \mathcal{S}(t)\,. \tag{3.37}$$

A widely used parametrisation of $\mathcal{S}(t)$ is given in [52]

$$\mathcal{S}(t) = \exp\left[-\frac{{\mathrm{C_A}}^2}{2}\,\mathcal{S}_2(R)\,\left(\frac{1+(at)^2}{1+(bt)^c}\right)t^2\right]\,, \tag{3.38}$$

where $\mathcal{S}_2$ is the NGLs coefficient at $\mathcal{O}(\alpha_s^2)$ and the parameters a, b and c are determined from fitting Eq. (3.38) to the output of the MC program of [52].

The resummed distribution, which imposes k_t clustering on the final state, can be written in the factorised form shown below

$$\Sigma(\Delta) = \exp\left[\Sigma_1(\Delta)\right]\, \mathcal{S}(t)\,\mathcal{C}^p(t)\,, \tag{3.39}$$

where $\mathcal{C}^p(t)$ is the CLs resummed form factor, and the all-orders result is currently only available via the MC code of [52].

In order to achieve full NLL accuracy in the large $\mathrm{N_c}$ limit with anti-k_t clustering, we have used the recently-published program `Gnole` [126, 127]. The following chapters provide a comprehensive discussion of this issue of resummation including CLs and/or NGLs.

Chapter 4

Dijet azimuthal decorrelation in e^+e^- annihilation

4.1 Introduction

The production of jets in e^+e^- collisions is a simple and clean environment, yet rich of physics, to test QCD and the Standard Model. It will be used in future colliders such as the ILC and FCC-ee in order to make precise measurements of QCD-related quantities, which together with detailed theoretical calculations will pave the way towards potential discovery of new-physics phenomena.

At lowest order two correlated jets are produced back-to-back with a relative azimuthal angle equal to π. At higher orders the jets manifest a decorrelation of azimuthal angle $\delta\phi$ which is enhanced near the back-to-back limit. The quantity $\delta\phi$, being sensitive to soft/collinear QCD effects, is of great interest in the phenomenology of perturbative and non-perturbative QCD dynamics. For instance it has been used to study unintegrated parton distribution functions in deep-inelastic $e-p$ scattering (DIS) [107] and small-x BFKL effects [108], as well as measurements of the QCD coupling at various scales [109]. Many studies have been devoted to the distribution of $\delta\phi$ in various processes, such as dijet production in $p-p$ [110–112] (and even $p-pb$ [113]) collisions and DIS [108, 114]. Experimentally, boson-jet (in pp collisions) [115] and lepton-jet or photon-jet (in DIS) [116, 117] decorrelations have been measured.

Near the back-to-back limit, the distribution of the azimuthal decorrelation is characterized by large logarithms preventing the convergence of the perturbative series, and thus need to be resummed to all orders. Depending on the nature of the algorithm being used to define the jets, the leading logarithms in this distribution can be double or single logarithms. For instance, in p_t-weighted recombination scheme of the k_t [118–120], anti-k_t [121] and Cambridge/Aachen algorithms [122, 123], the leading logarithms are double, $\alpha_s^n L^{2n}$, while in E-scheme recombination they are single, $\alpha_s^n L^n$, with $L = \ln(1/\delta\phi)$. In the former scheme, the jets recoil against emissions

everywhere in the phase space, and in particular soft *and* collinear emissions to these jets, which leads to the double logarithms in $\delta\phi$. On the other hand, in the latter (E-scheme), the jets recoil only against emissions that do not get clustered to them, and hence only away-from-jets emissions contribute to $\delta\phi$, resulting in leading soft wide-angle single logarithmic contributions.

In addition to this, the classification of the $\delta\phi$ observable, in E-scheme definition, falls in the "non-global" category, and as a consequence its distribution receives contributions from single non-global (NGLs) [52, 94] and/or clustering (CLs) [49, 50] logarithms. The resummation of these logarithms is not straightforward, and is usually performed numerically via Monte Carlo (MC) programs in the planar (large-N_c) limit.

In this chapter, we are interested in the calculation of NGLs and/or CLs for the $\delta\phi$ distribution both in the k_t and anti-k_t algorithms. We compute the coefficients of these logarithms as a function of the jet radius R up to $\mathcal{O}(\alpha_s^3)$, and at $\mathcal{O}(\alpha_s^4)$ in the anti-k_t algorithm at small R. We use the fixed-order MC program `EVENT2` [124, 125] in order to compare the leading singular behavior of the $\delta\phi$ distribution with our results at $\mathcal{O}(\alpha_s)$ and $\mathcal{O}(\alpha_s^2)$. We also compute the resummed NGLs and CLs at all orders in the large-N_c limit using the MC code of refs. [52, 94] as well as the recently-published program `Gnole` [126, 127] (in the anti-k_t algorithm). The latter program is also used to compute the resummed differential $\delta\phi$ distribution at next-to-leading logarithmic (NLL) accuracy, in which we additionally control all the sub-leading logarithms $\alpha_s^{n+1}L^n$ in the exponent of the resummation, and quantify the corresponding scale uncertainties.

This chapter is organized as follows. In the next section we compute at $\mathcal{O}(\alpha_s)$ the leading-order distribution focusing on the logarithmic contribution, and compare with fixed-order MC programs at this order. In section 3, we present the calculation of NGLs and CLs at $\mathcal{O}(\alpha_s^2)$ and show plots of the coefficients of these logarithms as a function of the jet radius and comment on the relative size of these coefficients. We also compare at this order the calculated $\delta\phi$ distribution with the output of the program `EVENT2`, thus confirming our results. In section 4 we extend the calculation to $\mathcal{O}(\alpha_s^3)$ and (in the anti-k_t algorithm and at small R) $\mathcal{O}(\alpha_s^4)$, and point out the significantly different color structure of NGLs in k_t clustering. In section 5 we present the all-orders resummation of the NGLs and/or CLs in the large-N_c limit up to LL accuracy for the k_t algorithm, and NLL accuracy in the anti-k_t clustering. Finally we draw our conclusions in section 6.

4.2 One-loop calculation and the global form factor

In this chapter we consider the process of dijet production in e^+e^- annihilation at centre-of-mass energy $\sqrt{s}$. The jets are reconstructed with the k_t [120] or anti-k_t [121] algorithms, suited

for e^+e^- annihilation, with merging and stopping distances d_{ij} and d_i defined by

$$d_{ij} = \min\left(E_i^{2p}, E_j^{2p}\right) \frac{1-\cos\theta_{ij}}{1-\cos R}\,, \qquad d_i = E_i^{2p}\,, \tag{4.1}$$

where $p = +1$ for the k_t algorithm and $p = -1$ for the anti-k_t algorithm. Here R is the jet radius, E_i is the energy of the i^{th} parton in the final state, and θ_{ij} is the opening angle between partons i and j. The algorithm sequentially merges objects i and j whenever d_{ij} is the smallest of all merging and stopping distances, and if an object i has its stopping distance as the smallest then it gets admitted to the list of final inclusive jets. The algorithm keeps recursing until all partons are clustered into jets. In this work, we assume the jet kinematics to be defined with E-scheme recombination, such that the 4-momentum of a merged object simply equals the vectorial sum of the momenta of its constituents.

At the Born level, the two jets are produced back-to-back, and their relative azimuthal angle (with respect to the beam axis) is exactly π. The observable we are interested in is the deviation from π of this relative azimuthal angle, $\delta\phi$, when soft gluons are emitted at higher orders. It is straightforward to obtain the following expression for $\delta\phi$ in terms of the transverse momenta of the emitted gluons κ_{ti} and their azimuthal angles φ_i, with respect to the *beam* axis

$$\delta\phi = \left|\sum_{i\notin\text{jets}} \frac{\kappa_{ti}}{p_t}\sin\varphi_i\right|, \tag{4.2}$$

where p_t is the jet transverse momentum. The (algebraic) sum is over all emitted gluons that are not clustered to any of the two measured (leading) jets. This definition is valid only at single leading logarithmic (LL) accuracy, and we shall give the proper definition, valid at NLL accuracy, in section 5. Furthermore, the expression of $\delta\phi$ in eq. (4.2) only applies in E-scheme recombination. Alternative jet recombination schemes exist for which the jet kinematics take a different form, e.g. the p_t-weighted scheme, and the resummation takes an entirely different structure [114].

At one loop the cumulative cross-section for events with azimuthal decorrelation $\delta\varphi$ less than some Δ, normalized to the Born cross-section, reads

$$\Sigma_1(\Delta) = -2\,\mathrm{C_F}\int \frac{\alpha_s(k_t)}{\pi}\,\frac{\mathrm{d}k_t}{k_t}\,\frac{\mathrm{d}\cos\theta}{\sin^2\theta}\,\frac{\mathrm{d}\phi}{2\pi}\,\omega^k_{q\bar{q}}\,\Theta_{\text{out}}(k)\,\Theta\left(\kappa_t|\sin\varphi|/p_t-\Delta\right), \tag{4.3}$$

where θ, ϕ and k_t are the polar angle, azimuthal angle and transverse momentum of the emitted soft gluon k, with respect to the *jet* (thrust) axis (the back-to-back outgoing jets are aligned along the z axis), $\mathrm{C_F}$ is the color factor associated with the emission of the gluon off the hard $q\bar{q}$ dipole, and α_s is the strong coupling with argument k_t. The invariant antenna function $\omega^k_{q\bar{q}}$

is given by

$$\omega_{q\bar{q}}^{k} = \frac{k_t^2}{2}\,\frac{p_q \cdot p_{\bar{q}}}{(p_q \cdot k)(p_{\bar{q}} \cdot k)} = 1\,, \tag{4.4}$$

with p_i denoting the momentum of particle i

$$p_q = \frac{\sqrt{s}}{2}(1,0,0,1)\,, \tag{4.5a}$$

$$p_{\bar{q}} = \frac{\sqrt{s}}{2}(1,0,0,-1)\,, \tag{4.5b}$$

$$k = E\,(1, \cos\phi \sin\theta, \sin\phi \sin\theta, \cos\theta)\,, \tag{4.5c}$$

where $k_t = E \sin\theta$. The constraint $\Theta_{\text{out}}(k)$ restricts the emitted gluon to be outside the jets and forbids it from being clustered to any of them in order to induce a non-zero azimuthal decorrelation. It depends on the jet radius R and is given, in the generalized algorithm, by

$$\Theta_{\text{out}}(k) = \Theta\left(\cos R - |\cos\theta|\right). \tag{4.6}$$

Since the soft emission is restricted to be outside both jets then there are no collinear logarithms associated with this observable. This means that the leading logarithms are single, which allows us at LL accuracy to simply change $\Theta(\kappa_t|\sin\varphi|/p_t - \Delta) \to \Theta(2\,k_t/\sqrt{s} - \Delta)$, since any factor multiplying k_t will only induce sub-leading logarithms. [1] We can then perform the integration over k_t using the one-loop running of the coupling (which formally enters the distribution at higher orders), and write the result in terms of the evolution parameter t defined by

$$t(\Delta) \equiv \int^{\sqrt{s}/2} \frac{\alpha_s(k_t)}{\pi}\,\frac{\mathrm{d}k_t}{k_t}\,\Theta\left(2\,k_t/\sqrt{s} - \Delta\right) = -\frac{1}{2\pi\beta_0}\ln(1-2\lambda)\,, \tag{4.7}$$

where $\lambda = \alpha_s(\sqrt{s}/2)\beta_0 \ln(1/\Delta)$ and β_0 is the one-loop coefficient of the QCD beta function. The angular integration is straightforward and we obtain

$$\Sigma_1(\Delta) = -2\,\mathrm{C_F}\,t(\Delta)\int_{-1}^{1}\frac{\mathrm{d}c}{1-c^2}\,\Theta\left(\cos R - |c|\right) = -2\,\mathrm{C_F}\,t(\Delta)\ln\frac{1+\cos R}{1-\cos R}\,, \tag{4.8}$$

with c standing for $\cos\theta$. Note that since only emissions in the inter-jet (gap) region are integrated over, this result may be cast in terms of the rapidity-gap width $\Delta\eta$

$$\Delta\eta \equiv \ln\frac{1+\cos R}{1-\cos R}\,. \tag{4.9}$$

The all-orders resummed global form factor is simply the exponential of the one-loop distribution. That is

$$\Sigma_{\text{global}}(\Delta) = \exp\left[-2\,\mathrm{C_F}\,t(\Delta)\,\Delta\eta\right]. \tag{4.10}$$

[1] Notice that κ_t and φ are different from k_t and ϕ.

An identical expression was also arrived at in ref. [128] for jet shapes in e^+e^- annihilation.

The leading-order result can be verified by comparing it with the output of the MC program `EVENT2` at $\mathcal{O}(\alpha_s)$ [124, 125]. Specifically we compare the differential distribution

$$\frac{2\pi}{\alpha_s}\frac{\mathrm{d}\Sigma_1}{\mathrm{d}L} = 4\,\mathrm{C_F}\,\ln\frac{1+\cos R}{1-\cos R}\,, \tag{4.11}$$

where $L = \ln\Delta$, with the same MC distribution, for the chosen value of $R = 0.5$. We show in figure 4.1 a plot of the difference between the MC distribution and the expansion of the resummation at $\mathcal{O}(\alpha_s)$, where, as expected, this difference tends to zero in the logarithmically-enhanced region.

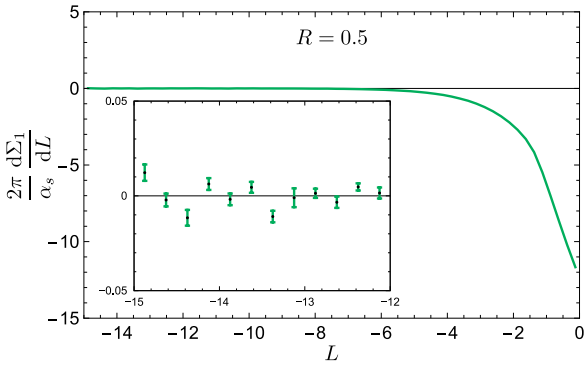

Figure 4.1: The difference between the leading-order `EVENT2` differential distribution $2\pi/\alpha_s\,\mathrm{d}\Sigma_1/\mathrm{d}L$ and the resummed distribution expanded at $\mathcal{O}(\alpha_s)$. The singular behavior of the MC distribution is exactly cancelled by the expanded result.

4.3 Two-loops calculation: NGLs and CLs

When employing the k_t or anti-k_t clustering algorithms with E-scheme recombination, the resummation of the azimuthal decorrelation distribution requires the treatment of NGLs and/or CLs. The corresponding cumulative distribution at $\mathcal{O}(\alpha_s^2)$ can then be split into three contributions

$$\Sigma_2(\Delta) = \frac{1}{2!}\left[\Sigma_1(\Delta)\right]^2 + \Sigma_2^{\mathrm{NG}}(\Delta) + \Sigma_2^{\mathrm{CL}}(\Delta)\,, \tag{4.12}$$

with $\Sigma_2^{\mathrm{CL}}(\Delta) = 0$ for anti-k_t clustering. Let us first discuss the NGLs contribution $\Sigma_2^{\mathrm{NG}}(\Delta)$ in both algorithms, and then compute the CLs contribution $\Sigma_2^{\mathrm{CL}}(\Delta)$ for k_t clustering.

4.3.1 Calculation of NGLs

The origin of NGLs at two loops is the emission of a soft gluon k_1 inside any of the two outgoing jets which itself emits a softer gluon k_2 outside the jets without being clustered back to them.

While this configuration results in a non-zero $\delta\phi$, its virtual correction (specifically when k_2 is virtual) gives $\delta\phi = 0$, and thus we have a real-virtual mis-cancellation of the soft singularities. We express the contribution of the uncancelled virtual correction to the integrated azimuthal decorrelation distribution as follows

$$\Sigma_2^{\mathrm{NG}}(\Delta) = \mathcal{S}_2(R)\,\frac{t^2}{2!}\,, \tag{4.13a}$$

$$\mathcal{S}_2(R) = -2\,\mathrm{C_F}\,\mathrm{C_A}\int \frac{\mathrm{d}c_1}{1-c_1^2}\,\frac{\mathrm{d}\phi_1}{2\pi}\,\frac{\mathrm{d}c_2}{1-c_2^2}\,\frac{\mathrm{d}\phi_2}{2\pi}\,\mathcal{A}_{q\bar{q}}^{12}\,\Xi_2^{\mathrm{NG}}(R)\,, \tag{4.13b}$$

where $\mathrm{C_A}$ is the color factor associated with the non-Abelian emission of gluon k_2 off k_1. The irreducible two-loops antenna function $\mathcal{A}_{q\bar{q}}^{12}$ is given by [93]

$$\mathcal{A}_{q\bar{q}}^{12} = \omega_{q\bar{q}}^{1}\left(\omega_{q1}^2 + \omega_{1\bar{q}}^2 - \omega_{q\bar{q}}^2\right) = \frac{1-c_1c_2}{1-c_1c_2-s_1s_2\cos(\phi_1-\phi_2)} - 1\,, \tag{4.14}$$

with $s_i \equiv \sin\theta_i$. The function Ξ_2^{NG} restricts the angular phase-space of integration and is given, in the anti-k_t and k_t algorithms respectively, by

$$\Xi_2^{\mathrm{NG,\,ak}_t} = \Theta_{\mathrm{in}}(k_1)\Theta_{\mathrm{out}}(k_2)\,, \tag{4.15a}$$

$$\Xi_2^{\mathrm{NG,\,k}_t} = \Theta_{\mathrm{in}}(k_1)\Theta_{\mathrm{out}}(k_2)\Theta(d_{12}-d_2)\,. \tag{4.15b}$$

The step function $\Theta(d_{12}-d_2)$ forbids gluon k_2 from being clustered back to the jet in the k_t algorithm. It is given by $\Theta(\cos R - \cos\theta_{12})$, with $\cos\theta_{12} = c_1c_2 + s_1s_2\cos(\phi_1-\phi_2)$.

In the anti-k_t algorithm the integration is simple and its result can be expressed in the same form as that of the rapidity-gap NGLs coefficient found in ref. [94]

$$\begin{aligned}\mathcal{S}_2^{\mathrm{ak}_t}(R) &= -\mathrm{C_F}\,\mathrm{C_A}\left[\frac{\pi^2}{6} + 2\Delta\eta^2 - 2\Delta\eta\ln\left(e^{2\Delta\eta}-1\right) - \mathrm{Li}_2\left(e^{-2\Delta\eta}\right) - \mathrm{Li}_2\left(1-e^{2\Delta\eta}\right)\right] \\ &= -\mathrm{C_F}\,\mathrm{C_A}\left[\frac{\pi^2}{3} - \frac{R^4}{8} - \frac{R^6}{24} - \frac{29\,R^8}{2560} + \mathcal{O}\left(R^{10}\right)\right],\end{aligned} \tag{4.16}$$

where $\Delta\eta(R)$ is defined in eq. (4.9). The above formula shows that in the limit $R \to 0$ the two-loops NGLs coefficient does not vanish, but rather reaches its maximum value. This feature was observed in ref. [94] and was ascribed to the fact that NGLs originate from the *edge* of jets, since this is the phase-space region where gluons k_1 and k_2 are collinear and thus the amplitude squared (4.14) is most singular.

In the k_t algorithm, and at small values of R (using small angles), we can write the NGLs

coefficient as

$$\mathcal{S}_2^{\mathrm{k}_t}(R\sim 0) = -8\,\mathrm{C_F}\,\mathrm{C_A}\int_0^1 \mathrm{d}\theta_1 \int_1^\infty \mathrm{d}\theta_2 \int_0^{2\pi} \frac{\mathrm{d}\phi}{2\pi}\,\frac{1}{(\theta_1^2+\theta_2^2)\sec\phi - 2\,\theta_1\,\theta_2}\times \\ \times\ \Theta\left(\theta_1^2+\theta_2^2-2\,\theta_1\,\theta_2\cos\phi-1\right) = -\frac{2\pi^2}{27}\,\mathrm{C_F}\,\mathrm{C_A}\,, \quad (4.17)$$

where we made the following changes of variables: $\phi = \phi_1 - \phi_2$ and $\theta_i \to R\,\theta_i$. Away from the small-R limit one may perform the integration numerically to obtain the full-R result for the two-loops coefficient of NGLs. We present the results in the following subsection together with the CLs coefficient.

4.3.2 CLs with k_t clustering

To compute the CLs we consider the Abelian primary emission of two strongly-ordered gluons directly off the hard $q\bar{q}$ dipole, whereby the harder gluon k_1 is inside one of the two jets and the softer k_2 is outside both of them, with the constraint $d_{12} < d_2$, such that gluon k_2 gets clustered into the jet by gluon k_1, which leads to $\delta\phi = 0$. However, when k_1 is virtual then gluon k_2 remains in the gap causing the hard jets to decorrelate. In this case we obtain a large single logarithmic contribution to the $\delta\phi$ distribution given by

$$\Sigma_2^{\mathrm{CL}}(\Delta) = \mathcal{C}_2^{\mathrm{k}_t}(R)\,\frac{t^2}{2!}\,, \quad (4.18a)$$

$$\mathcal{C}_2^{\mathrm{k}_t}(R) = 4\,\mathrm{C_F^2}\int \frac{\mathrm{d}c_1}{1-c_1^2}\,\frac{\mathrm{d}\phi_1}{2\pi}\,\frac{\mathrm{d}c_2}{1-c_2^2}\,\frac{\mathrm{d}\phi_2}{2\pi}\,w_{q\bar{q}}^1\,w_{q\bar{q}}^2\,\Theta(|c_1|-\cos R)\,\Theta(\cos R-|c_2|)\,\Theta(\cos\theta_{12}-\cos R)\,. \quad (4.18b)$$

Note again that $\mathcal{C}_2^{\mathrm{ak}_t}(R) = 0$, as there are no CLs for anti-k_t clustering.

First, let us consider the small-R limit of this integral. In this case we may write

$$\mathcal{C}_2^{\mathrm{k}_t}(R\sim 0) = 8\,\mathrm{C_F^2}\int_0^1 \frac{\mathrm{d}\theta_1}{\theta_1}\int_1^\infty \frac{\mathrm{d}\theta_2}{\theta_2}\int_0^{2\pi}\frac{\mathrm{d}\phi}{2\pi}\,\Theta\left(-\theta_1^2-\theta_2^2+2\,\theta_1\,\theta_2\cos\phi+1\right) = \frac{5\pi^2}{27}\,\mathrm{C_F^2}\,. \quad (4.19)$$

Away from this small-R limit we perform the integration numerically. We show in figure 4.2 a plot of the coefficients of NGLs and CLs at $\mathcal{O}(\alpha_s^2)$ as a function of the jet radius R. Also shown is the combined coefficient of CLs and NGLs in the k_t algorithm; $\mathcal{F}_2^{\mathrm{k}_t} = \mathcal{S}_2^{\mathrm{k}_t} + \mathcal{C}_2^{\mathrm{k}_t}$.

Notice that NGLs coefficient in the k_t clustering algorithm is significantly smaller than that in the anti-k_t. The CLs coefficient is positive and quite small, with the advantage that it cancels the NGLs coefficient, particularly at small values of R. Note that the overall coefficient $\mathcal{F}_2$ is less than 1 for values of R smaller than about 0.5. For small R values, the anti-k_t NGLs

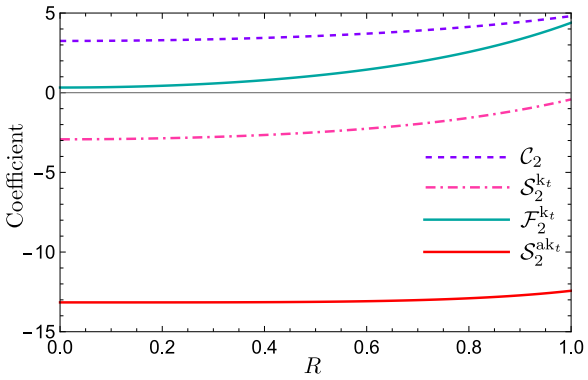

Figure 4.2: CLs and NGLs coefficients at two loops with k_t and anti-k_t clustering.

coefficient computed here is identical to that found for the single hemisphere mass [129] and jet mass with a jet veto [128].

4.3.3 Comparison to EVENT2

We compare our two-loops results with the exact MC distribution at $\mathcal{O}(\alpha_s^2)$ obtained with the `EVENT2` program. The latter splits the distribution at NLO into three color contributions; $\mathcal{O}(\mathrm{C_F^2})$, $\mathcal{O}(\mathrm{C_F\,C_A})$ and $\mathcal{O}(\mathrm{C_F\,T_f\,n_f})$, with $\mathrm{T_f} = 1/2$ being the normalization constant of the generators of the SU(3) group in the fundamental representation and $\mathrm{n_f} = 5$ is the number of active quark flavors. The expansion of the resummed distribution at this order, including running coupling effects, is written, after differentiating with respect to L, as

$$\left(\frac{2\pi}{\alpha_s}\right)^2 \frac{\mathrm{d}\Sigma_2}{\mathrm{d}L} = \left[\mathrm{C_F^2}\,4\left(4\,\Delta\eta^2 + \mathcal{C}_2\right) - \mathrm{C_F\,C_A}\,\frac{4}{3}\left(3\,\mathcal{S}_2 + 11\Delta\eta\right) + \mathrm{C_F\,T_f\,n_f}\,\frac{16}{3}\,\Delta\eta\right] L + \mathcal{O}(1)\,. \tag{4.20}$$

At this order this differential distribution is linear in L, but does not capture the $\mathcal{O}(1)$ constant, which, in the cumulative integrated distribution, is an NLL $\mathcal{O}(\alpha_s^2\,L)$ term. We plot the difference between the MC distribution and the expansion (4.20) for each color contribution separately. All curves should tend towards a constant when L grows large and negative. The results are shown in figure 4.3. Here the $\mathcal{O}(\mathrm{C_F^2})$ part contains the CLs coefficient in k_t clustering, while the $\mathcal{O}(\mathrm{C_F\,C_A})$ term contains the NGLs coefficient both in k_t and anti-k_t algorithms. The $\mathcal{O}(\mathrm{C_F\,T_f\,n_f})$ contribution is algorithm independent at LL accuracy, but the NLL $\mathcal{O}(1)$ constant does depend on the jet algorithm.

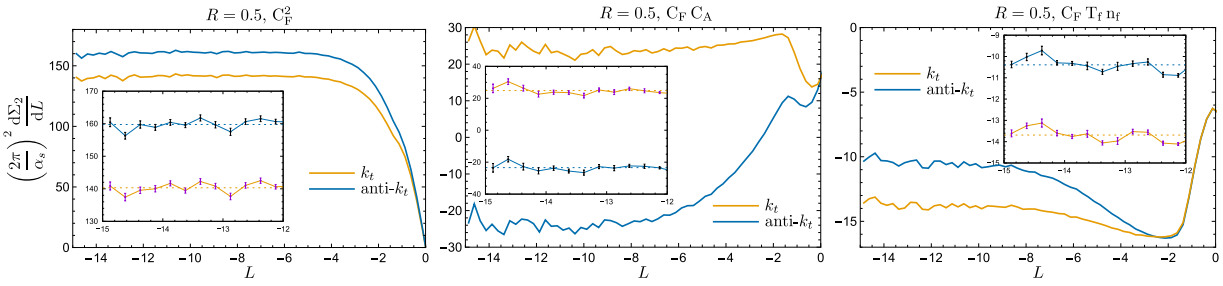

Figure 4.3: The difference between the NLO EVENT2 differential distribution $(2\pi/\alpha_s)^2\,\mathrm{d}\Sigma_2/\mathrm{d}L$ and the resummed distribution expanded at $\mathcal{O}(\alpha_s^2)$. The leading logarithmic behavior of the MC distribution $\mathcal{O}(\alpha_s^2 L)$ is cancelled, leaving a constant behavior at large values of L.

4.4 NGLs and CLs at three loops

4.4.1 NGLs at three loops

At $\mathcal{O}(\alpha_s^3)$, the cumulative distribution can be written as follows

$$\Sigma_3(\Delta) = \frac{1}{3!}\left[\Sigma_1(\Delta)\right]^3 + \Sigma_1(\Delta)\times\Sigma_2^{\mathrm{NG}}(\Delta) + \Sigma_1(\Delta)\times\Sigma_2^{\mathrm{CL}}(\Delta) + \Sigma_3^{\mathrm{NG}}(\Delta) + \Sigma_3^{\mathrm{CL}}(\Delta)\,. \tag{4.21}$$

Focusing first on the *pure* NGLs contribution Σ_3^{NG} (i.e., excluding the cross-talk between the one-loop global and two-loops non-global logarithms) in the anti-k_t algorithm, we may write it in the form

$$\Sigma_3^{\mathrm{NG,ak}_t}(\Delta) = \mathcal{S}_3^{\mathrm{ak}_t}(R)\,\frac{t^3}{3!}\,, \tag{4.22a}$$

$$\mathcal{S}_3^{\mathrm{ak}_t}(R) = 2\,\mathrm{C_F}\,\mathrm{C_A^2}\int\left(\prod_{i=1}^{3}\frac{\mathrm{d}c_i}{1-c_i^2}\,\frac{\mathrm{d}\phi_i}{2\pi}\right)\left[\mathcal{A}_{q\bar{q}}^{12}\,\bar{\mathcal{A}}_{q\bar{q}}^{13}\,\Theta_{\mathrm{in}}(k_1)\Theta_{\mathrm{out}}(k_2)\Theta_{\mathrm{out}}(k_3) + \right.$$
$$\left. -\mathcal{B}_{q\bar{q}}^{123}\,\Theta_{\mathrm{in}}(k_1)\Theta_{\mathrm{in}}(k_2)\Theta_{\mathrm{out}}(k_3)\right]\,, \tag{4.22b}$$

where we define $\bar{\mathcal{A}}_{q\bar{q}}^{13} = \mathcal{A}_{q\bar{q}}^{13}/\omega_{q\bar{q}}^{1}$, and the 3-loops irreducible cascade antenna function is given by

$$\mathcal{B}_{q\bar{q}}^{123} = \omega_{q\bar{q}}^{1}\left[\mathcal{A}_{q1}^{23} + \mathcal{A}_{1\bar{q}}^{23} - \mathcal{A}_{q\bar{q}}^{23}\right]. \tag{4.23}$$

It is worth mentioning that, for the cascade term, there is a non-negligible contribution from the configuration in which gluon k_1 is in one jet emitting gluon k_2 in the other jet which itself emits the softest gluon k_3 in the gap between the two jets. At small values of R the integration is quite simple and yields the result

$$\mathcal{S}_3^{\mathrm{ak}_t}(R\sim 0) = \mathrm{C_F}\,\mathrm{C_A^2}\,2\,\zeta_3\,. \tag{4.24}$$

Notice that this result is twice that found for the hemisphere mass observable [102]. Away from the small-R limit the integration can be performed numerically and we shall present the results

in the next subsection.

The *pure* NGLs contribution in the k_t algorithm is given by an identical form to that of the anti-k_t (4.22a)

$$\Sigma_3^{\mathrm{NG,k_t}}(\Delta) = \mathcal{S}_3^{\mathrm{k_t}}(R)\,\frac{t^3}{3!}\,. \tag{4.25}$$

We perform for the first time in the literature a calculation of NGLs in the k_t algorithm beyond two loops. Due to non-linearity of k_t clustering we shall find a class of NGLs that have a non-standard color factor, namely $\mathrm{C_F^2\,C_A}$ at $\mathcal{O}(\alpha_s^3)$. Such terms usually (in anti-k_t clustering) only arise in the cross-talk of the expansion of the primary-emission global form factor (4.10) at $\mathcal{O}(\alpha_s)$ together with NGLs at $\mathcal{O}(\alpha_s^2)$, i.e., the term $\Sigma_1(\Delta)\times\Sigma_2^{\mathrm{NG}}(\Delta)$ in eq. (4.21). However, in the k_t algorithm, we find them as "pure" irreducible NGLs. That is, they are part of the term $\Sigma_3^{\mathrm{NG}}(\Delta)$ in eq. (4.21).

To proceed, we consider three types of emissions at $\mathcal{O}(\alpha_s^3)$, as shown in figure 4.4: (a) one primary + two correlated emissions, (b) ladder emissions, and (c) cascade emissions. In each case we consider all possible virtual-correction Feynman diagrams as well as angular configurations of the emitted gluons that affect the clustering procedure, and look for a mis-match between the soft divergences of these emissions.

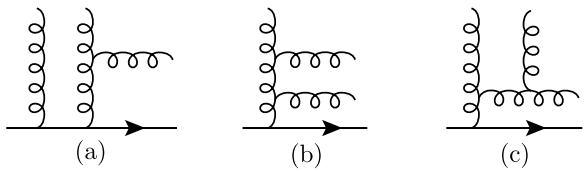

Figure 4.4: The three types of emissions to consider for NGLs calculation at $\mathcal{O}(\alpha_s^3)$: (a) one primary + two correlated emissions, (b) ladder emissions, and (c) cascade emissions.

Starting first with type (a) contributions, there are three possible permutations of the gluons. [2] For the permutation in which k_3 is emitted in correlation with k_2, and which has a squared amplitude $4\,\mathrm{C_F^2\,C_A}\,\omega^1_{q\bar{q}}\,\mathcal{A}^{23}_{q\bar{q}}$, we find that the angular phase space of integration that yields a logarithmic contribution is given by

$$\begin{aligned}\Xi_{31}^{\mathrm{NG,k_t}}(R) = {}& \Theta_{\mathrm{in}}(k_1)\Theta_{\mathrm{in}}(k_2)\Theta_{\mathrm{out}}(k_3)\Theta(d_3-d_{13})\Theta(d_{23}-d_3)+\\ &+\Theta_{\mathrm{out}}(k_1)\Theta_{\mathrm{in}}(k_2)\Theta_{\mathrm{out}}(k_3)\Theta(d_{23}-d_3)+\\ &-\Theta_{\mathrm{in}}(k_1)\Theta_{\mathrm{out}}(k_2)\Theta_{\mathrm{out}}(k_3)\Theta(d_{13}-d_3)\Theta(d_{23}-d_3)\Theta(d_2-d_{12})\,.\end{aligned} \tag{4.26}$$

To see how one obtains this result let us give one example of angular configurations that result in a logarithmic contribution. There are four Feynman diagrams in this case, shown in figure

[2] Note that for all permutations the transverse momenta of the three gluons are strongly ordered as follows: $k_{t1} \gg k_{t2} \gg k_{t3}$.

4.5. Consider the situation when particles k_3 and k_2 are outside the jet regions, $d_{3j} > d_3$ and $d_{2j} > d_2$, while particle k_1 is inside, $d_{1j} < d_1$. In this scenario, both diagrams in which k_1 is virtual (i.e., diagrams (3) and (4) in figure 4.5) yield $\delta\phi \neq 0$, since in both diagrams particle k_2 is real and remains in the gap region after applying the clustering. However, these two diagrams contribute equally and with opposite signs, so they cancel each other. For the remaining two diagrams, (1) and (2), we have a mismatch when particle k_2 gets pulled inside the jet by the real particle k_1 while k_3 remains in the gap. This happens when d_{12} is smaller than d_2, and both d_{13} and d_{23} are greater than d_3. While in diagram (1) we have a real unclustered gluon k_3 in the gap region (i.e., it forms a jet on its own) giving $\delta\phi \neq 0$, in diagram (2) the gap is empty and the hard jets are exactly back-to-back with $\delta\phi = 0$. The virtual-correction diagram (2) contributes fully to the cumulative distribution while the real-emission diagram (1) cancels this contribution only up to $\delta\phi = \Delta$, leaving uncancelled virtual-correction contributions with a negative sign. This is the last term in eq. (4.26).

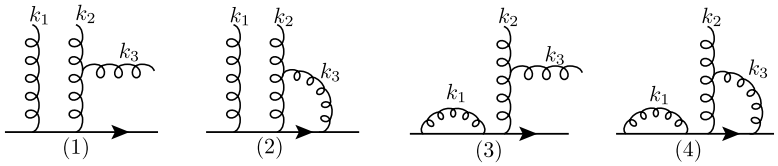

Figure 4.5: Feynman diagrams corresponding to the squared amplitude $4\,\mathrm{C_F^2}\,\mathrm{C_A}\,\omega^1_{q\bar{q}}\,\mathcal{A}^{23}_{q\bar{q}}$.

Similarly, we obtain for the second and third gluon permutations of type (a) diagrams, with squared amplitudes $4\,\mathrm{C_F^2}\,\mathrm{C_A}\,\omega^2_{q\bar{q}}\,\mathcal{A}^{13}_{q\bar{q}}$ and $4\,\mathrm{C_F^2}\,\mathrm{C_A}\,\omega^3_{q\bar{q}}\,\mathcal{A}^{12}_{q\bar{q}}$, respectively, as well as type (b) (ladder-emission) contributions, with squared amplitude $2\,\mathrm{C_F}\,\mathrm{C_A^2}\,\bar{\mathcal{A}}^{12}_{q\bar{q}}\,\mathcal{A}^{13}_{q\bar{q}}$, the same phase space function. It is given by

$$\begin{aligned}\Xi^{\mathrm{NG},\mathrm{k}_t}_{32}(R) = {}& \Theta_{\mathrm{in}}(k_1)\Theta_{\mathrm{in}}(k_2)\Theta_{\mathrm{out}}(k_3)\Theta(d_{13}-d_3)\Theta(d_3-d_{23}) + \\ & + \Theta_{\mathrm{in}}(k_1)\Theta_{\mathrm{out}}(k_2)\Theta_{\mathrm{out}}(k_3)\Theta(d_{13}-d_3)\Theta(d_3-d_{23}) + \\ & + \Theta_{\mathrm{in}}(k_1)\Theta_{\mathrm{out}}(k_2)\Theta_{\mathrm{out}}(k_3)\Theta(d_{13}-d_3)\Theta(d_{23}-d_3)\Theta(d_{12}-d_2)\,. \end{aligned} \tag{4.27}$$

Finally, for type (c) (cascade emission) contributions, corresponding to the squared amplitude $2\,\mathrm{C_F}\,\mathrm{C_A^2}\,\mathcal{B}^{123}_{q\bar{q}}$, the phase space function reads

$$\begin{aligned}\Xi^{\mathrm{NG},\mathrm{k}_t}_{33}(R) = {}& -\Theta_{\mathrm{in}}(k_1)\Theta_{\mathrm{in}}(k_2)\Theta_{\mathrm{out}}(k_3)\Theta(d_{13}-d_3)\Theta(d_{23}-d_3) - \\ & - \Theta_{\mathrm{in}}(k_1)\Theta_{\mathrm{out}}(k_2)\Theta_{\mathrm{out}}(k_3)\Theta(d_{13}-d_3)\Theta(d_{23}-d_3)\Theta(d_2-d_{12})\,. \end{aligned} \tag{4.28}$$

Before performing the integration, we subtract off the part of the phase space that produces the interference term between the one-loop global primary logarithm and the two-loops NGLs,

which only comes from type (a) emissions. For the first permutation of gluons, this part of phase space is identified by the second term in eq. (4.26), $\Theta_{\text{out}}(k_1)\Theta_{\text{in}}(k_2)\Theta_{\text{out}}(k_3)\Theta(d_{23}-d_3)$, where gluon k_1 reproduces the one-loop global term (4.8) and the other correlated gluons, k_2 and k_3, give the two-loops NGLs (eq. (4.13b) with phase space (4.15b)). However, for the other two gluon permutations of type (a) emissions, the phase space (4.27) does not simply contain such interference terms. Strictly speaking, this means that NGLs do not cleanly factorize from the global form factor in the k_t algorithm. Nevertheless, we can manually add and subtract the interference terms and write the total distribution in the factorizable form (4.21).

We can then write the "pure" NGLs coefficient $\mathcal{S}_3^{\text{k}_t}$, given in eq. (4.25), in the following form

$$\mathcal{S}_3^{\text{k}_t}(R) = \mathcal{S}_3^{(a)}(R) + \mathcal{S}_3^{(b)+(c)}(R)\,, \tag{4.29}$$

where we split the result according to the color factor, such that for type (a) emissions we have

$$\mathcal{S}_3^{(a)}(R) = 4\,\text{C}_\text{F}^2\,\text{C}_\text{A}\int\left(\prod_{i=1}^{3}\frac{\text{d}c_i}{1-c_i^2}\,\frac{\text{d}\phi_i}{2\pi}\right)\left[\omega_{q\bar{q}}^1\,\mathcal{A}_{q\bar{q}}^{23}\,\widetilde{\Xi}_{31}(R)+\omega_{q\bar{q}}^2\,\mathcal{A}_{q\bar{q}}^{13}\,\widetilde{\Xi}_{32}(R)+\omega_{q\bar{q}}^3\,\mathcal{A}_{q\bar{q}}^{12}\,\widetilde{\Xi}_{33}(R)\right], \tag{4.30}$$

with modified phase space that subtracts away the interference terms

$$\widetilde{\Xi}_{31}(R) = \Xi_{31}^{\text{NG},\text{k}_t}(R) - \Theta_{\text{out}}(k_1)\Theta_{\text{in}}(k_2)\Theta_{\text{out}}(k_3)\Theta(d_{23}-d_3)\,, \tag{4.31a}$$

$$\widetilde{\Xi}_{32}(R) = \Xi_{32}^{\text{NG},\text{k}_t}(R) - \Theta_{\text{in}}(k_1)\Theta_{\text{out}}(k_2)\Theta_{\text{out}}(k_3)\Theta(d_{13}-d_3)\,, \tag{4.31b}$$

$$\widetilde{\Xi}_{33}(R) = \Xi_{32}^{\text{NG},\text{k}_t}(R) - \Theta_{\text{in}}(k_1)\Theta_{\text{out}}(k_2)\Theta_{\text{out}}(k_3)\Theta(d_{12}-d_2)\,, \tag{4.31c}$$

and for type (b) and (c) emissions

$$\mathcal{S}_3^{(b)+(c)}(R) = 2\,\text{C}_\text{F}\,\text{C}_\text{A}^2\int\left(\prod_{i=1}^{3}\frac{\text{d}c_i}{1-c_i^2}\,\frac{\text{d}\phi_i}{2\pi}\right)\left[\mathcal{A}_{q\bar{q}}^{12}\,\bar{\mathcal{A}}_{q\bar{q}}^{13}\,\Xi_{32}^{\text{NG},\text{k}_t}(R)+\mathcal{B}_{q\bar{q}}^{123}\,\Xi_{33}^{\text{NG},\text{k}_t}(R)\right]. \tag{4.32}$$

We are now in a position to perform the integrations numerically as a function of the jet radius R. We show the results in the next subsection, in which we also compute the clustering logarithmic contribution at $\mathcal{O}(\alpha_s^3)$.

4.4.2 CLs with k_t clustering at three loops

Following the same steps as for NGLs calculation, the phase space clustering function at $\mathcal{O}(\alpha_s^3)$ for the CLs contribution, which results from the mismatch of soft singularities between real and virtual emissions of three primary soft gluons, with a squared amplitude $8\,\text{C}_\text{F}^3\,w_{q\bar{q}}^1\,w_{q\bar{q}}^2\,w_{q\bar{q}}^3$,

is given by

$$\begin{aligned}\Xi_3^{\mathrm{CL},\mathrm{k}_t}(R) = &- \Theta_{\mathrm{in}}(k_1)\Theta_{\mathrm{in}}(k_2)\Theta_{\mathrm{out}}(k_3)\Theta(d_3-d_{13})\Theta(d_3-d_{23}) - \\ &- \Theta_{\mathrm{out}}(k_1)\Theta_{\mathrm{in}}(k_2)\Theta_{\mathrm{out}}(k_3)\Theta(d_3-d_{23}) - \\ &- \Theta_{\mathrm{in}}(k_1)\Theta_{\mathrm{out}}(k_2)\Theta_{\mathrm{out}}(k_3)\Theta(d_3-d_{13}) - \\ &- \Theta_{\mathrm{in}}(k_1)\Theta_{\mathrm{out}}(k_2)\Theta_{\mathrm{out}}(k_3)\Theta(d_{13}-d_3)\Theta(d_{23}-d_3)\Theta(d_2-d_{12})\,. \end{aligned} \tag{4.33}$$

Note that the above phase-space clustering function is similar (but not exactly identical) to that found for the jet mass observable [53]. Extracting the interference terms between the CLs at two loops and the global logarithm at one loop, i.e., the term $\Sigma_1(\Delta)\times\Sigma_2^{\mathrm{CL}}(\Delta)$ in eq. (4.21), we reduce the above phase space function to that of the "pure" CLs contribution as

$$\begin{aligned}\widetilde{\Xi}_3^{\mathrm{CL},\mathrm{k}_t}(R) = &- \Theta_{\mathrm{in}}(k_1)\Theta_{\mathrm{in}}(k_2)\Theta_{\mathrm{out}}(k_3)\Theta(d_3-d_{13})\Theta(d_3-d_{23}) + \\ &+ \Theta_{\mathrm{in}}(k_1)\Theta_{\mathrm{out}}(k_2)\Theta_{\mathrm{out}}(k_3)\Theta(d_2-d_{12})[1-\Theta(d_{13}-d_3)\Theta(d_{23}-d_3)]\,. \end{aligned} \tag{4.34}$$

Then, the clustering logarithmic contribution to the cumulative cross-section is given by

$$\Sigma_3^{\mathrm{CL}}(\Delta) = \mathcal{C}_3^{\mathrm{k}_t}(R)\,\frac{t^3}{3!}\,, \tag{4.35a}$$

$$\mathcal{C}_3^{\mathrm{k}_t}(R) = 8\,\mathrm{C_F^3}\int\left(\prod_{i=1}^{3}\frac{\mathrm{d}c_i}{1-c_i^2}\,\frac{\mathrm{d}\phi_i}{2\pi}\right) w_{q\bar{q}}^1\, w_{q\bar{q}}^2\, w_{q\bar{q}}^3\,\widetilde{\Xi}_3^{\mathrm{CL},\mathrm{k}_t}(R)\,. \tag{4.35b}$$

We show in figure 4.6 a plot of the coefficients of NGLs and CLs in the k_t and anti-k_t algorithms as a function of the jet radius R. Shown also is the combined coefficient $\mathcal{F}_3^{\mathrm{k}_t} = \mathcal{S}_3^{\mathrm{k}_t} + \mathcal{C}_3^{\mathrm{k}_t}$ for the k_t algorithm.

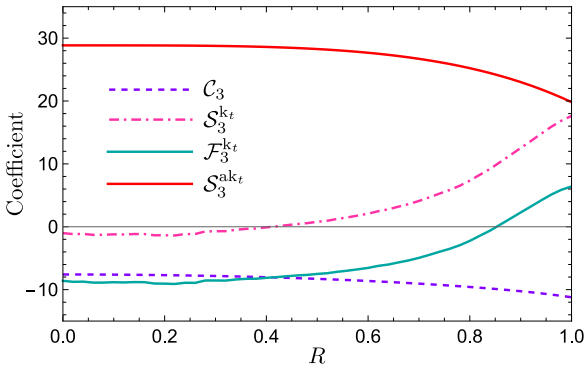

Figure 4.6: CLs and NGLs coefficients at three loops with k_t and anti-k_t clustering.

As in the previous section, we notice that the NGLs coefficient in the anti-k_t algorithm at this order is also quite large. Clearly, the application of the k_t clustering has reduced the

significance of NGLs by almost a factor of 30 for values less than $R \sim 0.6$. The CLs coefficient is also small such that the overall coefficient $\mathcal{F}_3$ is smaller in magnitude than the $\mathcal{S}_3^{\mathrm{ak}_t}$ by about a factor of 3 for most values of R.

4.5 Four loops and beyond

4.5.1 Four-loops NGLs with anti-k_t at small R

The calculation of NGLs with anti-k_t clustering proceeds in a similar manner at fourth order, and can easily be deduced from previous calculations of NGLs in the literature. In fact, the phase space of integration is similar to that of the hemisphere mass distribution reported in ref. [102], and thus the cumulative cross-section, at this order, may be cast in the following way

$$\Sigma_4^{\mathrm{ak}_t}(\Delta) = \frac{1}{4!}\left[\Sigma_1(\Delta)\right]^4 + \frac{1}{2!}\left[\Sigma_1(\Delta)\right]^2 \Sigma_2^{\mathrm{NG,ak}_t}(\Delta) + \Sigma_1(\Delta)\,\Sigma_3^{\mathrm{NG,ak}_t}(\Delta) + \frac{1}{2!}\left[\Sigma_2^{\mathrm{NG,ak}_t}(\Delta)\right]^2 + \Sigma_4^{\mathrm{NG,ak}_t}(\Delta)\,, \tag{4.36}$$

with pure NGLs contribution given by

$$\Sigma_4^{\mathrm{NG,ak}_t}(\Delta) = \mathcal{S}_4^{\mathrm{ak}_t}(R)\,\frac{t^4}{4!}\,, \tag{4.37a}$$

$$\begin{aligned}
\mathcal{S}_4^{\mathrm{ak}_t}(R) = {} & 2\,\mathrm{C_F}\,\mathrm{C_A^3}\int\left(\prod_{i=1}^{4}\frac{\mathrm{d}c_i}{1-c_i^2}\,\frac{\mathrm{d}\phi_i}{2\pi}\right)\Big[-\mathcal{A}_{q\bar{q}}^{12}\,\bar{\mathcal{A}}_{q\bar{q}}^{13}\,\bar{\mathcal{A}}_{q\bar{q}}^{14}\,\Theta_{\mathrm{in}}(k_1)\Theta_{\mathrm{out}}(k_2)\Theta_{\mathrm{out}}(k_3)\Theta_{\mathrm{out}}(k_4) + \\
& + 3\,\bar{\mathcal{A}}_{q\bar{q}}^{12}\,\mathcal{B}_{q\bar{q}}^{134}\,\Theta_{\mathrm{in}}(k_1)\Theta_{\mathrm{out}}(k_2)\Theta_{\mathrm{in}}(k_3)\Theta_{\mathrm{out}}(k_4) + \mathfrak{U}_{q\bar{q}}^{1234}\,\Theta_{\mathrm{in}}(k_1)\Theta_{\mathrm{in}}(k_2)\Theta_{\mathrm{out}}(k_3)\Theta_{\mathrm{out}}(k_4) - \\
& - \mathcal{C}_{q\bar{q}}^{1234}\,\Theta_{\mathrm{in}}(k_1)\Theta_{\mathrm{in}}(k_2)\Theta_{\mathrm{in}}(k_3)\Theta_{\mathrm{out}}(k_4)\Big] - \\
& - 2\,\mathrm{C_F}\,\mathrm{C_A^3}\left(1-\frac{2\,\mathrm{C_F}}{\mathrm{C_A}}\right)\int\left(\prod_{i=1}^{4}\frac{\mathrm{d}c_i}{1-c_i^2}\,\frac{\mathrm{d}\phi_i}{2\pi}\right)\mathbf{A}_{q\bar{q}}^{1234}\Theta_{\mathrm{in}}(k_1)\Theta_{\mathrm{in}}(k_2)\Theta_{\mathrm{out}}(k_3)\Theta_{\mathrm{out}}(k_4)\,,
\end{aligned} \tag{4.37b}$$

where the irreducible antenna functions read [93]

$$\mathcal{C}_{q\bar{q}}^{1234} = w_{q\bar{q}}^{1}\left(\mathcal{B}_{q1}^{234} + \mathcal{B}_{1\bar{q}}^{234} - \mathcal{B}_{q\bar{q}}^{234}\right), \tag{4.38a}$$

$$\mathfrak{U}_{q\bar{q}}^{1234} = w_{q\bar{q}}^{1}\left(\mathcal{A}_{q1}^{23}\,\bar{\mathcal{A}}_{q1}^{24} + \mathcal{A}_{1\bar{q}}^{23}\,\bar{\mathcal{A}}_{1\bar{q}}^{24} - \mathcal{A}_{q\bar{q}}^{23}\,\bar{\mathcal{A}}_{q\bar{q}}^{24}\right), \tag{4.38b}$$

$$\begin{aligned}
\mathbf{A}_{q\bar{q}}^{1234} = {} & \omega_{q\bar{q}}^{1}\,\omega_{q1}^{2}\left(\bar{\mathcal{A}}_{q\bar{q}}^{23} - \bar{\mathcal{A}}_{q1}^{23}\right)\left(\bar{\mathcal{A}}_{q1}^{24} - \bar{\mathcal{A}}_{1\bar{q}}^{24}\right) + \omega_{q\bar{q}}^{1}\,\omega_{1\bar{q}}^{2}\left(\bar{\mathcal{A}}_{q\bar{q}}^{23} - \bar{\mathcal{A}}_{1\bar{q}}^{23}\right)\left(\bar{\mathcal{A}}_{1\bar{q}}^{24} - \bar{\mathcal{A}}_{q1}^{24}\right) - \\
& - \omega_{q\bar{q}}^{1}\,\omega_{q\bar{q}}^{2}\left(\bar{\mathcal{A}}_{q1}^{23} - \bar{\mathcal{A}}_{q\bar{q}}^{23}\right)\left(\bar{\mathcal{A}}_{1\bar{q}}^{24} - \bar{\mathcal{A}}_{q\bar{q}}^{24}\right) + k_3 \leftrightarrow k_4\,.
\end{aligned} \tag{4.38c}$$

At small values of R the integration has been performed in ref. [102], and the corresponding result is given by

$$\mathcal{S}_4^{\mathrm{ak}_t}(R \sim 0) = -\mathrm{C_F}\,\mathrm{C_A^3}\,\zeta_4\left[\frac{29}{4} - \left(1 - \frac{2\,\mathrm{C_F}}{\mathrm{C_A}}\right)\right]. \tag{4.39}$$

4.5.2 LL resummation

In this section we present numerical results for the resummation of NGLs and CLs in the large-N_c approximation. For this we use the MC code first developed in refs. [52, 94] with modification of k_t clustering in terms of distances (4.1). The results are shown in figure 4.7 for the resummed cumulative distribution Σ as a function of the evolution parameter t (4.7), for the particular value of the jet radius $R = 0.5$. Shown in the figure are: results for the (primary) global distribution (black curve), obtained by running the MC program using anti-k_t clustering and allowing only for primary emissions, and the full anti-k_t distribution (solid pink curve) which additionally includes NGLs at large N_c. We observe the very large impact of NGLs on the distribution, reducing the global form factor by a factor of 10 for $t = 0.3$.

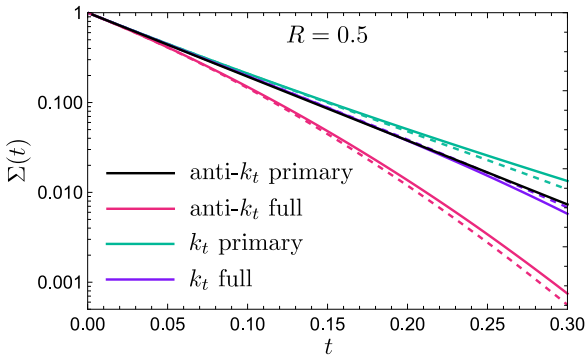

Figure 4.7: Numerically resummed NGLs and CLs at large N_c.

We also show in the same figure the primary-emission distribution obtained by running the above-mentioned program with k_t clustering (solid green curve), which includes the global form factor together with the resummed CLs, as well as the overall distribution in k_t clustering which includes in addition the resummed NGLs (solid purple curve). We observe that the distribution in k_t clustering is affected by both CLs and NGLs, but the combined impact of the two is noticeably small. This means that CLs tend to cancel NGLs in k_t clustering, as noted with the fixed-order calculations performed above.

Moreover, we show in figure 4.7 the analytical results for the resummed distribution in each case (dashed lines), which are estimated from the observed pattern of exponentiation

$$\Sigma(\Delta) = \exp\left[\Sigma_1(\Delta)\right] \exp\left[\sum_{i=2}^{\infty} \Sigma_i^{\mathrm{NG}}(\Delta)\right] \exp\left[\sum_{i=2}^{\infty} \Sigma_i^{\mathrm{CL}}(\Delta)\right]. \tag{4.40}$$

It is clear that the truncation of the series at $i = 3$ in the exponent, though quite close to the numerical result, does not give an accurate fit of the MC distribution. This means that higher-order contributions cannot be ignored.

4.5.3 NLL resummation with anti-k_t

We present here a resummed result for the azimuthal decorrelation distribution with anti-k_t clustering at NLL accuracy in the large-N_c limit, obtained using the recently-published program `Gnole` [126,127]. The distribution can be obtained from this program by defining our observable within the code, using the full definition rather than the LL approximation (4.2). Explicitly written the former reads

$$\delta\phi = \left| \sin^{-1} \sum_{i \notin \text{jets}} \frac{k_{\perp i}}{p_{tr}} \right|, \tag{4.41}$$

where $k_{\perp i}$ is the component of the transverse momentum of the emission i perpendicular to the thrust (or leading jet) axis, and p_{tr} is the recoiling jet's transverse momentum. For simplicity we take the jets to be at threshold, i.e., transverse to the beam direction.

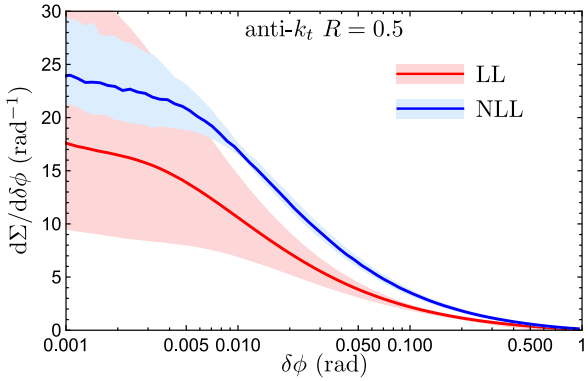

Figure 4.8: NLL numerical resummation of the $\delta\phi$ distribution at large N_c.

In figure 4.8 we present the results for the NLL resummed distribution together with the LL one, both obtained with `Gnole`. We note here that the LL distribution is obtained using the definition of the observable (4.41), while that obtained with the MC code of refs. [52,94] (figure 4.7) is essentially equivalent to the transverse energy distribution (in other words, definition 4.2 without the $\sin\phi$ part). This does in fact numerically affect the distribution even at LL accuracy. [3]

We observe that the NLL corrections to the distribution are quite important, just like the transverse energy distribution shown in ref. [127]. Furthermore, the scale-uncertainty band, obtained by varying the renormalization and resummation scales by factors of 2 and 1/2 around their central values ($\mu_R = \sqrt{s}$ and $Q_0 = \sqrt{s}/2$, respectively, with $\sqrt{s} = M_Z$), gets significantly reduced in the NLL curve. It is worth mentioning that one still needs to account for the matching in order to fully control all sub-leading NLL logarithms at the tail of the distribution.

[3] Note that it is not possible to change the definition of the observable in the MC code of refs. [52,94].

We note that the actual distribution does not possess a Sudakov peak at low values of $\delta\phi$, instead it tends towards a constant value. This is explained by the fact that the very low values of $\delta\phi$ are not suppressed by soft emissions, but are rather enhanced by vectorial cancellation of semi-hard emissions.

4.6 Summary

The azimuthal decorrelation $\delta\phi$ for dijet production in e^+e^- annihilation, is a typical example of a jet shape distribution that promise to provide valuable information on perturbative and non-perturbative QCD dynamics. Employing the four vector recombination scheme ($E-$ scheme), the observable at hand is non-global. One of the main complications that arise in such observables particularly at leading logarithmic accuracy, are two fold. On the one side, non-global logarithms will arise in the jet shape distribution when the jets are defined using both the k_t and anti$-k_t$ clustering procedures. On the other side new logarithmic contributions, clustering logs in the independent emission piece will show up at the said logarithmic accuracy, when the k_t clustering algorithm is applied. These logarithms are jet-algorithm dependent, and start to appear at two loops and are quite delicate to compute.

In this chapter we have calculated the full-R expression analytically at two loops and numerically at three loops for the anti-k_t jet algorithm for NGLs. At four loops, they have been determined only for small-R values for the same said jet algorithm. For the k_t clustering algorithm, calculations have been performed up to three loops and only numerically. In the k_t algorithm, we have unearthed "pure" non-global contributions with color factor $\mathrm{C}_\mathrm{F}^2\,\mathrm{C}_\mathrm{A}$ at $\mathcal{O}(\alpha_s^3)$ that have no alike in the anti-k_t algorithm, due to non-linearity of the k_t algorithm.

Moreover, CLs, which are absent in the anti-k_t algorithm, have been computed numerically up to three loops. The usual reduction in the significance of NGLs due to k_t clustering has been observed confirming previous findings. Furthermore, the combined impact of NGLs and CLs on the distribution is observed to be very small which has important phenomenological implications in terms of accuracy of the resummed distribution. Our results at two loops have been checked against the output of the MC program `EVENT2`.

Numerical estimates of the all-orders distribution has been presented both at LL and NLL accuracy. The achievement of the latter accuracy have been made possible by the recently-published `Gnole` code, thus achieving state-of-the-art accuracy for the resummation of this quantity.

In the next chapter we present an attempt to analytically resum non-global logarithms to all orders using the BMS equation. The hemisphere mass distribution in e^+e^- collisions will serve as a generic example of non-global event shape observables.

Chapter 5

Eikonal amplitudes and non-global logarithms from the BMS equation

5.1 Introduction

Achieving precision in the calculation of QCD observables at particle colliders is usually hindered by many perturbative and non-perturbative issues. The resummation of large logarithms is one such issue. Uncanceled virtual emissions above some scale Q_0 up to a renormalisation scale $\mu_{\rm R}$ contribute to the integrated distribution of the observable in question when real emissions above Q_0 are cut, leading to logarithms of the form $\alpha_s^n \ln^m(Q_0/\mu_{\rm R})$, with $m \leq 2n$ for observables sensitive to soft and/or collinear emissions (e.g., jet mass), while $m \leq n$ for observables sensitive to soft wide-angle emissions alone (e.g., energy flow into gaps between jets). In this paper we consider the former case of double logarithmic enhancements, i.e., up to $(\alpha_s\, L^2)^n$, with $L = \ln(Q_0/\mu_{\rm R})$.

In the leading logarithmic (LL) accuracy all double logarithms of the form $\alpha_s^n L^{n+1}$ in the exponent of the distribution are resummed, and in the next-to-leading logarithmic (NLL) accuracy all single logarithms $\alpha_s^n L^n$ are additionally resummed. The resummation of these large logarithms is particulary quite simple for observables that are inclusive over emissions in the entire angular phase space since typically a limited number of gluon emissions needs to be considered in order to reproduce the all-orders behaviour of the distribution of the said observables.

However, most of the observables that are interesting for new physics, are sensitive to radiation only in a restricted region of phase space and pointed out as non-global. The topic of resummation of NGLs has seen a lot of interest in the literature, see the introductory chapter 1. In this chapter we consider the integrated hemisphere mass distribution in the process $e^+e^- \to q\bar{q}$, and propose a solution to the BMS equation for NGLs in the form of an exponential. The exponent is written as a series in the strong coupling (or equivalently the evolution parameter), and we show how it may be resummed by illustrating the partial resummation of the two-loops

term in the exponent. The results we find are consistent with those obtained by Shwartz and Zhu in Ref. [96] which were written as an expansion in the coupling in the actual distribution and not in the exponent. The benefit of writing the series in the exponent is to avoid obvious interference terms that pop up in the series expansion. The proposed solution paves the way for a clearer picture for all-orders resummation as it subtracts away any such interferences. Additionally, the present work serves as a stringent test on the validity of both the BMS equation as well as the work done in Refs. [93, 102], by showing how Eikonal amplitudes used in the latter references are correctly reproduced by the BMS equation at large N_c up to six loops. We recall that the Eikonal amplitudes squared were computed at finite N_c in [93].

This chapter is organised as follows. In section 2 we define the observable and introduce our notation. In section 3 we write down the BMS equation and propose its solution as an exponential of a series in the strong coupling. We explicity treat each order in the exponent up to sixth order in the coupling, hence we extract Eikonal squared amplitudes from the BMS equation and compare with previous results in the literature, in section 4. In section 5 we perform necessary integrations in order to obtain the coefficients of the NGLs in the exponent up to five loops in the exponent. We show that the expansion of our result agrees with that found in Refs. [93, 96]. We then show how the resummation of the terms in the exponent may be achieved by considering only the resummation of the two-loops result. Finally, in section 6, we draw our conclusions.

5.2 Kinematics, observable and notation

To illustrate the resummation of NGLs and extract Eikonal amplitudes from the BMS equation we consider a simple observable, namely the hemisphere mass in dijet events in e^+e^- annihilation processes, where the hard scattering is accompanied with strongly-ordered soft gluon emissions $\omega_n \ll \cdots \ll \omega_2 \ll \omega_1 \ll Q$, with Q the hard scale and ω_i the energy of the i^{th} emission. The four-momenta of the outgoing quark (a), anti-quark (b) and gluons (i) are given by:

$$p_a = \frac{Q}{2}\,(1,0,0,1)\,, \tag{5.1a}$$

$$p_b = \frac{Q}{2}\,(1,0,0,-1)\,, \tag{5.1b}$$

$$k_i = \omega_i\,(1,\sin\theta_i\cos\phi_i,\sin\theta_i\sin\phi_i,\cos\theta_i)\,, \tag{5.1c}$$

where recoil effects are negligible in the single-logarithmic approximation. Here θ_i and ϕ_i are the polar and azimuthal angles of the i^{th} emission.

To compare our findings of Eikonal amplitudes to those presented in Ref. [93] we follow the same notation introduced therein. We define the *antenna* functions, which carry the dynamical

structure of the squared matrix elements, as follows:

$$w_{ab}^{i} = \omega_i^2 \, \frac{p_a \cdot p_b}{(p_a \cdot k_i)\,(k_i \cdot p_b)}\,, \tag{5.2a}$$

$$\mathcal{A}_{ab}^{ij} = w_{ab}^{i}\left(w_{ai}^{j} + w_{ib}^{j} - w_{ab}^{j}\right), \tag{5.2b}$$

$$\mathcal{B}_{ab}^{ijk} = w_{ab}^{i}\left(\mathcal{A}_{ai}^{jk} + \mathcal{A}_{ib}^{jk} - \mathcal{A}_{ab}^{jk}\right), \tag{5.2c}$$

$$\mathcal{C}_{ab}^{ijk\ell} = w_{ab}^{i}\left(\mathcal{B}_{ai}^{jk\ell} + \mathcal{B}_{ib}^{jk\ell} - \mathcal{B}_{ab}^{jk\ell}\right), \tag{5.2d}$$

$$\mathcal{D}_{ab}^{ijk\ell m} = w_{ab}^{i}\left(\mathcal{C}_{ai}^{jk\ell m} + \mathcal{C}_{ib}^{jk\ell m} - \mathcal{C}_{ab}^{jk\ell m}\right), \tag{5.2e}$$

$$\mathcal{E}_{ab}^{ijk\ell mn} = w_{ab}^{i}\left(\mathcal{D}_{ai}^{jk\ell mn} + \mathcal{D}_{ib}^{jk\ell mn} - \mathcal{D}_{ab}^{jk\ell mn}\right). \tag{5.2f}$$

Additionally we defined the reduced antenna functions $\bar{\mathcal{A}}_{ab}^{ij} = \mathcal{A}_{ab}^{ij}/w_{ab}^{i}$, and similarly for the other functions. The basic dipole antenna function w_{ab}^{i} may be recast as:

$$\begin{aligned} w_{ab}^{i} &= \frac{(ab)}{(ai)(ib)}\,, \\ (ij) &= 1 - \cos\theta_{ij} = 1 - c_i\,c_j - s_i\,s_j\cos\phi_{ij}\,, \end{aligned} \tag{5.3}$$

where, for compactness, we have adopted the notation $c_i \equiv \cos\theta_i$, $s_i \equiv \sin\theta_i$, and $\phi_{ij} = \phi_i - \phi_j$.

The observable we are interested in is the normalised (squared) invariant mass of the right hemisphere $\mathcal{H}_R$ (in the direction of the quark a):

$$\begin{aligned} \rho &= \left(p_a + \sum_{i\in\mathcal{H}_R} k_i\right)^2 /Q^2 \\ &= \sum_{i\in\mathcal{H}_R} 2\,k_i\cdot p_a/Q^2 = \sum_{i\in\mathcal{H}_R} x_i\,(1-\cos\theta_i)\,, \end{aligned} \tag{5.4}$$

where the sum runs over all gluon emissions inside the right hemisphere $\mathcal{H}_R$, and $x_i = \omega_i/Q$ is the energy fraction of the i^{th} emission.

5.3 The BMS equation and its solution

The hemisphere mass distribution is sensitive to soft and/or collinear gluon emissions leading to large logarithms $L = \ln(1/\rho)$ in the integrated distribution $\sigma(\rho)$ of this observable. At leading order in color (also known as the large-$\mathrm{N_c}$ approximation), this distribution satisfies a non-linear integro-differential equation known as the BMS equation [95]:

$$\frac{\partial\mathcal{G}_{ab}(t)}{\partial t} = \mathrm{N_c}\int\frac{\mathrm{d}\Omega_k}{4\pi}\,w_{ab}^{k}\left(\Theta_k^{\text{out}}\,\mathcal{G}_{ak}(t)\,\mathcal{G}_{kb}(t) - \mathcal{G}_{ab}(t)\right), \tag{5.5}$$

where the hemisphere mass distribution is just $\sigma(\rho) = \mathcal{G}_{ab}(t)$. The quantity $\mathcal{G}_{ab}(t)$ is generally interpreted as the probability that a given dipole (ab) whose directions are determined by solid angles Ω_a and Ω_b emits radiation which contributes to the hemisphere mass with a value less than ρ. We shall confine ourselves in the present work to the specific dipole $(ab) = (q\bar{q})$ fixed by $c_a = +1$ and $c_b = -1$, or equivalently $\theta_a = 0$ and $\theta_b = \pi$. The evolution parameter t is related to ρ by:

$$t = \frac{1}{\pi}\int_\rho^1 \frac{\mathrm{d}x}{x}\,\alpha_s(Q\,x) = -\frac{1}{2\pi\beta_0}\,\ln\left(1 - 2\alpha_s\beta_0 L\right), \tag{5.6}$$

with β_0 the one-loop coefficient of the QCD β function and the second equality holds at one-loop. In Eq. (5.5) $\mathrm{d}\Omega_k = \mathrm{d}c_k\mathrm{d}\phi_k$ is the differential solid angle of the emission k, and the step function Θ_k^{out} restricts this emission to be outside the measured hemisphere $\mathcal{H}_R$, thus $\Theta_k^{\text{out}} = \Theta(-c_k)$. We additionally have $\Theta_k^{\text{in}} = 1 - \Theta_k^{\text{out}} = \Theta(c_k)$. The solution to the BMS equation is unique with the initial condition $\mathcal{G}_{ab}(t = 0) = 1$. Typical values of t for phenomenological studies are in the range $0 \leq t \lesssim 0.5$.

The first term $\Theta_k^{\text{out}}\,\mathcal{G}_{ak}(t)\,\mathcal{G}_{kb}(t)$ in Eq. (5.5) represents real emission contributions while the subtracted term $\mathcal{G}_{ab}(t)$ represents the virtual-corrections, and they are both (when integrated) separately divergent when the emission is collinear to one of the hard dipoles. This collinear singularity is cancelled in the sum of the two terms. To avoid these divergences we rewrite the BMS equation in an alternative way: To avoid these divergences we rewrite the BMS equation in an alternative way:

$$\frac{\partial\mathcal{G}_{ab}(t)}{\partial t} = \mathrm{N_c}\int\frac{\mathrm{d}\Omega_k}{4\pi}\,w_{ab}^k\,\Theta_k^{\text{out}}\left(\mathcal{G}_{ak}(t)\,\mathcal{G}_{kb}(t) - \mathcal{G}_{ab}(t)\right) - \mathrm{N_c}\int\frac{\mathrm{d}\Omega_k}{4\pi}\,w_{ab}^k\,\Theta_k^{\text{in}}\,\mathcal{G}_{ab}(t)\,. \tag{5.7}$$

Equation (5.7) as it stands is still ill-defined, since there is another collinear singularity in the second term associated with emissions parallel to the quark (right-hemisphere) direction. This issue was also raised in Ref. [99]. In fact, the BMS equation was originally written for away-from-jets energy flow observables which are free from contributions of such emissions. Observables of this kind are sensitive only to soft wide-angle emissions and thus only have single logarithms. On the contrary, the hemisphere mass distribution has both single and double logarithms. This explains the origin of the divergence in Eq. (5.7). In order for the BMS equation to be valid in our case a kinematical cutoff needs to be applied to the second term in (5.7), namely a collinear cutoff $1 - c_k > \rho$. This cutoff naturally arises when using the "measurement operator" procedure to account for real and virtual contributions to the hemisphere mass as explained in Ref. [102].

This collinear singularity, however, only affects the resummation of double logarithms, which typically results in a Sudakov form factor, and does not enter the resummation of non-global logarithms. To see this, we recall that [94] non-global logarithms result from emissions near the boundary between the two hemispheres which is away from both quark and anti-quark

directions. Said differently, collinear emissions to the quark and anti-quark do not contribute to non-global logarithms. Since we are interested only in the resummation of non-global logarithms in this paper, and since the double logarithmic (Sudakov) form factor has been well treated before (see Ref. [104] and the Review [105]), we can therefore discard this divergence in the current paper.

5.3.1 Exponential solution

Based on the observation made in Ref. [102] about the possible exponentiation of NGLs, and given that the derivative of the function $\mathcal{G}_{ab}(t)$ in the BMS equation reproduces a phase-space integral over somewhat the same function, it is natural to propose an exponential solution with a series in the exponent of the form:

$$\mathcal{G}_{ab}(t) = \exp\left(\sum_{n=1}^{\infty} \frac{1}{n!}\, \mathcal{S}_{ab}^{(n)}\, \mathrm{N_c^n}\, t^n\right), \tag{5.8}$$

where $\mathcal{S}_{ab}^{(n)}$ are fixed coefficients. This proposed solution satisfies the boundary condition mentioned above at $t = 0$ and has the primary-emission Sudakov form factor (the term $n = 1$ in the exponent). This exponential form avoids the unnecessary dealing with "interference" terms discussed in Ref. [102], which can be seen here by expanding the exponential. The BMS equation does in fact admit this solution since, as we shall see, all the coefficients $\mathcal{S}_{ab}^{(n)}$ in the exponent are fully determined recursively down to the Sudakov term $\mathcal{S}_{ab}^{(1)}$, which too is fully determined.

Although the BMS equation is valid only at leading colour, one can write the series in the exponent in terms of the color factors $\mathrm{C_F} = (\mathrm{N_c^2} - 1)/(2\,\mathrm{N_c})$ and $\mathrm{C_A} = \mathrm{N_c}$ by merely replacing $\mathrm{N_c^n} \to 2\,\mathrm{C_F}\,\mathrm{C_A^{n-1}}$, where at large $\mathrm{N_c}$ we have $2\mathrm{C_F} = \mathrm{C_A} = \mathrm{N_c}$. This fact helps us *partially* restore the full color structure of the resummed non-global logarithms at finite $\mathrm{N_c}$. Further finite-$\mathrm{N_c}$ corrections totally not accounted for by the BMS equation, and which contribute a factor σ_{corr} (first appearing at $\mathcal{O}(\alpha_s^4)$) to the fully resummed distribution, are also required, such that:

$$\sigma_{\mathrm{full\,N_c}}(\rho) = \sigma_{\mathrm{large\,N_c}}(\rho) \times \sigma_{\mathrm{corr}}(\rho)\,, \tag{5.9a}$$

$$\sigma_{\mathrm{corr}}(\rho) = 1 + \mathcal{O}(\alpha_s^4)\,. \tag{5.9b}$$

The first term in $\sigma_{\mathrm{corr}}(\rho)$ was computed in Ref. [102] to be:

$$\frac{1}{4!}\,\bar{\alpha}_s^4\, L^4\, \mathrm{C_F}\, \mathrm{C_A^3} \left(\frac{1}{2} - \frac{\mathrm{C_F}}{\mathrm{C_A}}\right) \zeta_4\,, \tag{5.10}$$

with $\bar{\alpha}_s = \alpha_s/\pi$ and ζ is the Riemann zeta function.

5.3.2 Iteration of the series coefficients

We now show how the coefficients in the exponent of the exponential solution maybe found iteratively. Taking the derivative of the solution (5.8) with respect to t and renaming the summation index we obtain:

$$\frac{\partial \mathcal{G}_{ab}(t)}{\partial t} = \left(\sum_{n=0}^{\infty} \frac{1}{n!} \mathcal{S}_{ab}^{(n+1)} \, \mathrm{N_c}^{n+1} \, t^n \right) \times \mathcal{G}_{ab}(t) \,, \tag{5.11}$$

where we note that the sum here starts at $n = 0$. Substituting into the BMS equation and dividing both sides by $\mathrm{N_c}\, \mathcal{G}_{ab}(t)$ we obtain:

$$\begin{aligned} \sum_{n=0}^{\infty} \frac{1}{n!} \mathcal{S}_{ab}^{(n+1)} \, (\mathrm{N_c}\, t)^n = &- \int \frac{\mathrm{d}\Omega_k}{4\pi} \, \Theta_k^{\mathrm{in}} \, w_{ab}^k + \int \frac{\mathrm{d}\Omega_k}{4\pi} \, \Theta_k^{\mathrm{out}} \times \\ \times \, w_{ab}^k \left(\exp \left[\sum_{n=1}^{\infty} \frac{1}{n!} \left(\mathcal{S}_{ak}^{(n)} + \mathcal{S}_{kb}^{(n)} - \mathcal{S}_{ab}^{(n)} \right) (\mathrm{N_c}\, t)^n \right] - 1 \right) . \end{aligned} \tag{5.12}$$

In order to extract the coefficients $\mathcal{S}_{ab}^{(n)}$ at any order n it suffices to equate coefficients of $(\mathrm{N_c} t)^n$ from both sides of this equation. At zeroth order (equating coefficients of $(\mathrm{N_c}\, t)^0$) we have:

$$\mathcal{S}_{ab}^{(1)} = - \int \frac{\mathrm{d}\Omega_1}{4\pi} \, \Theta_1^{\mathrm{in}} \, w_{ab}^1 \,, \tag{5.13}$$

where we have set $k = 1$ to represent the first emission. This is the coefficient in the exponent of the Sudakov form factor. As stated earlier, this term is divergent and can be regulated by placing a collinear cutoff on the polar integration. However, this divergence is irrelevant for the calculation of NGLs and thus will not be considered further.

At higher loops we may write:

$$\begin{aligned} \sum_{n=1}^{\infty} \frac{1}{n!} \mathcal{S}_{ab}^{(n+1)} \, (\mathrm{N_c}\, t)^n = &\int \frac{\mathrm{d}\Omega_1}{4\pi} \, \Theta_1^{\mathrm{out}} \, w_{ab}^1 \times \\ \times \left(\exp \left[\sum_{n=1}^{\infty} \frac{1}{n!} \left(\mathcal{S}_{a1}^{(n)} + \mathcal{S}_{1b}^{(n)} - \mathcal{S}_{ab}^{(n)} \right) (\mathrm{N_c}\, t)^n \right] - 1 \right) . \end{aligned} \tag{5.14}$$

Denoting $\mathcal{X}_n = \mathcal{S}^{(n)}_{a1} + \mathcal{S}^{(n)}_{1b} - \mathcal{S}^{(n)}_{ab}$, and using the fact that:

$$\begin{aligned}
&\exp\left(\sum_{n=1}^{\infty} \frac{(\mathrm{N_c}\, t)^n}{n!}\, \mathcal{X}_n\right) - 1 = \frac{(\mathrm{N_c}\, t)^1}{1!}\, \mathcal{X}_1 + \\
&+ \frac{(\mathrm{N_c}\, t)^2}{2!} \left(\mathcal{X}_1^2 + \mathcal{X}_2\right) + \frac{(\mathrm{N_c}\, t)^3}{3!} \left(\mathcal{X}_1^3 + 3\, \mathcal{X}_1\, \mathcal{X}_2 + \mathcal{X}_3\right) + \\
&+ \frac{(\mathrm{N_c}\, t)^4}{4!} \left(\mathcal{X}_1^4 + 6\, \mathcal{X}_1^2\, \mathcal{X}_2 + 3\, \mathcal{X}_2^2 + 4\, \mathcal{X}_1\, \mathcal{X}_3 + \mathcal{X}_4\right) + \\
&+ \frac{(\mathrm{N_c}\, t)^5}{5!} \left(\mathcal{X}_1^5 + 10\, \mathcal{X}_1^3\, \mathcal{X}_2 + 15\, \mathcal{X}_1\, \mathcal{X}_2^2 + 10\, \mathcal{X}_1^2\, \mathcal{X}_3 + \right. \\
&\qquad \left. + 10\, \mathcal{X}_2\, \mathcal{X}_3 + 5\, \mathcal{X}_1\, \mathcal{X}_4 + \mathcal{X}_5\right) + \\
&+ \frac{(\mathrm{N_c}\, t)^6}{6!} \left(\mathcal{X}_1^6 + 15\, \mathcal{X}_1^4\, \mathcal{X}_2 + 45\, \mathcal{X}_1^2\, \mathcal{X}_2^2 + 15\, \mathcal{X}_2^3 + 20\, \mathcal{X}_1^3\, \mathcal{X}_3 + \right. \\
&\qquad + 60\, \mathcal{X}_1\, \mathcal{X}_2\, \mathcal{X}_3 + 10\, \mathcal{X}_3^2 + 15\, \mathcal{X}_1^2\, \mathcal{X}_4 + 15\, \mathcal{X}_2\, \mathcal{X}_4 + \\
&\qquad \left. + 6\, \mathcal{X}_1\, \mathcal{X}_5 + \mathcal{X}_6\right) + \mathcal{O}(t^7) \\
&\equiv \sum_{n=1}^{\infty} \frac{1}{n!}\, \mathcal{F}^{(n)}_{ab}(k_1)\, (\mathrm{N_c}\, t)^n\,,
\end{aligned} \tag{5.15}$$

we are able to compute all the coefficients $\mathcal{S}^{(n)}_{ab}$ recursively:

$$\mathcal{S}^{(n+1)}_{ab} = \int \frac{\mathrm{d}\Omega_1}{4\pi}\, \Theta^{\mathrm{out}}_1\, w^1_{ab}\, \mathcal{F}^{(n)}_{ab}(k_1)\,, \qquad n \geq 1\,, \tag{5.16}$$

where we note that all $\mathcal{F}^{(n)}_{ab}(k_1)$ are written as combinations of the functions χ_m with $m \leq n$. This means that the $(n+1)^{\mathrm{th}}$-order coefficient $\mathcal{S}^{(n+1)}_{ab}$ is written in terms of lower-order terms recursively. In what follows bellow we illustrate the evaluation of these coefficients up to sixth order. Going to higher orders is in principle possible though cumbersome.

5.3.3 Results up to six loops

The leading order at which NGLs first appear is the two-loops order, that is $\mathcal{O}(\alpha_s^2)$. At this order we have:

$$\begin{aligned}
\mathcal{S}^{(2)}_{ab} &= \int \frac{\mathrm{d}\Omega_1}{4\pi}\, \Theta^{\mathrm{out}}_1\, w^1_{ab}\, \mathcal{F}^{(1)}_{ab}(k_1) \\
&= \int \frac{\mathrm{d}\Omega_1}{4\pi}\, \Theta^{\mathrm{out}}_1\, w^1_{ab}\, \mathcal{X}_1 \\
&= \int \frac{\mathrm{d}\Omega_1}{4\pi}\, \Theta^{\mathrm{out}}_1\, w^1_{ab} \left(\mathcal{S}^{(1)}_{a1} + \mathcal{S}^{(1)}_{1b} - \mathcal{S}^{(1)}_{ab}\right) \\
&= -\int \frac{\mathrm{d}\Omega_1}{4\pi} \frac{\mathrm{d}\Omega_2}{4\pi}\, \Theta^{\mathrm{out}}_1\, \Theta^{\mathrm{in}}_2\, w^1_{ab} \left(w^2_{a1} + w^2_{1b} - w^2_{ab}\right) \\
&= -\int \frac{\mathrm{d}\Omega_{12}}{(4\pi)^2}\, \Theta^{\mathrm{out}}_1\, \Theta^{\mathrm{in}}_2\, \mathcal{A}^{12}_{ab}\,,
\end{aligned} \tag{5.17}$$

where we substituted the expressions for $\mathcal{S}^{(1)}_{ij}$ from the relation (5.13), and used the shorthand notation $\mathrm{d}\Omega_{12\ldots m} \equiv \mathrm{d}\Omega_1 \mathrm{d}\Omega_2 \ldots \mathrm{d}\Omega_m$.

At three loops we find:

$$\begin{aligned}\mathcal{S}^{(3)}_{ab} &= \int \frac{\mathrm{d}\Omega_1}{4\pi}\, \Theta^{\text{out}}_1\, w^1_{ab} \times \left[\left(\mathcal{S}^{(1)}_{a1} + \mathcal{S}^{(1)}_{1b} - \mathcal{S}^{(1)}_{ab}\right)^2 + \mathcal{S}^{(2)}_{a1} + \mathcal{S}^{(2)}_{1b} - \mathcal{S}^{(2)}_{ab}\right] \\ &= \int \frac{\mathrm{d}\Omega_{123}}{(4\pi)^3}\, \Theta^{\text{out}}_1\, \Theta^{\text{in}}_2\, \Theta^{\text{in}}_3\, \mathcal{A}^{12}_{ab}\, \bar{\mathcal{A}}^{13}_{ab} - \int \frac{\mathrm{d}\Omega_{123}}{(4\pi)^3}\, \Theta^{\text{out}}_1\, \Theta^{\text{out}}_2\, \Theta^{\text{in}}_3\, \mathcal{B}^{123}_{ab}\,. \end{aligned} \tag{5.18}$$

Similarly, at four loops we have the result:

$$\begin{aligned}\mathcal{S}^{(4)}_{ab} &= \int \frac{\mathrm{d}\Omega_1}{4\pi}\, \Theta^{\text{out}}_1\, w^1_{ab} \Bigg[\left(\mathcal{S}^{(1)}_{a1} + \mathcal{S}^{(1)}_{1b} - \mathcal{S}^{(1)}_{ab}\right)^3 + \\ &\quad + 3\left(\mathcal{S}^{(1)}_{a1} + \mathcal{S}^{(1)}_{1b} - \mathcal{S}^{(1)}_{ab}\right)\left(\mathcal{S}^{(2)}_{a1} + \mathcal{S}^{(2)}_{1b} - \mathcal{S}^{(2)}_{ab}\right) + \mathcal{S}^{(3)}_{a1} + \mathcal{S}^{(3)}_{1b} - \mathcal{S}^{(3)}_{ab}\Bigg] \\ &= -\int \frac{\mathrm{d}\Omega_{1234}}{(4\pi)^4}\, \Theta^{\text{out}}_1\, \Theta^{\text{in}}_2\, \Theta^{\text{in}}_3\, \Theta^{\text{in}}_4\, \mathcal{A}^{12}_{ab}\, \bar{\mathcal{A}}^{13}_{ab}\, \bar{\mathcal{A}}^{14}_{ab} + \\ &\quad + 3\int \frac{\mathrm{d}\Omega_{1234}}{(4\pi)^4}\, \Theta^{\text{out}}_1\, \Theta^{\text{in}}_2\, \Theta^{\text{out}}_3\, \Theta^{\text{in}}_4\, \mathcal{A}^{12}_{ab}\, \bar{\mathcal{B}}^{134}_{ab} + \\ &\quad + \int \frac{\mathrm{d}\Omega_{1234}}{(4\pi)^4}\, \Theta^{\text{out}}_1\, \Theta^{\text{out}}_2\, \Theta^{\text{in}}_3\, \Theta^{\text{in}}_4\, \mathfrak{A}^{1234}_{ab} - \\ &\quad - \int \frac{\mathrm{d}\Omega_{1234}}{(4\pi)^4}\, \Theta^{\text{out}}_1\, \Theta^{\text{out}}_2\, \Theta^{\text{out}}_3\, \Theta^{\text{in}}_4\, \mathcal{C}^{1234}_{ab}\,. \end{aligned} \tag{5.19}$$

where, inline with the notation used in Ref. [93], we introduced:

$$\mathfrak{A}^{ijk\ell}_{ab} = w^i_{ab}\left(\mathcal{A}^{jk}_{ai}\bar{\mathcal{A}}^{j\ell}_{ai} + \mathcal{A}^{jk}_{ib}\bar{\mathcal{A}}^{j\ell}_{ib} - \mathcal{A}^{jk}_{ab}\bar{\mathcal{A}}^{j\ell}_{ab}\right). \tag{5.20}$$

Furthermore, to present the five-loops coefficient, we introduce, as in Ref. [93]:

$$\mathbb{A}^{ijk\ell m}_{ab} = w^i_{ab}\left(\mathcal{A}^{jk}_{ai}\bar{\mathcal{A}}^{j\ell}_{ai}\bar{\mathcal{A}}^{jm}_{ai} + \mathcal{A}^{jk}_{ib}\bar{\mathcal{A}}^{j\ell}_{ib}\bar{\mathcal{A}}^{jm}_{ib} - \mathcal{A}^{jk}_{ab}\bar{\mathcal{A}}^{j\ell}_{ab}\bar{\mathcal{A}}^{jm}_{ab}\right), \tag{5.21a}$$

$$\tilde{\mathfrak{A}}^{ijk\ell m}_{ab} = w^i_{ab}\left(\mathcal{A}^{jk}_{ai}\bar{\mathcal{B}}^{j\ell m}_{ai} + \mathcal{A}^{jk}_{ib}\bar{\mathcal{B}}^{j\ell m}_{ib} - \mathcal{A}^{jk}_{ab}\bar{\mathcal{B}}^{j\ell m}_{ab}\right), \tag{5.21b}$$

$$\mathfrak{B}^{ijk\ell m}_{ab} = w^i_{ab}\left(\mathfrak{A}^{jk\ell m}_{ai} + \mathfrak{A}^{jk\ell m}_{ib} - \mathfrak{A}^{jk\ell m}_{ab}\right). \tag{5.21c}$$

Then, the five-loops coefficient reads:

$$\begin{aligned}\mathcal{S}^{(5)}_{ab} &= \int \frac{\mathrm{d}\Omega_1}{4\pi}\, w^1_{ab}\, \Theta^{\text{out}}_1 \Bigg[\left(\mathcal{S}^{(1)}_{a1} + \mathcal{S}^{(1)}_{1b} - \mathcal{S}^{(1)}_{ab}\right)^4 + \\ &\quad + 6\left(\mathcal{S}^{(1)}_{a1} + \mathcal{S}^{(1)}_{1b} - \mathcal{S}^{(1)}_{ab}\right)^2\left(\mathcal{S}^{(2)}_{a1} + \mathcal{S}^{(2)}_{1b} - \mathcal{S}^{(2)}_{ab}\right) + \\ &\quad + 4\left(\mathcal{S}^{(1)}_{a1} + \mathcal{S}^{(1)}_{1b} - \mathcal{S}^{(1)}_{ab}\right)\left(\mathcal{S}^{(3)}_{a1} + \mathcal{S}^{(3)}_{1b} - \mathcal{S}^{(3)}_{ab}\right) + \\ &\quad + 3\left(\mathcal{S}^{(2)}_{a1} + \mathcal{S}^{(2)}_{1b} - \mathcal{S}^{(2)}_{ab}\right)^2 + \mathcal{S}^{(4)}_{a1} + \mathcal{S}^{(4)}_{1b} - \mathcal{S}^{(4)}_{ab}\Bigg]. \end{aligned} \tag{5.22}$$

Substituting in terms of the antennas functions we find at this order:

$$\begin{aligned}
\mathcal{S}^{(5)}_{ab} = &\int \frac{\mathrm{d}\Omega_{12345}}{(4\pi)^5}\,\Theta^{\text{out}}_1\,\Theta^{\text{in}}_2\,\Theta^{\text{in}}_3\,\Theta^{\text{in}}_4\,\Theta^{\text{in}}_5\,\mathcal{A}^{12}_{ab}\,\bar{\mathcal{A}}^{13}_{ab}\,\bar{\mathcal{A}}^{14}_{ab}\,\bar{\mathcal{A}}^{15}_{ab} - \\
&- 6\int \frac{\mathrm{d}\Omega_{12345}}{(4\pi)^5}\,\Theta^{\text{out}}_1\,\Theta^{\text{out}}_2\,\Theta^{\text{in}}_3\,\Theta^{\text{in}}_4\,\Theta^{\text{in}}_5\,\mathcal{B}^{123}_{ab}\,\bar{\mathcal{A}}^{14}_{ab}\,\bar{\mathcal{A}}^{15}_{ab} + \\
&+ 3\int \frac{\mathrm{d}\Omega_{12345}}{(4\pi)^5}\,\Theta^{\text{out}}_1\,\Theta^{\text{out}}_2\,\Theta^{\text{in}}_3\,\Theta^{\text{out}}_4\,\Theta^{\text{in}}_5\,\mathcal{B}^{123}_{ab}\,\bar{\mathcal{B}}^{145}_{ab} - \\
&- 4\int \frac{\mathrm{d}\Omega_{12345}}{(4\pi)^5}\,\Theta^{\text{out}}_1\,\Theta^{\text{out}}_2\,\Theta^{\text{in}}_3\,\Theta^{\text{in}}_4\,\Theta^{\text{in}}_5\,\mathcal{A}^{15}_{ab}\,\bar{\mathfrak{A}}^{1234}_{ab} + \\
&+ 4\int \frac{\mathrm{d}\Omega_{12345}}{(4\pi)^5}\,\Theta^{\text{out}}_1\,\Theta^{\text{out}}_2\,\Theta^{\text{out}}_3\,\Theta^{\text{in}}_4\,\Theta^{\text{in}}_5\,\mathcal{A}^{15}_{ab}\,\bar{\mathcal{C}}^{1234}_{ab} - \\
&- \int \frac{\mathrm{d}\Omega_{12345}}{(4\pi)^5}\,\Theta^{\text{out}}_1\,\Theta^{\text{out}}_2\,\Theta^{\text{in}}_3\,\Theta^{\text{in}}_4\,\Theta^{\text{in}}_5\,\mathbb{A}^{12345}_{ab} + \\
&+ 3\int \frac{\mathrm{d}\Omega_{12345}}{(4\pi)^5}\,\Theta^{\text{out}}_1\,\Theta^{\text{out}}_2\,\Theta^{\text{in}}_3\,\Theta^{\text{out}}_4\,\Theta^{\text{in}}_5\,\tilde{\mathfrak{A}}^{12345}_{ab} + \\
&+ \int \frac{\mathrm{d}\Omega_{12345}}{(4\pi)^5}\,\Theta^{\text{out}}_1\,\Theta^{\text{out}}_2\,\Theta^{\text{out}}_3\,\Theta^{\text{in}}_4\,\Theta^{\text{in}}_5\,\mathfrak{B}^{12345}_{ab} - \\
&- \int \frac{\mathrm{d}\Omega_{12345}}{(4\pi)^5}\,\Theta^{\text{out}}_1\,\Theta^{\text{out}}_2\,\Theta^{\text{out}}_3\,\Theta^{\text{out}}_4\,\Theta^{\text{in}}_5\,\mathcal{D}^{12345}_{ab}\,.
\end{aligned} \tag{5.23}$$

For the presentation of the six-loops result we shall need the following definitions:

$$\mathbb{B}^{ijk\ell mn}_{ab} = w^i_{ab}\left(\mathbb{A}^{jk\ell mn}_{ai} + \mathbb{A}^{jk\ell mn}_{ib} - \mathbb{A}^{jk\ell mn}_{ab}\right), \tag{5.24a}$$

$$\tilde{\mathfrak{B}}^{ijk\ell mn}_{ab} = w^i_{ab}\left(\tilde{\mathfrak{A}}^{jk\ell mn}_{ai} + \tilde{\mathfrak{A}}^{jk\ell mn}_{ib} - \tilde{\mathfrak{A}}^{jk\ell mn}_{ab}\right), \tag{5.24b}$$

$$\mathfrak{C}^{ijk\ell mn}_{ab} = w^i_{ab}\left(\mathfrak{B}^{jk\ell mn}_{ai} + \mathfrak{B}^{jk\ell mn}_{ib} - \tilde{\mathfrak{B}}^{jk\ell mn}_{ab}\right). \tag{5.24c}$$

At this order we have:

$$\begin{aligned}
\mathcal{S}^{(6)}_{ab} = &\int \frac{\mathrm{d}\Omega_1}{4\pi}\,w^1_{ab}\,\Theta^{\text{out}}_1\Bigg[\left(\mathcal{S}^{(1)}_{a1} + \mathcal{S}^{(1)}_{1b} - \mathcal{S}^{(1)}_{ab}\right)^5 + \\
&+ 10\left(\mathcal{S}^{(1)}_{a1} + \mathcal{S}^{(1)}_{1b} - \mathcal{S}^{(1)}_{ab}\right)^3\left(\mathcal{S}^{(2)}_{a1} + \mathcal{S}^{(2)}_{1b} - \mathcal{S}^{(2)}_{ab}\right) + \\
&+ 15\left(\mathcal{S}^{(1)}_{a1} + \mathcal{S}^{(1)}_{1b} - \mathcal{S}^{(1)}_{ab}\right)\left(\mathcal{S}^{(2)}_{a1} + \mathcal{S}^{(2)}_{1b} - \mathcal{S}^{(2)}_{ab}\right)^2 + \\
&+ 10\left(\mathcal{S}^{(1)}_{a1} + \mathcal{S}^{(1)}_{1b} - \mathcal{S}^{(1)}_{ab}\right)^2\left(\mathcal{S}^{(3)}_{a1} + \mathcal{S}^{(3)}_{1b} - \mathcal{S}^{(3)}_{ab}\right) + \\
&+ 10\left(\mathcal{S}^{(2)}_{a1} + \mathcal{S}^{(2)}_{1b} - \mathcal{S}^{(2)}_{ab}\right)\left(\mathcal{S}^{(3)}_{a1} + \mathcal{S}^{(3)}_{1b} - \mathcal{S}^{(3)}_{ab}\right) + \\
&+ 5\left(\mathcal{S}^{(1)}_{a1} + \mathcal{S}^{(1)}_{1b} - \mathcal{S}^{(1)}_{ab}\right)\left(\mathcal{S}^{(4)}_{a1} + \mathcal{S}^{(4)}_{1b} - \mathcal{S}^{(4)}_{ab}\right) + \\
&+ \mathcal{S}^{(5)}_{a1} + \mathcal{S}^{(5)}_{1b} - \mathcal{S}^{(5)}_{ab}\Bigg].
\end{aligned} \tag{5.25}$$

Explicitly written we have:

$$
\begin{aligned}
\mathcal{S}^{(6)}_{ab} = &- \int \frac{\mathrm{d}\Omega_{1\dots6}}{(4\pi)^6}\, \Theta_1^{\mathrm{out}}\Theta_2^{\mathrm{out}}\Theta_3^{\mathrm{out}}\Theta_4^{\mathrm{out}}\Theta_5^{\mathrm{out}}\Theta_6^{\mathrm{in}}\, \mathcal{E}^{123456}_{ab} \\
&- \int \frac{\mathrm{d}\Omega_{1\dots6}}{(4\pi)^6}\, \Theta_1^{\mathrm{out}}\Theta_2^{\mathrm{in}}\Theta_3^{\mathrm{in}}\Theta_4^{\mathrm{in}}\Theta_5^{\mathrm{in}}\Theta_6^{\mathrm{in}}\, \mathcal{A}^{12}_{ab}\bar{\mathcal{A}}^{13}_{ab}\bar{\mathcal{A}}^{14}_{ab}\bar{\mathcal{A}}^{15}_{ab}\bar{\mathcal{A}}^{16}_{ab} \\
&+ 10 \int \frac{\mathrm{d}\Omega_{1\dots6}}{(4\pi)^6}\, \Theta_1^{\mathrm{out}}\Theta_2^{\mathrm{in}}\Theta_3^{\mathrm{in}}\Theta_4^{\mathrm{in}}\Theta_5^{\mathrm{out}}\Theta_6^{\mathrm{in}}\, \mathcal{A}^{12}_{ab}\bar{\mathcal{A}}^{13}_{ab}\bar{\mathcal{A}}^{14}_{ab}\bar{\mathcal{B}}^{156}_{ab} \\
&- 15 \int \frac{\mathrm{d}\Omega_{1\dots6}}{(4\pi)^6}\, \Theta_1^{\mathrm{out}}\Theta_2^{\mathrm{in}}\Theta_3^{\mathrm{out}}\Theta_4^{\mathrm{in}}\Theta_5^{\mathrm{out}}\Theta_6^{\mathrm{in}}\, \mathcal{A}^{12}_{ab}\bar{\mathcal{B}}^{134}_{ab}\bar{\mathcal{B}}^{156}_{ab} \\
&- 10 \int \frac{\mathrm{d}\Omega_{1\dots6}}{(4\pi)^6}\, \Theta_1^{\mathrm{out}}\Theta_2^{\mathrm{in}}\Theta_3^{\mathrm{in}}\Theta_4^{\mathrm{out}}\Theta_5^{\mathrm{out}}\Theta_6^{\mathrm{in}}\, \mathcal{A}^{12}_{ab}\bar{\mathcal{A}}^{13}_{ab}\bar{\mathcal{C}}^{1456}_{ab} \\
&+ 10 \int \frac{\mathrm{d}\Omega_{1\dots6}}{(4\pi)^6}\, \Theta_1^{\mathrm{out}}\Theta_2^{\mathrm{out}}\Theta_3^{\mathrm{in}}\Theta_4^{\mathrm{out}}\Theta_5^{\mathrm{out}}\Theta_6^{\mathrm{in}}\, \mathcal{B}^{123}_{ab}\bar{\mathcal{C}}^{1456}_{ab} \\
&+ 10 \int \frac{\mathrm{d}\Omega_{1\dots6}}{(4\pi)^6}\, \Theta_1^{\mathrm{out}}\Theta_2^{\mathrm{in}}\Theta_3^{\mathrm{in}}\Theta_4^{\mathrm{out}}\Theta_5^{\mathrm{in}}\Theta_6^{\mathrm{in}}\, \mathcal{A}^{12}_{ab}\bar{\mathcal{A}}^{13}_{ab}\bar{\mathfrak{A}}^{1456}_{ab} \\
&- 10 \int \frac{\mathrm{d}\Omega_{1\dots6}}{(4\pi)^6}\, \Theta_1^{\mathrm{out}}\Theta_2^{\mathrm{out}}\Theta_3^{\mathrm{in}}\Theta_4^{\mathrm{out}}\Theta_5^{\mathrm{in}}\Theta_6^{\mathrm{in}}\, \mathcal{B}^{123}_{ab}\bar{\mathfrak{A}}^{1456}_{ab} \\
&+ 5 \int \frac{\mathrm{d}\Omega_{1\dots6}}{(4\pi)^6}\, \Theta_1^{\mathrm{out}}\Theta_2^{\mathrm{in}}\Theta_3^{\mathrm{out}}\Theta_4^{\mathrm{in}}\Theta_5^{\mathrm{in}}\Theta_6^{\mathrm{in}}\, \mathcal{A}^{12}_{ab}\bar{\mathbb{A}}^{13456}_{ab} \\
&- 15 \int \frac{\mathrm{d}\Omega_{1\dots6}}{(4\pi)^6}\, \Theta_1^{\mathrm{out}}\Theta_2^{\mathrm{in}}\Theta_3^{\mathrm{out}}\Theta_4^{\mathrm{in}}\Theta_5^{\mathrm{out}}\Theta_6^{\mathrm{in}}\, \mathcal{A}^{12}_{ab}\bar{\bar{\mathfrak{A}}}^{13456}_{ab} \\
&- 5 \int \frac{\mathrm{d}\Omega_{1\dots6}}{(4\pi)^6}\, \Theta_1^{\mathrm{out}}\Theta_2^{\mathrm{in}}\Theta_3^{\mathrm{out}}\Theta_4^{\mathrm{out}}\Theta_5^{\mathrm{in}}\Theta_6^{\mathrm{in}}\, \mathcal{A}^{12}_{ab}\bar{\mathfrak{B}}^{13456}_{ab} \\
&+ 5 \int \frac{\mathrm{d}\Omega_{1\dots6}}{(4\pi)^6}\, \Theta_1^{\mathrm{out}}\Theta_2^{\mathrm{in}}\Theta_3^{\mathrm{out}}\Theta_4^{\mathrm{out}}\Theta_5^{\mathrm{out}}\Theta_6^{\mathrm{in}}\, \mathcal{A}^{12}_{ab}\bar{\mathcal{D}}^{13456}_{ab} + \\
&+ \int \frac{\mathrm{d}\Omega_{1\dots6}}{(4\pi)^6}\, \Theta_1^{\mathrm{out}}\Theta_2^{\mathrm{out}}\Theta_3^{\mathrm{in}}\Theta_4^{\mathrm{in}}\Theta_5^{\mathrm{in}}\Theta_6^{\mathrm{in}}\, \mathcal{J}^{123456}_{ab} \\
&- 6 \int \frac{\mathrm{d}\Omega_{1\dots6}}{(4\pi)^6}\, \Theta_1^{\mathrm{out}}\Theta_2^{\mathrm{out}}\Theta_3^{\mathrm{out}}\Theta_4^{\mathrm{in}}\Theta_5^{\mathrm{in}}\Theta_6^{\mathrm{in}}\, \mathcal{K}^{123456}_{ab} \\
&+ 3 \int \frac{\mathrm{d}\Omega_{1\dots6}}{(4\pi)^6}\, \Theta_1^{\mathrm{out}}\Theta_2^{\mathrm{out}}\Theta_3^{\mathrm{out}}\Theta_4^{\mathrm{in}}\Theta_5^{\mathrm{out}}\Theta_6^{\mathrm{in}}\, \mathcal{L}^{123456}_{ab} \\
&+ 4 \int \frac{\mathrm{d}\Omega_{1\dots6}}{(4\pi)^6}\, \Theta_1^{\mathrm{out}}\Theta_2^{\mathrm{out}}\Theta_3^{\mathrm{out}}\Theta_4^{\mathrm{out}}\Theta_5^{\mathrm{in}}\Theta_6^{\mathrm{in}}\, \mathcal{P}^{123456}_{ab} \\
&- 4 \int \frac{\mathrm{d}\Omega_{1\dots6}}{(4\pi)^6}\, \Theta_1^{\mathrm{out}}\Theta_2^{\mathrm{out}}\Theta_3^{\mathrm{out}}\Theta_4^{\mathrm{in}}\Theta_5^{\mathrm{in}}\Theta_6^{\mathrm{in}}\, \mathcal{Q}^{123456}_{ab} \\
&- \int \frac{\mathrm{d}\Omega_{1\dots6}}{(4\pi)^6}\, \Theta_1^{\mathrm{out}}\Theta_2^{\mathrm{out}}\Theta_3^{\mathrm{out}}\Theta_4^{\mathrm{in}}\Theta_5^{\mathrm{in}}\Theta_6^{\mathrm{in}}\, \mathbb{B}^{123456}_{ab} \\
&+ 3 \int \frac{\mathrm{d}\Omega_{1\dots6}}{(4\pi)^6}\, \Theta_1^{\mathrm{out}}\Theta_2^{\mathrm{out}}\Theta_3^{\mathrm{out}}\Theta_4^{\mathrm{in}}\Theta_5^{\mathrm{out}}\Theta_6^{\mathrm{in}}\, \tilde{\mathfrak{B}}^{123456}_{ab} \\
&+ \int \frac{\mathrm{d}\Omega_{1\dots6}}{(4\pi)^6}\, \Theta_1^{\mathrm{out}}\Theta_2^{\mathrm{out}}\Theta_3^{\mathrm{out}}\Theta_4^{\mathrm{out}}\Theta_5^{\mathrm{in}}\Theta_6^{\mathrm{in}}\, \mathfrak{C}^{123456}_{ab}\,,
\end{aligned}
\tag{5.26}
$$

where

$$
\mathcal{J}^{ijk\ell mn}_{ab} = w^i_{ab}\left(\mathcal{A}^{jk}_{ai}\bar{\mathcal{A}}^{j\ell}_{ai}\bar{\mathcal{A}}^{jm}_{ai}\bar{\mathcal{A}}^{jn}_{ai} + \mathcal{A}^{jk}_{ib}\bar{\mathcal{A}}^{j\ell}_{ib}\bar{\mathcal{A}}^{jm}_{ib}\bar{\mathcal{A}}^{jn}_{ib} - \mathcal{A}^{jk}_{ab}\bar{\mathcal{A}}^{j\ell}_{ab}\bar{\mathcal{A}}^{jm}_{ab}\bar{\mathcal{A}}^{jn}_{ab}\right), \tag{5.27a}
$$

$$\mathcal{K}_{ab}^{ijk\ell mn} = w_{ab}^{i}\left(\mathcal{B}_{ai}^{jk\ell}\bar{\mathcal{A}}_{ai}^{jm}\bar{\mathcal{A}}_{ai}^{jn} + \mathcal{B}_{ib}^{jk\ell}\bar{\mathcal{A}}_{ib}^{jm}\bar{\mathcal{A}}_{ib}^{jn} - \mathcal{B}_{ab}^{jk\ell}\bar{\mathcal{A}}_{ab}^{jm}\bar{\mathcal{A}}_{ab}^{jn}\right), \tag{5.27b}$$

$$\mathcal{L}_{ab}^{ijk\ell mn} = w_{ab}^{i}\left(\mathcal{B}_{ai}^{jk\ell}\bar{\mathcal{B}}_{ai}^{jmn} + \mathcal{B}_{ib}^{jk\ell}\bar{\mathcal{B}}_{ib}^{jmn} - \mathcal{B}_{ab}^{jk\ell}\bar{\mathcal{B}}_{ab}^{jmn}\right), \tag{5.27c}$$

$$\mathcal{P}_{ab}^{ijk\ell mn} = w_{ab}^{i}\left(\mathcal{A}_{ai}^{jn}\bar{\mathcal{C}}_{ai}^{jk\ell m} + \mathcal{A}_{ib}^{jn}\bar{\mathcal{C}}_{ib}^{jk\ell m} - \mathcal{A}_{ab}^{jn}\bar{\mathcal{C}}_{ab}^{jk\ell m}\right), \tag{5.27d}$$

$$\mathcal{Q}_{ab}^{ijk\ell mn} = w_{ab}^{i}\left(\mathcal{A}_{ai}^{jn}\bar{\mathfrak{A}}_{ai}^{jk\ell m} + \mathcal{A}_{ib}^{jn}\bar{\mathfrak{A}}_{ib}^{jk\ell m} - \mathcal{A}_{ab}^{jn}\bar{\mathfrak{A}}_{ab}^{jk\ell m}\right). \tag{5.27e}$$

At this point we emphasise that the unintegrated results $\mathcal{S}_{ab}^{(n)}$ that we have presented are in fact very general and applicable to the computation of the distribution of any non-global observable, at large $\mathrm{N_c}$. The evaluation of these integrals for the specific case of the hemisphere mass distribution will be presented in section 5. Before doing so, we show, in the next section, how Eikonal amplitudes squared for the emission of soft energy-ordered gluons up to six-loops at large $\mathrm{N_c}$ maybe extracted from the above expressions for $\mathcal{S}_{ab}^{(n)}$.

5.4 Eikonal amplitudes from the BMS equation

The integrals involved in the evaluation of each of the coefficients $\mathcal{S}_{ab}^{(n)}$ correctly reproduce the squared Eikonal amplitudes for the emission of n soft energy-ordered gluons. The phase space of these integrals encodes the impact of the "measurement operator", introduced in Ref. [96], on the various squared amplitudes corresponding to all possible real/virtual gluon configurations at a given order n, in addition to the possible angular configurations (inside or outside the measured region). Furthermore, the constant integers that appear in front of the integrals merely result from identical contributions of different permutations of the emitted gluons. Take, for instance, the four-loops term from Eq. (5.18):

$$3\int \frac{\mathrm{d}\Omega_{1234}}{(4\pi)^4}\,\Theta_1^{\mathrm{out}}\,\Theta_2^{\mathrm{in}}\,\Theta_3^{\mathrm{out}}\,\Theta_4^{\mathrm{in}}\,\mathcal{A}_{ab}^{12}\,\bar{\mathcal{B}}_{ab}^{134}\,. \tag{5.28}$$

This term can be rewritten as:

$$\int \frac{\mathrm{d}\Omega_{1234}}{(4\pi)^4}\Big[\Theta_1^{\mathrm{out}}\,\Theta_2^{\mathrm{in}}\,\Theta_3^{\mathrm{out}}\,\Theta_4^{\mathrm{in}}\,\mathcal{A}_{ab}^{12}\,\bar{\mathcal{B}}_{ab}^{134} + \Theta_1^{\mathrm{out}}\,\Theta_2^{\mathrm{out}}\,\Theta_3^{\mathrm{in}}\,\Theta_4^{\mathrm{in}}\,\mathcal{A}_{ab}^{13}\,\bar{\mathcal{B}}_{ab}^{124} + \\ + \Theta_1^{\mathrm{out}}\,\Theta_2^{\mathrm{out}}\,\Theta_3^{\mathrm{in}}\,\Theta_4^{\mathrm{in}}\,\mathcal{A}_{ab}^{14}\,\bar{\mathcal{B}}_{ab}^{123}\Big]\,. \tag{5.29}$$

These three terms actually give identical results after integration, but each of them originates from a different term in the amplitude squared that comes from one of the permutations of the emitted gluons. The color factor associated with the amplitudes that we extract at n^{th} order is, at large $\mathrm{N_c}$, $\mathrm{N_c^n}$. As stated before, we invoke the replacement $\mathrm{N_c^n} \to 2\,\mathrm{C_F}\,\mathrm{C_A^{n-1}}$ in order to partially restore the full $\mathrm{N_c}$ color structure of the squared amplitudes.

It should be emphasised, though, that the results presented in the previous section explicitly

reproduce just what was referred to in Ref. [93] as the "*irreducible*" parts of the squared amplitudes at a given order. The "*reducible*" parts of the squared Eikonal amplitudes are related to the interference terms that one obtains by expanding the proposed exponential solution (5.8). The reducible parts of the squared amplitudes at order n are written purely in terms of squared amplitudes at previous orders $m < n$. Extracting these amplitudes is trivial and we shall show the results below.

In remaining part of this section we present the emission squared amplitudes deduced from the exponential solution of the BMS equation up to six loops. We follow the notation of Ref. [93], where $\mathcal{W}^{X}_{12\ldots m}$ represents the m-gluon emission amplitude squared with real-virtual configurations denoted by X. For instance, $\mathcal{W}^{\rm RVR}_{123}$ is the squared amplitude of emission of 3 gluons with k_1 and k_3 being real and k_2 being virtual. We shall only present the real emission amplitudes. The virtual corrections may readily be deduced from the latter as explained in Ref. [93].

The squared amplitude for the emission of a single soft gluon ($n = 1$) off a dipole (ab) is read from the expression of $\mathcal{S}^{(1)}_{ab}$ (5.13) to be:

$$\mathcal{W}^{\rm R}_{1} = 2\,{\rm C_F}\,w^{1}_{ab}\,. \tag{5.30}$$

At two loops, the emission squared amplitude is given by:

$$\mathcal{W}^{\rm RR}_{12} = \mathcal{W}^{\rm R}_{1}\mathcal{W}^{\rm R}_{2} + \overline{\mathcal{W}}^{\rm RR}_{12}\,, \tag{5.31}$$

where the irreducible two-loops part is read from $\mathcal{S}^{(2)}_{ab}$ (last line of Eq. (5.17)) to be:

$$\overline{\mathcal{W}}^{\rm RR}_{12} = 2\,{\rm C_F}\,{\rm C_A}\,\mathcal{A}^{12}_{ab}\,. \tag{5.32}$$

At three loops we have:

$$\mathcal{W}^{\rm RR}_{123} = \mathcal{W}^{\rm R}_{1}\mathcal{W}^{\rm R}_{2}\mathcal{W}^{\rm R}_{3} + \mathcal{W}^{\rm R}_{1}\overline{\mathcal{W}}^{\rm RR}_{23} + \mathcal{W}^{\rm R}_{2}\overline{\mathcal{W}}^{\rm RR}_{13} + \mathcal{W}^{\rm R}_{3}\overline{\mathcal{W}}^{\rm RR}_{12} + \overline{\mathcal{W}}^{\rm RRR}_{123}\,, \tag{5.33}$$

with the totally irreducible component (read from Eq. (5.18)):

$$\overline{\mathcal{W}}^{\rm RRR}_{123} = 2{\rm C_F}{\rm C}^2_{\rm A}\left(\mathcal{A}^{12}_{ab}\,\bar{\mathcal{A}}^{13}_{ab} + \mathcal{B}^{123}_{ab}\right). \tag{5.34}$$

We note here that the minus sign associated with the term $\mathcal{B}^{123}_{ab}$ in (5.18), as well as the different phase space of integration in the two terms of this equation, results from consideration of virtual contributions. This is clearly explained in Ref. [102]. For instance, the contribution $\Theta^{\rm out}_1\,\Theta^{\rm in}_2\,\Theta^{\rm in}_3\,\mathcal{A}^{12}_{ab}\,\bar{\mathcal{A}}^{13}_{ab}$ is associated with the irreducible part of the squared amplitude of emission

$\overline{\mathcal{W}}^{\mathrm{RVR}}_{123}$ with gluon k_2 being virtual:

$$\overline{\mathcal{W}}^{\mathrm{RVR}}_{123} = -2\mathrm{C_F}\mathrm{C_A^2}\mathcal{A}^{12}_{ab}\bar{\mathcal{A}}^{13}_{ab}\,, \tag{5.35}$$

while the contribution $\Theta^{\mathrm{out}}_1\,\Theta^{\mathrm{out}}_2\,\Theta^{\mathrm{in}}_3\,\mathcal{B}^{123}_{ab}$ is associated with the contribution of the sum of the two terms $\overline{\mathcal{W}}^{\mathrm{RVR}}_{123} + \overline{\mathcal{W}}^{\mathrm{RRR}}_{123}$, as explained in Ref. [102].

The four loops emission squared amplitude is given by:

$$\begin{aligned}\mathcal{W}^{\mathrm{RRRR}}_{1234} = \mathcal{W}^{\mathrm{R}}_1\mathcal{W}^{\mathrm{R}}_2\mathcal{W}^{\mathrm{R}}_3\mathcal{W}^{\mathrm{R}}_4 + \Big(\mathcal{W}^{\mathrm{R}}_1\mathcal{W}^{\mathrm{R}}_2\overline{\mathcal{W}}^{\mathrm{RR}}_{34} + \mathrm{perm.}\Big) + \Big(\overline{\mathcal{W}}^{\mathrm{RR}}_{12}\overline{\mathcal{W}}^{\mathrm{RR}}_{34} + \mathrm{perm.}\Big) \\ + \Big(\mathcal{W}^{\mathrm{R}}_1\overline{\mathcal{W}}^{\mathrm{RRR}}_{234} + \mathrm{perm.}\Big) + \overline{\mathcal{W}}^{\mathrm{RRRR}}_{1234} + \text{finite-}\mathrm{N_c}\text{ contributions}\,,\end{aligned} \tag{5.36}$$

where "perm." stands for all possible permutations of the gluons that do not reproduce the same term twice (in order to avoid double counting). The irreducible part of the squared amplitude at this order is read from Eq. (5.19) to be:

$$\overline{\mathcal{W}}^{\mathrm{RRRR}}_{1234} = 2\mathrm{C_F}\mathrm{C_A^3}\left(\mathcal{A}^{12}_{ab}\bar{\mathcal{A}}^{13}_{ab}\bar{\mathcal{A}}^{14}_{ab} + \mathfrak{A}^{1234}_{ab} + \mathcal{C}^{1234}_{ab} + \mathcal{A}^{12}_{ab}\bar{\mathcal{B}}^{134}_{ab} + \mathcal{A}^{13}_{ab}\bar{\mathcal{B}}^{124}_{ab} + \mathcal{A}^{14}_{ab}\bar{\mathcal{B}}^{123}_{ab}\right). \tag{5.37}$$

The five loops emission squared amplitude is given by:

$$\begin{aligned}\mathcal{W}^{\mathrm{RRRRR}}_{12345} = \mathcal{W}^{\mathrm{R}}_1\mathcal{W}^{\mathrm{R}}_2\mathcal{W}^{\mathrm{R}}_3\mathcal{W}^{\mathrm{R}}_4\mathcal{W}^{\mathrm{R}}_5 + \Big(\mathcal{W}^{\mathrm{R}}_1\mathcal{W}^{\mathrm{R}}_2\mathcal{W}^{\mathrm{R}}_3\overline{\mathcal{W}}^{\mathrm{RR}}_{45} + \mathrm{perm.}\Big) + \\ + \Big(\mathcal{W}^{\mathrm{R}}_1\overline{\mathcal{W}}^{\mathrm{RR}}_{23}\overline{\mathcal{W}}^{\mathrm{RR}}_{45} + \mathrm{permu.}\Big) + \Big(\mathcal{W}^{\mathrm{R}}_1\mathcal{W}^{\mathrm{R}}_2\overline{\mathcal{W}}^{\mathrm{RRR}}_{345} + \mathrm{perm.}\Big) + \\ + \Big(\overline{\mathcal{W}}^{\mathrm{RR}}_{12}\overline{\mathcal{W}}^{\mathrm{RRR}}_{345} + \mathrm{perm.}\Big) + \Big(\mathcal{W}^{\mathrm{R}}_1\overline{\mathcal{W}}^{\mathrm{RRRR}}_{2345} + \mathrm{perm.}\Big) + \\ + \overline{\mathcal{W}}^{\mathrm{RRRRR}}_{12345} + \text{finite-}\mathrm{N_c}\text{ contributions}\,.\end{aligned} \tag{5.38}$$

The irreducible contribution can be read from Eq. (5.23):

$$\begin{aligned}\overline{\mathcal{W}}^{\mathrm{RRRRR}}_{12345} = 2\,\mathrm{C_F}\mathrm{C_A^4}\,\Big(\mathcal{D}^{12345}_{ab} + \mathcal{A}^{12}_{ab}\,\bar{\mathcal{A}}^{13}_{ab}\,\bar{\mathcal{A}}^{14}_{ab}\,\bar{\mathcal{A}}^{15}_{ab} + \mathcal{B}^{123}_{ab}\,\bar{\mathcal{A}}^{14}_{ab}\,\bar{\mathcal{A}}^{15}_{ab} + \mathcal{B}^{124}_{ab}\,\bar{\mathcal{A}}^{13}_{ab}\,\bar{\mathcal{A}}^{15}_{ab} + \\ + \mathcal{B}^{125}_{ab}\,\bar{\mathcal{A}}^{13}_{ab}\,\bar{\mathcal{A}}^{14}_{ab} + \mathcal{B}^{134}_{ab}\,\bar{\mathcal{A}}^{12}_{ab}\,\bar{\mathcal{A}}^{15}_{ab} + \mathcal{B}^{135}_{ab}\,\bar{\mathcal{A}}^{12}_{ab}\,\bar{\mathcal{A}}^{14}_{ab} + \mathcal{B}^{145}_{ab}\,\bar{\mathcal{A}}^{12}_{ab}\,\bar{\mathcal{A}}^{13}_{ab} + \\ + \mathcal{B}^{123}_{ab}\,\bar{\mathcal{B}}^{145}_{ab} + \mathcal{B}^{124}_{ab}\,\bar{\mathcal{B}}^{135}_{ab} + \mathcal{B}^{125}_{ab}\,\bar{\mathcal{B}}^{134}_{ab} + \mathcal{A}^{15}_{ab}\,\bar{\mathfrak{A}}^{1234}_{ab} + \mathcal{A}^{14}_{ab}\,\bar{\mathfrak{A}}^{1235}_{ab} + \\ + \mathcal{A}^{13}_{ab}\,\bar{\mathfrak{A}}^{1245}_{ab} + \mathcal{A}^{12}_{ab}\,\bar{\mathfrak{A}}^{1345}_{ab} + \mathcal{A}^{15}_{ab}\,\bar{\mathcal{C}}^{1234}_{ab} + \mathcal{A}^{14}_{ab}\,\bar{\mathcal{C}}^{1235}_{ab} + \mathcal{A}^{13}_{ab}\,\bar{\mathcal{C}}^{1245}_{ab} + \\ + \mathcal{A}^{12}_{ab}\,\bar{\mathcal{C}}^{1345}_{ab} + \tilde{\mathfrak{A}}^{12345}_{ab} + \tilde{\mathfrak{A}}^{12435}_{ab} + \tilde{\mathfrak{A}}^{12534}_{ab} + \mathbb{A}^{12345}_{ab} + \mathfrak{B}^{12345}_{ab}\Big)\,.\end{aligned} \tag{5.39}$$

At six loops we have

$$\begin{aligned}\mathcal{W}^{\mathrm{RRRRRR}}_{123456} =&\mathcal{W}^{\mathrm{R}}_1\mathcal{W}^{\mathrm{R}}_2\mathcal{W}^{\mathrm{R}}_3\mathcal{W}^{\mathrm{R}}_4\mathcal{W}^{\mathrm{R}}_5\mathcal{W}^{\mathrm{R}}_6 + \Big(\mathcal{W}^{\mathrm{R}}_1\mathcal{W}^{\mathrm{R}}_2\mathcal{W}^{\mathrm{R}}_3\mathcal{W}^{\mathrm{R}}_4\overline{\mathcal{W}}^{\mathrm{RR}}_{56} + \text{perm.}\Big) + \\ &+ \Big(\mathcal{W}^{\mathrm{R}}_1\mathcal{W}^{\mathrm{R}}_2\overline{\mathcal{W}}^{\mathrm{RR}}_{34}\overline{\mathcal{W}}^{\mathrm{RR}}_{56} + \text{perm.}\Big) + \Big(\overline{\mathcal{W}}^{\mathrm{RR}}_{12}\overline{\mathcal{W}}^{\mathrm{RR}}_{34}\overline{\mathcal{W}}^{\mathrm{RR}}_{56} + \text{perm.}\Big) + \\ &+ \Big(\mathcal{W}^{\mathrm{R}}_1\mathcal{W}^{\mathrm{R}}_2\mathcal{W}^{\mathrm{R}}_3\overline{\mathcal{W}}^{\mathrm{RRR}}_{456} + \text{perm.}\Big) + \Big(\mathcal{W}^{\mathrm{R}}_1\overline{\mathcal{W}}^{\mathrm{RR}}_{23}\overline{\mathcal{W}}^{\mathrm{RRR}}_{456} + \text{perm.}\Big) + \\ &+ \Big(\overline{\mathcal{W}}^{\mathrm{RRR}}_{123}\overline{\mathcal{W}}^{\mathrm{RRR}}_{456} + \text{perm.}\Big) + \Big(\overline{\mathcal{W}}^{\mathrm{RR}}_{12}\overline{\mathcal{W}}^{\mathrm{RRRR}}_{3456} + \text{perm.}\Big) + \\ &+ \Big(\mathcal{W}^{\mathrm{R}}_1\mathcal{W}^{\mathrm{R}}_2\overline{\mathcal{W}}^{\mathrm{RRRR}}_{3456} + \text{perm.}\Big) + \Big(\mathcal{W}^{\mathrm{R}}_1\overline{\mathcal{W}}^{\mathrm{RRRRR}}_{23456} + \text{perm.}\Big) + \\ &+ \overline{\mathcal{W}}^{\mathrm{RRRRRR}}_{123456} + \text{finite-N}_\mathrm{c}\text{ contributions}\,, \end{aligned} \tag{5.40}$$

where the irreducible contribution at this order is deduced from Eq. (5.26) to be:

$$\begin{aligned}\overline{\mathcal{W}}^{\mathrm{RRRRR}}_{123456} =& \mathcal{A}^{12}_{ab}\bar{\mathcal{A}}^{13}_{ab}\bar{\mathcal{A}}^{14}_{ab}\bar{\mathcal{A}}^{15}_{ab}\bar{\mathcal{A}}^{16}_{ab}+ \\ &+ \mathcal{A}^{12}_{ab}\bar{\mathcal{A}}^{13}_{ab}\bar{\mathcal{A}}^{14}_{ab}\bar{\mathcal{B}}^{156}_{ab} + \mathcal{A}^{12}_{ab}\bar{\mathcal{A}}^{13}_{ab}\bar{\mathcal{A}}^{15}_{ab}\bar{\mathcal{B}}^{146}_{ab} + \mathcal{A}^{12}_{ab}\bar{\mathcal{A}}^{13}_{ab}\bar{\mathcal{A}}^{16}_{ab}\bar{\mathcal{B}}^{145}_{ab} + \mathcal{A}^{12}_{ab}\bar{\mathcal{A}}^{14}_{ab}\bar{\mathcal{A}}^{15}_{ab}\bar{\mathcal{B}}^{136}_{ab}+ \\ &+ \mathcal{A}^{12}_{ab}\bar{\mathcal{A}}^{14}_{ab}\bar{\mathcal{A}}^{16}_{ab}\bar{\mathcal{B}}^{135}_{ab} + \mathcal{A}^{12}_{ab}\bar{\mathcal{A}}^{15}_{ab}\bar{\mathcal{A}}^{16}_{ab}\bar{\mathcal{B}}^{134}_{ab} + \mathcal{A}^{13}_{ab}\bar{\mathcal{A}}^{14}_{ab}\bar{\mathcal{A}}^{15}_{ab}\bar{\mathcal{B}}^{126}_{ab} + \mathcal{A}^{13}_{ab}\bar{\mathcal{A}}^{14}_{ab}\bar{\mathcal{A}}^{16}_{ab}\bar{\mathcal{B}}^{125}_{ab}+ \\ &+ \mathcal{A}^{13}_{ab}\bar{\mathcal{A}}^{15}_{ab}\bar{\mathcal{A}}^{16}_{ab}\bar{\mathcal{B}}^{124}_{ab} + \mathcal{A}^{14}_{ab}\bar{\mathcal{A}}^{15}_{ab}\bar{\mathcal{A}}^{16}_{ab}\bar{\mathcal{B}}^{123}_{ab}+ \\ &+ \mathcal{A}^{12}_{ab}\bar{\mathcal{B}}^{134}_{ab}\bar{\mathcal{B}}^{156}_{ab} + \mathcal{A}^{12}_{ab}\bar{\mathcal{B}}^{135}_{ab}\bar{\mathcal{B}}^{146}_{ab} + \mathcal{A}^{12}_{ab}\bar{\mathcal{B}}^{136}_{ab}\bar{\mathcal{B}}^{145}_{ab} + \mathcal{A}^{13}_{ab}\bar{\mathcal{B}}^{124}_{ab}\bar{\mathcal{B}}^{156}_{ab} + \mathcal{A}^{13}_{ab}\bar{\mathcal{B}}^{125}_{ab}\bar{\mathcal{B}}^{146}_{ab}+ \\ &+ \mathcal{A}^{13}_{ab}\bar{\mathcal{B}}^{126}_{ab}\bar{\mathcal{B}}^{145}_{ab} + \mathcal{A}^{14}_{ab}\bar{\mathcal{B}}^{123}_{ab}\bar{\mathcal{B}}^{156}_{ab} + \mathcal{A}^{14}_{ab}\bar{\mathcal{B}}^{125}_{ab}\bar{\mathcal{B}}^{136}_{ab} + \mathcal{A}^{14}_{ab}\bar{\mathcal{B}}^{126}_{ab}\bar{\mathcal{B}}^{135}_{ab} + \mathcal{A}^{15}_{ab}\bar{\mathcal{B}}^{123}_{ab}\bar{\mathcal{B}}^{146}_{ab}+ \\ &+ \mathcal{A}^{15}_{ab}\bar{\mathcal{B}}^{124}_{ab}\bar{\mathcal{B}}^{136}_{ab} + \mathcal{A}^{15}_{ab}\bar{\mathcal{B}}^{126}_{ab}\bar{\mathcal{B}}^{134}_{ab} + \mathcal{A}^{16}_{ab}\bar{\mathcal{B}}^{123}_{ab}\bar{\mathcal{B}}^{145}_{ab} + \mathcal{A}^{16}_{ab}\bar{\mathcal{B}}^{124}_{ab}\bar{\mathcal{B}}^{135}_{ab} + \mathcal{A}^{16}_{ab}\bar{\mathcal{B}}^{125}_{ab}\bar{\mathcal{B}}^{134}_{ab}+ \\ &+ \mathcal{A}^{12}_{ab}\bar{\mathcal{A}}^{13}_{ab}\bar{\mathcal{C}}^{1456}_{ab} + \mathcal{A}^{12}_{ab}\bar{\mathcal{A}}^{14}_{ab}\bar{\mathcal{C}}^{1356}_{ab} + \mathcal{A}^{12}_{ab}\bar{\mathcal{A}}^{15}_{ab}\bar{\mathcal{C}}^{1346}_{ab} + \mathcal{A}^{12}_{ab}\bar{\mathcal{A}}^{16}_{ab}\bar{\mathcal{C}}^{1345}_{ab} + \mathcal{A}^{13}_{ab}\bar{\mathcal{A}}^{14}_{ab}\bar{\mathcal{C}}^{1256}_{ab}+ \\ &+ \mathcal{A}^{13}_{ab}\bar{\mathcal{A}}^{15}_{ab}\bar{\mathcal{C}}^{1246}_{ab} + \mathcal{A}^{13}_{ab}\bar{\mathcal{A}}^{16}_{ab}\bar{\mathcal{C}}^{1245}_{ab} + \mathcal{A}^{14}_{ab}\bar{\mathcal{A}}^{15}_{ab}\bar{\mathcal{C}}^{1236}_{ab} + \mathcal{A}^{14}_{ab}\bar{\mathcal{A}}^{16}_{ab}\bar{\mathcal{C}}^{1235}_{ab} + \mathcal{A}^{15}_{ab}\bar{\mathcal{A}}^{16}_{ab}\bar{\mathcal{C}}^{1234}_{ab}+ \\ &+ \mathcal{B}^{123}_{ab}\bar{\mathcal{C}}^{1456}_{ab} + \mathcal{B}^{124}_{ab}\bar{\mathcal{C}}^{1356}_{ab} + \mathcal{B}^{125}_{ab}\bar{\mathcal{C}}^{1346}_{ab} + \mathcal{B}^{126}_{ab}\bar{\mathcal{C}}^{1345}_{ab} + \mathcal{B}^{134}_{ab}\bar{\mathcal{C}}^{1256}_{ab} + \mathcal{B}^{135}_{ab}\bar{\mathcal{C}}^{1246}_{ab}+ \\ &+ \mathcal{B}^{136}_{ab}\bar{\mathcal{C}}^{1245}_{ab} + \mathcal{B}^{145}_{ab}\bar{\mathcal{C}}^{1236}_{ab} + \mathcal{B}^{146}_{ab}\bar{\mathcal{C}}^{1235}_{ab} + \mathcal{B}^{156}_{ab}\bar{\mathcal{C}}^{1234}_{ab}+ \\ &+ \mathcal{A}^{12}_{ab}\bar{\mathcal{A}}^{13}_{ab}\bar{\mathfrak{A}}^{1456}_{ab} + \mathcal{A}^{12}_{ab}\bar{\mathcal{A}}^{14}_{ab}\bar{\mathfrak{A}}^{1356}_{ab} + \mathcal{A}^{12}_{ab}\bar{\mathcal{A}}^{15}_{ab}\bar{\mathfrak{A}}^{1346}_{ab} + \mathcal{A}^{12}_{ab}\bar{\mathcal{A}}^{16}_{ab}\bar{\mathfrak{A}}^{1345}_{ab}+ \\ &+ \mathcal{A}^{13}_{ab}\bar{\mathcal{A}}^{14}_{ab}\bar{\mathfrak{A}}^{1256}_{ab} + \mathcal{A}^{13}_{ab}\bar{\mathcal{A}}^{15}_{ab}\bar{\mathfrak{A}}^{1246}_{ab} + \mathcal{A}^{13}_{ab}\bar{\mathcal{A}}^{16}_{ab}\bar{\mathfrak{A}}^{1245}_{ab} + \mathcal{A}^{14}_{ab}\bar{\mathcal{A}}^{15}_{ab}\bar{\mathfrak{A}}^{1236}_{ab} + \mathcal{A}^{14}_{ab}\bar{\mathcal{A}}^{16}_{ab}\bar{\mathfrak{A}}^{1235}_{ab}+ \\ &+ \mathcal{A}^{15}_{ab}\bar{\mathcal{A}}^{16}_{ab}\bar{\mathfrak{A}}^{1234}_{ab}+ \\ &+ \mathcal{B}^{123}_{ab}\bar{\mathfrak{A}}^{1456}_{ab} + \mathcal{B}^{124}_{ab}\bar{\mathfrak{A}}^{1356}_{ab} + \mathcal{B}^{125}_{ab}\bar{\mathfrak{A}}^{1346}_{ab} + \mathcal{B}^{126}_{ab}\bar{\mathfrak{A}}^{1345}_{ab} + \mathcal{B}^{134}_{ab}\bar{\mathfrak{A}}^{1256}_{ab} + \mathcal{B}^{135}_{ab}\bar{\mathfrak{A}}^{1246}_{ab}+ \\ &+ \mathcal{B}^{136}_{ab}\bar{\mathfrak{A}}^{1245}_{ab} + \mathcal{B}^{145}_{ab}\bar{\mathfrak{A}}^{1236}_{ab} + \mathcal{B}^{146}_{ab}\bar{\mathfrak{A}}^{1235}_{ab} + \mathcal{B}^{156}_{ab}\bar{\mathfrak{A}}^{1234}_{ab}+ \\ &+ \mathcal{A}^{12}_{ab}\bar{\mathbb{A}}^{13456}_{ab} + \mathcal{A}^{13}_{ab}\bar{\mathbb{A}}^{12456}_{ab} + \mathcal{A}^{14}_{ab}\bar{\mathbb{A}}^{12356}_{ab} + \mathcal{A}^{15}_{ab}\bar{\mathbb{A}}^{12346}_{ab} + \mathcal{A}^{16}_{ab}\bar{\mathbb{A}}^{12345}_{ab}+ \\ &+ \mathcal{A}^{12}_{ab}\bar{\tilde{\mathfrak{A}}}^{13456}_{ab} + \mathcal{A}^{12}_{ab}\bar{\tilde{\mathfrak{A}}}^{13546}_{ab} + \mathcal{A}^{12}_{ab}\bar{\tilde{\mathfrak{A}}}^{13645}_{ab} + \mathcal{A}^{13}_{ab}\bar{\tilde{\mathfrak{A}}}^{12456}_{ab} + \mathcal{A}^{13}_{ab}\bar{\tilde{\mathfrak{A}}}^{12546}_{ab} + \mathcal{A}^{13}_{ab}\bar{\tilde{\mathfrak{A}}}^{12645}_{ab}+ \\ &+ \mathcal{A}^{14}_{ab}\bar{\tilde{\mathfrak{A}}}^{12356}_{ab} + \mathcal{A}^{14}_{ab}\bar{\tilde{\mathfrak{A}}}^{12536}_{ab} + \mathcal{A}^{14}_{ab}\bar{\tilde{\mathfrak{A}}}^{12635}_{ab} + \mathcal{A}^{15}_{ab}\bar{\tilde{\mathfrak{A}}}^{12346}_{ab} + \mathcal{A}^{15}_{ab}\bar{\tilde{\mathfrak{A}}}^{12436}_{ab} + \mathcal{A}^{15}_{ab}\bar{\tilde{\mathfrak{A}}}^{12634}_{ab}+ \\ &+ \mathcal{A}^{16}_{ab}\bar{\tilde{\mathfrak{A}}}^{12345}_{ab} + \mathcal{A}^{16}_{ab}\bar{\tilde{\mathfrak{A}}}^{12435}_{ab} + \mathcal{A}^{16}_{ab}\bar{\tilde{\mathfrak{A}}}^{12534}_{ab}+ \\ &+ \mathcal{A}^{12}_{ab}\bar{\mathfrak{B}}^{13456}_{ab} + \mathcal{A}^{13}_{ab}\bar{\mathfrak{B}}^{12456}_{ab} + \mathcal{A}^{14}_{ab}\bar{\mathfrak{B}}^{12356}_{ab} + \mathcal{A}^{15}_{ab}\bar{\mathfrak{B}}^{12346}_{ab} + \mathcal{A}^{16}_{ab}\bar{\mathfrak{B}}^{12345}_{ab}+ \\ &+ \mathcal{A}^{12}_{ab}\bar{\mathcal{D}}^{13456}_{ab} + \mathcal{A}^{13}_{ab}\bar{\mathcal{D}}^{12456}_{ab} + \mathcal{A}^{14}_{ab}\bar{\mathcal{D}}^{12356}_{ab} + \mathcal{A}^{15}_{ab}\bar{\mathcal{D}}^{12346}_{ab} + \mathcal{A}^{16}_{ab}\bar{\mathcal{D}}^{12345}_{ab}+ \end{aligned} \tag{5.41}$$

$$+\mathcal{K}_{ab}^{123456}+\mathcal{K}_{ab}^{123546}+\mathcal{K}_{ab}^{123645}+\mathcal{K}_{ab}^{124536}+\mathcal{K}_{ab}^{124635}+\mathcal{K}_{ab}^{125634}+\mathcal{L}_{ab}^{123456}+$$
$$+\mathcal{L}_{ab}^{123546}+\mathcal{L}_{ab}^{123645}+\mathcal{P}_{ab}^{123456}+\mathcal{P}_{ab}^{123465}+\mathcal{P}_{ab}^{123564}+\mathcal{P}_{ab}^{124563}+\mathcal{Q}_{ab}^{123456}+$$
$$+\mathcal{Q}_{ab}^{123465}+\mathcal{Q}_{ab}^{123564}+\mathcal{Q}_{ab}^{124563}+\tilde{\mathfrak{B}}_{ab}^{123456}+\tilde{\mathfrak{B}}_{ab}^{123546}+\tilde{\mathfrak{B}}_{ab}^{123645}+\mathcal{J}_{ab}^{123456}+$$
$$+\mathbb{B}_{ab}^{123456}+\mathfrak{C}_{ab}^{123456}+\mathcal{E}_{ab}^{123456}\,. \tag{5.42}$$

Notice how the integer coefficient that multiplies each integral in Eq. (5.26) exactly corresponds to the number of possible iterations of gluons in the squared amplitude. The result at six loops has not been previously reported in the literature and we have deduced it here from the BMS equation. Furthermore, we have verified this result by comparing it to the output of the `Mathematica` Program `EikAmp` [93]. Recall that `EikAmp` additionally produces contributions that are subleading in colour, i.e., finite-$\mathrm{N_c}$ contributions, and thus provides squared amplitudes that are more accurate in terms of the colour structure.

5.5 NGLs in the hemisphere mass distribution

We present in this section the results of integrations for the coefficients $\mathcal{S}_{ab}^{(n)}$ of NGLs up to $n=5$, in the case of back-to-back di-jet production events in e^+e^- collisions, where we measure the invariant mass of the hemisphere defined by one of the jets. The iterative structure of the integrals suggests the use of Goncharov polylogarithms (GPLs), symbols and co-product machinery [86] which greatly simplifies the analytical computations of the said integrations [96]. This results we report herein serve as confirmation of the semi-analytical calculations carried out in Ref. [102]. We leave the details of the integrations to appendix B and confine ourselves here to only state the full result up to fifth order.

The resummed hemisphere mass distribution may be expressed as follows:

$$\sigma(\rho)=\sigma^{\mathrm{P}}(\rho)\,\times\,\sigma^{\mathrm{NG}}(\rho)\,, \tag{5.43}$$

where $\sigma^{\mathrm{P}}(\rho)$ is the primary Sudakov form factor given by [106]:

$$\sigma^{\mathrm{P}}(\rho)=\frac{1}{\Gamma[1+\mathcal{R}'(\rho)]}\,\exp\left[-\mathcal{R}(\rho)-\gamma_E\,\mathcal{R}'(\rho)\right], \tag{5.44}$$

The term $\sigma^{\mathrm{NG}}(\rho)$ is the resummed non-global factor given by:

$$\sigma^{\mathrm{NG}}(t)=\exp\left(-\frac{(\mathrm{N_c}t)^2}{2!}\frac{\zeta_2}{2}+\frac{(\mathrm{N_c}t)^3}{3!}\frac{\zeta_3}{2}-\frac{(\mathrm{N_c}t)^4}{4!}\frac{29\,\zeta_4}{16}+\right.$$
$$\left.+\,\frac{(\mathrm{N_c}t)^5}{5!}\left[\frac{17}{4}\zeta_5+\frac{1}{2}\zeta_2\zeta_3\right]+\mathcal{O}(t^6)\right), \tag{5.45}$$

where the five-loops result has been deduced from previous results in the literature [96, 102].

The fixed-order expansion of this result gives

$$\sigma(\rho)^{\rm NG} = 1 - \frac{\pi^2}{24}(\mathrm{N_c}t)^2 + \frac{\zeta_3}{12}(\mathrm{N_c}t)^3 + \frac{\pi^4}{34\,560}(\mathrm{N_c}t)^4 + \\ + \left(-\frac{1}{360}\pi^2\zeta_3 + \frac{17}{480}\zeta_5\right)(\mathrm{N_c}t)^5, \tag{5.46}$$

which confirms the results obtained in Refs. [96, 102].

Since we have not computed higher NGLs coefficients, we can make a crude estimate of how large they may be. We do so by fitting the exponential solution (5.8) truncated at seventh order to the full numerical resummation of NGLs obtained by the evolution code of Ref. [52]. The fitting values that we have obtained are:

$$\mathcal{S}_{ab}^{(6)} = -\,13.34\,, \tag{5.47a}$$

$$\mathcal{S}_{ab}^{(7)} = +\,15.03\,. \tag{5.47b}$$

The numerical values for the coefficients that multiply $(\mathrm{N_c}t)^n$ in (5.45) up to fifth order (n=5) are shown in Table 5.1. Also shown in the same table are the estimated coefficients at 6 and 7 loops based on the fitting values above (5.47). We note that for typical phenomenological studies $\mathrm{N_c}t \lesssim 1$. Combined with the observations that the numerical values for the coefficients shown in Table 5.1 become smaller at each higher order, it is expected that the series in the exponent (5.45) should converge fairly quickly.

Order	Coefficient
2	−0.411
3	+0.100
4	−0.082
5	+0.045
6	−0.018
7	+0.003

Table 5.1: Coefficients multiplying $\mathrm{N_c}t$ at order n.

In the next subsection, we discuss the resummation of the pure ladder terms to all orders.

5.5.1 Two-loops ladder resummation

In this section we show how a class of terms that appear at each order in the perturbative expansion of NGLs distribution may be resummed in the exponent (5.8) to all orders. Such a class of terms, dubbed "ladder" terms [1] [102], seems to exhibit a symmetry pattern and starts

[1] The Feynman diagrams corresponding to these terms look like a ladder. See Fig. 5.1.

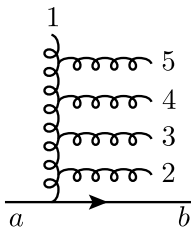

Figure 5.1: Diagrammatic representation of the ladder terms up to fifth order.

at two-loops by the expression (5.17):

$$\mathcal{S}^{(2)}_{ab} = -\int \frac{\mathrm{d}\Omega_{12}}{(4\pi)^2}\,\Theta_1^{\mathrm{out}}\,\Theta_2^{\mathrm{in}}\,\mathcal{A}^{12}_{ab}\,. \tag{5.48}$$

At higher orders ($n \geq 2$) they appear as:

$$(-1)^{n-1}\int \frac{\mathrm{d}\Omega_{12\ldots n}}{(4\pi)^n}\,\Theta_1^{\mathrm{out}}\,\omega^1_{ab}\prod_{i=2}^{n}\Theta_i^{\mathrm{in}}\bar{\mathcal{A}}^{1i}_{ab}\,. \tag{5.49}$$

They may be depicted by the Feynman diagrams shown in Fig. 5.1. The result of integration of a given ladder term at order n is given by the formula:

$$(-1)^{n-1}\,(n-1)!\zeta_n/2\,, \qquad n \geq 2\,, \tag{5.50}$$

Summing these terms to all orders in the exponent yields the result:

$$\begin{aligned}&\exp\left[\sum_{n=2}^{\infty}\frac{(-1)^{n-1}\,(n-1)!}{2}\,\zeta_n\,\frac{(N_c t)^n}{n!}\right]\\ &= \frac{1}{\sqrt{\Gamma(\mathrm{N_c}t+1)}}\exp\left[-\frac{\gamma_E}{2}\,\mathrm{N_c}\,t\right].\end{aligned} \tag{5.51}$$

An analogous result to the above was derived in Ref. [96] by means of solving the BMS equation up to two loops while ignoring higher-loop terms. Eq. (5.51) also corresponds to the first radiator $R^{(1)}_{ab}(t)$ in Eq. (5.3) of Ref. [95] [2]. This means that the exponential solution (5.8) may be factored out into a product of infinite exponential terms (or equivalently a sum of infinite terms in the exponent), each of which resums a specific class of terms that exhibit a given symmetry pattern. What we have computed above, i.e., ladder terms, is just the first obvious class of such terms. Possibility of computing the other less trivial classes will be postponed for future publications.

We show in figure 5.2 a plot of the ratio $\sigma^{\mathrm{NG}}/\sigma^{\mathrm{DS}}$, where σ^{DS} is a parametrisation function that was obtained in Ref. [52] by fitting to the output of a Monte Carlo dipole evolution code

[2] Notice that the evolution parameter t is denoted as δ in [95].

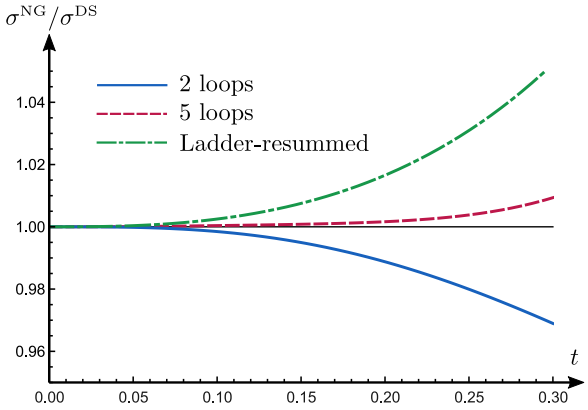

Figure 5.2: Plots of the ratios $\sigma^{\rm NG}/\sigma^{\rm DS}$ as a function of t including terms in (5.8) up to 2 loops, up to 5 loops in the exponent, and ladder terms resummed factor (5.51).

developed therein to resum NGLs at large $\mathrm{N_c}$. It is given by:

$$\sigma^{\rm DS}(t) = \exp\left[-\mathrm{C_F}\,\mathrm{C_A}\,\frac{\pi^2}{12}\,\frac{1+(0.85\,\mathrm{C_A}\,t/2)^2}{1+(0.86\,\mathrm{C_A}\,t/2)^{1.33}}\right]. \tag{5.52}$$

We show in figure 5.2 three cases for $\sigma^{\rm NG}$. In one case we truncate the series in the exponent (5.45) at two loops keeping only the leading term in the exponent. We notice that the exponential result differs only at the level of a maximum of 3% for values of t up to 0.3. In the second case we truncate the series in the exponent at fifth order. Here we see that the 5-loops resummed result performs better than the two-loops result with discrepancy less than 1% for values of t up to ~ 0.3 (which is equivalent to a value of $L = \ln(1/\rho) = 5.3$ or $\rho = 0.005$). This indicates that adding a few more terms in the exponent one should be able to obtain a reliably good agreement with the full numerical resummation of NGLs $\sigma^{\rm DS}$.

The resummed factor for the ladder terms (blue curve), on the other hand, does not seem to perform any better than the two-loops case (green dotted curve). This indicates that the formula we proposed in Eq. (5.8) is equivalent to that proposed in Ref. [95] (Eq. (5.3)) in the sense that in both cases it is necessary to compute higher-loop terms/classes in order to get a reliable analytical result that matches the full numerical one.

5.6 Summary

In the current work we have shown how to extract the Eikonal squared amplitudes for the emission of soft energy-ordered gluons at large $\mathrm{N_c}$ from the non-linear integro-differential BMS equation. The explicit formulae for these amplitudes have been given up to the sixth order in the strong coupling. The latter have actually been deduced from the explicit formulae of the coefficients of NGLs distribution $\mathcal{S}_{ab}^{(n)}$, for which the BMS equation was initially developed. The expressions of $\mathcal{S}_{ab}^{(n)}$ are general and may be applied to the computation of any non-global QCD observable. All that is needed is a simple change of the limits of the phase space integrals.

Moreover, we have explicitly verified that the squared amplitudes extracted from the BMS equation coincide with those presented in our previous work [93] in the large N_c limit. The results of the latter reference were obtained by means of a `Mathematica` code that implements the dipole formula in the Eikonal approximation and captures the full colour dependence of the amplitudes.

We additionally carried out analytical evaluations of the various integrals corresponding to the NGLs coefficients $\mathcal{S}_{ab}^{(n)}$ up to fourth order for the specific case of hemisphere jet mass. We have thus confirmed the semi-numerical calculations presented previously in [102]. The fifth and sixth order computations are quite delicate and will be presented in future publications. Furthermore, we compared our results to the full numerical resummation of Ref. [52] and found that the more higher terms in the exponent of the proposed solution (5.8) the better the agreement is for larger intervals of the evolution parameter t. Nonetheless, and as previously pointed out in the literature, the exponential of the two-loops result gives a good approximation for the full resummation for values of t up to ~ 0.3.

We have also elaborated on the observation that the solution of the BMS equation may be represented by a product of infinite exponential factors each of which resums a class of terms contributing to the NGLs distribution. We have computed the first of such resummed factors, which corresponds to a class of terms whose Feynman diagrams resemble a ladder shape. It turns out, however, that such a solution does not differ much than the solution we proposed in (5.8) in view of the fact that higher-loop terms cannot be neglected and should be computed for a precise and reliable solution to the BMS equation.

Chapter 6

Conclusions

As stated in this thesis, jets are ubiquitous in collider phenomenology and with the larger data set that will be generated by Run 3 of the LHC and the future e^+e^- colliders (FCC-ee and ILC), jet substructure tools are crucial in particle physics. An important application of jet substructure in jet physics is in the description of QCD background and searches for new particles decaying hadronically. In particular, in this thesis we focused on the study of event and jet shapes distributions that can provide information about the internal structure of the QCD jets (background), possibly enabling for the differentiation of the jet's partonic origin, using the traditional perturbative QCD approach.

In chapter 4 of this thesis, we studied the jet shape distribution, azimuthal decorrelation for high-p_t QCD di-jet production in e^+e^- annihilation. We examined non-global and clustering logarithms in the distribution of the aforementioned observable and we presented analytical calculations both at fixed-order up to four loops and numerically resummed them to all orders in the large-$\mathrm{N_c}$ approximation. We discovered that at small R the coefficients are identical to those in the single hemisphere jet mass observable. In light of the fact that experimental jet measurements usually use large values of the jet parameter R, we also computed the full logarithmic structure of the said shape distribution in the full R limit for both the anti-k_t and k_t algorithms up to three loops. The NGLs significance reduction associated with k_t clustering was confirmed in this study. It was further observed that NGLs and CLs together have a very small effect on the distribution and the accuracy of the resummed distribution is therefore important from a phenomenological standpoint. The difference between the numerical and analytical differential distributions at $\mathcal{O}(\alpha_s)$ and $\mathcal{O}(\alpha_s^2)$ indicating that singular terms have been eliminated completely. As a final step, we calculated the resummed distribution at NLL accuracy using the program Gnole, thereby obtaining state-of-the-art accuracy. Based on scale uncertainty and accuracy, NLL resummation shows a better distribution and so it would be interesting to investigate the impact of NLL effects with k_t clustering in a future work. Of similar worthiness is computing NGLs and CLs at four-loops with full R dependence. Furthermore, we

will also adress non-perturbative corrections, fixed-order matching, statistical and systematic uncertainties.

In chapter 5 of this thesis we addressed the BMS equation describing the evolution of the leading NGLs at large N_c at single logarithmic accuracy up to four loops for the hemisphere mass distribution in $e^+e^- \to$ di-jet events. We proposed an exponential solution arrived at in Ref [102], which was, however, extended herein to resum both the Sudakov and NGLs at large N_c. This latter being a series in the strong coupling α_s. We substituted the proposed solution into the BMS equation and we obtained recurrence relations make the computation of the NGLs coefficient possible. We additionally showed that the squared amplitudes for the emission of soft energy-ordered gluons are correctly embedded in the explicit formulae of the coefficients of NGLs distribution $\mathcal{S}^n_{ab}$, and explicitly verify that they coincide with those derived in previous works in the literature in the large-Nc limit up to sixth order in the strong coupling. Furthermore, we were able to analytically compute the leading NGLs coefficients up to four loops. Whereas our calculation is full up to four loops, the difficulties encountered in some integrals which are far from simple to integrate make it incomplete at five and higher loops. Furthermore, for the pure ladder terms, we could investigate what happens at higher loops and identify a pattern and resum theme to all orders to the best possible accuracy.

The current work may be extended in various ways. These include, to name few, (a) analytically computing the fifth and sixth order NGLs coefficients, (b) considering other non-global jet shape distributions up to sixth order, (c) exploring the effect of jet algorithms and jet radii on NGLs distributions up to sixth order, and (d) exploiting new developments in mathematics especially in the field of non-linear integro-differential equations in the hope of finding an analytical solution to the BMS equation. The latter attempt may be possible in the near future given the fact the BMS equation is analogous to quite few well known equations in physics, such as the Batlisky-Kovchegov (BK) equation (see [98] and references therein) that have been thoroughly studied for a long time. We hope to address some of theses issues in the near future.

Appendix A

e^+e^- annihilation at one loop

In this appendix we explicitly present the calculation of the squared amplitude for one-loop virtual corrections for the process ($e^+e^- \to qqg$) and show that in the Eikonal approximation, the virtual cross section turns out to contain exactly the same soft and collinear divergences existing in the real emission contribution. To do so, the virtual corrections at this order are depicted in Fig. A.1. Since we are interesting in the case of on mass-shell (anti) quark, the contributions of the self energy diagrams are defined to be zero (the gluon is emitted and absorbed by the same (anti)quark leg ($p_1^2 = p_2^2 = 0$)) and the only one-loop diagram contributing is the vertex correction ($p_1.p_2$). The corresponding amplitude reads

$$iM_1^v = \bar{u}(p_1, i)\,(-i\,g_s\,t^a_{il}\,\gamma^\mu) \int \frac{\mathrm{d}^4k}{(2\pi)^4}\,\frac{-i}{k^2+i\epsilon}\,\frac{i(\not{p}_1+\not{k})}{(p_1+k)^2+i\epsilon}\,B_0\times$$
$$\times\ \frac{i(\not{p}_2+\not{k})}{(p_2-k)^2+i\epsilon}\,(i\,g_s\,t^a_{lj}\,\gamma^\mu)\,v(p_2, j)\,. \tag{A.1}$$

Using the Eikonal approximation we can neglect the loop momentum k in the numerator and k^2 in the denominator ($k^2 \ll p.k$) which is off mass-shell (virtual) though ($k^2 \neq 0$). Performing

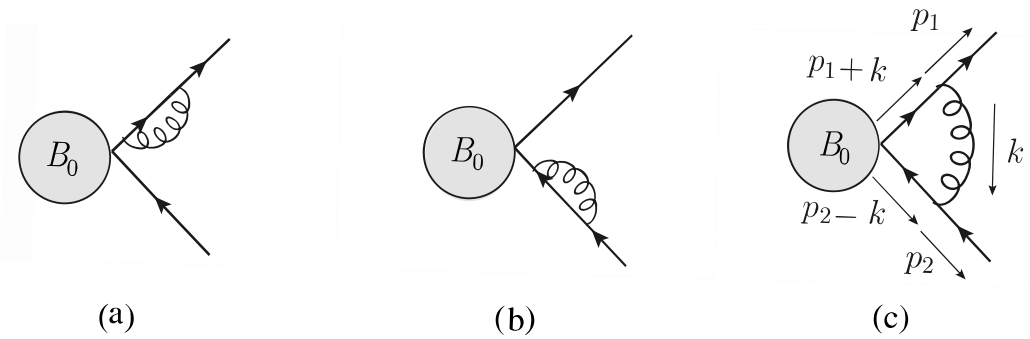

Figure A.1: The basic Feynman diagrams for virtual one-loop corrections to the born amplitude $e^-e^+ \to q\bar{q}$.

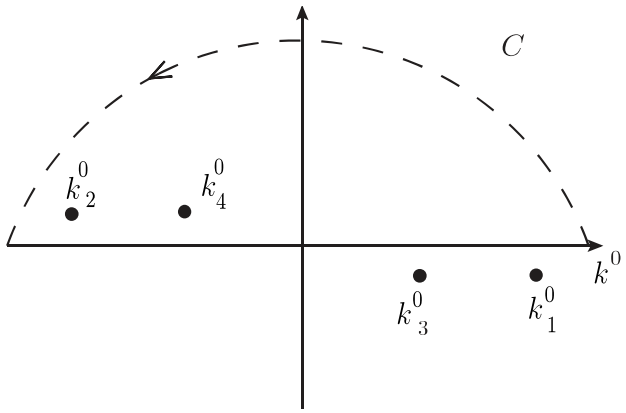

Figure A.2: Poles of the integrand in Eq. (A.2) in the complex plane k^0.

the usual Dirac algebra we obtain

$$\begin{aligned} iM_1^v &= (-i)\, g_s^2\, \mathrm{C_F}\, [\bar{u}(p_1,i)\, B_0\, v(p_2,j)\, \delta_{ij}] \int \frac{\mathrm{d}^4k}{(2\pi)^4}\, \frac{1}{(k^2+i\epsilon)}\, \frac{(p_1.p_2)}{(p_1.k+i\epsilon)(p_2.k+i\epsilon)} \\ &= (-i)\, g_s^2\, \mathrm{C_F}\, (iM_0) \int \frac{\mathrm{d}^4k}{(2\pi)^4}\, \frac{1}{(k^2+i\epsilon)}\, \frac{(p_1.p_2)}{(p_1.k+i\epsilon)(p_2.k+i\epsilon)}\,. \end{aligned} \tag{A.2}$$

The four-momenta of the outgoing quark, anti-quark and gluon are given in the center of mass frame by

$$\begin{aligned} p_1 &= \frac{\sqrt{s}}{2}(1,0,0,1)\,, \\ p_2 &= \frac{\sqrt{s}}{2}(1,0,0,-1)\,, \\ k &\equiv (k^0,k^1,k^2,k^3) = (k^0,\vec{k}), \quad \vec{k} = (\vec{k_t},k^3)\,. \end{aligned} \tag{A.3}$$

We can evaluate the above integral using contour integration techniques. Substituting the results into Eq. (A.2), we find

$$M_1^v = (-i)\, g_s^2\, \mathrm{C_F}\, M_0 \int \frac{\mathrm{d}^3\vec{k}}{(2\pi)^3} \int_{-\infty}^{+\infty} \frac{\mathrm{d}k^0}{k^0}\, \frac{1}{(k^0-k_1^0)\,(k^0-k_2^0)\,(k^0-k_3^0)\,(k^0-k_4^0)}\,. \tag{A.4}$$

Eq. (A.4) has four pols in the complex k^0 plane, and they are presented in Fig. A.2

$$k_1^0 = |\vec{k}| - i\epsilon\,; \quad k_2^0 = -|\vec{k}| + i\epsilon\,; \quad k_3^0 = k^3 - i\epsilon\,; \quad k_4^0 = -k^3 + i\epsilon\,.$$

Closing the contour from below, we note that poles with negative imaginary parts are outside the semicircle, and hence do not contribute when performing the residue theorem that finally gives

$$M_1^v = -\, g_s^2\, \mathrm{C_F}\, M_0 \int \frac{\mathrm{d}^3\vec{k}}{(2\pi)^3} \left[\frac{(p_1.p_2)}{2|\vec{k}|\,(p_1.k)(p_2.k)} - \frac{1}{(k^3-i\epsilon)\,|\vec{k_t}|^2} \right]. \tag{A.5}$$

The second integral which is a purely imaginary part, is called "Coulomb (or Glauber) phase ", and its final result is given by

$$\int \frac{\mathrm{d}^3\vec{k}}{(2\pi)^3}\,\frac{1}{(k^3-i\epsilon)\,|\vec{k_t}|^2} = \frac{i\pi}{(2\pi)^2}\int \frac{\mathrm{d}k_t}{k_t}\,, \tag{A.6}$$

where $k_t = |\vec{k_t}|$. The one-loop correction to the cross section at order α_s is proportional to $|M_0 + M_v^1|^2$

$$|M_1^v + M_0|^2 = |M_0|^2 + M_0\, M_1^{v\dagger} + M_1^v\, M_0^\dagger\,.$$

The squared amplitude actually involves three terms; the squared of the first element is of order α_s^2 which is higher than our accuracy and thus would be dropped. The squared of the second term is the usual born cross section while the last one which is of order α_s, is dubbed the interference term and given by

$$\begin{aligned} M_0^\dagger\, M_1^v + M_1^{v\dagger}\, M_0 = \mathrm{C_F}\, g_s^2\, |M_0|^2 \Bigg[&- \int \frac{\mathrm{d}^3k}{(2\pi)^3\, 2E_g}\,\frac{(p_1.p_2)}{(p_1.k)\,(p_2.k)} + i\pi \int \frac{\mathrm{d}k}{(2\pi)^2\, k} \\ &- \int \frac{\mathrm{d}^3k}{(2\pi)^3\, 2E_g}\,\frac{(p_1.p_2)}{(p_1.k)\,(p_2.k)} - i\pi \int \frac{\mathrm{d}k}{(2\pi)^2\, k}\Bigg] \\ &= -2\,\mathrm{C_F}\, g_s^2\, |M_0|^2 \int \frac{\mathrm{d}^3k}{(2\pi)^3\, 2E_g}\,\frac{(p_1.p_2)}{(p_1.k)\,(p_2.k)}\,. \end{aligned} \tag{A.7}$$

We note that the Coulomb term completely cancels in the sum, and the one-loop contribution turns out to be exactly identical to the real emission squared amplitude given in Eq. (2.50) up to a sign.

Appendix B

Calculation of NGLs coefficients

B.1 One and two-loop calculations

We evaluate in this section the integral (5.13) which gives the one-loop Sudakov coefficient $\mathcal{S}_{ij}^{(1)}$ for arbitrary dipole (ij). We introduce the following brackets:

$$\{ij\} = 1 + c_i\, c_j + s_i\, s_j \cos\phi_{ij}\,, \tag{B.1a}$$

$$[ij] = 1 + c_i\, c_j - s_i\, s_j \cos\phi_{ij}\,, \tag{B.1b}$$

where we remind the reader that $c_i = \cos\theta_i, s_i = \sin\theta_i$ and $\phi_{ij} = \phi_i - \phi_j$. First, we carry out the azimuthal average

$$\mathcal{I}_{ij}(c_k) = \int_0^{2\pi} \frac{\mathrm{d}\phi_k}{2\pi}\, \frac{(ij)}{(ik)\,(jk)}\,, \tag{B.2}$$

using contour integration techniques to obtain

$$\begin{aligned}\mathcal{I}_{ij}(c_k) = \mathcal{I}_{ij}^{(1)}(c_k)\,[\Theta(c_k - c_i) - \Theta(c_j - c_k)] + \\ + \mathcal{I}_{ij}^{(2)}(c_k)\,[\Theta(c_k - c_i) - \Theta(c_k - c_j)]\,,\end{aligned} \tag{B.3}$$

with

$$\mathcal{I}_{ij}^{(1)} = \frac{(ij)}{[ij] - 2\,(c_i + c_j)\,c_k + \{ij\}c_k^2}\left[\frac{1 - c_i c_k}{c_k - c_i} + \frac{1 - c_j c_k}{c_k - c_j}\right]\,, \tag{B.4a}$$

$$\mathcal{I}_{ij}^{(2)} = \frac{1}{1 - c_k^2}\left[\frac{1 - c_i c_k}{c_k - c_i} - \frac{1 - c_j c_k}{c_k - c_j}\right]. \tag{B.4b}$$

Evaluating the polar integration results in a collinear divergence, as explained in the main text (see Ref. [102] for the detailed calculation of such a term).

The two-loops integral which represents the leading NGLs coefficient reads:

$$\mathcal{S}_{ij}^{(2)} = -\int_{-1}^{0} \frac{\mathrm{d}c_\ell}{2}\frac{\mathrm{d}\phi_\ell}{2\pi}\frac{(ij)}{(i\ell)(j\ell)}\int_0^1 \frac{\mathrm{d}c_k}{2}\left[\mathcal{I}_{i\ell}(c_k)+\mathcal{I}_{\ell j}(c_k)-\mathcal{I}_{ij}(c_k)\right]. \tag{B.5}$$

For the case $(ij)=(aj)$ with $c_j<0$ and $c_a=1$ one simply finds:

$$\mathcal{S}_{aj}^{(2)} = -\frac{\zeta_2}{2}. \tag{B.6}$$

Moreover, for the simpler case $(ij)=(ab)$ with $c_a=1$ and $c_b=-1$ one obtains:

$$\mathcal{S}_{ab}^{(2)} = -\frac{\zeta_2}{2}. \tag{B.7}$$

Finally for $(ij)=(ib)$, with i an arbitrary leg outside the measured hemisphere ($c_i<0$) one has:

$$\mathcal{S}_{ib}^{(2)} = -\frac{1}{2}\left(\zeta_2 - \mathrm{Li}_2\left[\frac{2c_i}{c_i-1}\right]\right). \tag{B.8}$$

B.2 Three-loops calculations

The coefficient of the NGLs at three-loops for the hemisphere mass distribution in di-jet events in e^+e^- collisions is given by

$$\begin{aligned}\mathcal{S}_{ab}^{(3)} = &\int_{-1}^{0}\frac{\mathrm{d}c_1}{2}\int_0^{2\pi}\frac{\mathrm{d}\phi_1}{2\pi}\int_0^1\frac{\mathrm{d}c_2}{2}\int_0^{2\pi}\frac{\mathrm{d}\phi_2}{2\pi}\int_0^1\frac{\mathrm{d}c_3}{2}\int_0^{2\pi}\frac{\mathrm{d}\phi_3}{2\pi}\mathcal{A}_{ab}^{12}\bar{\mathcal{A}}_{ab}^{13}- \\ &-\int_{-1}^{0}\frac{\mathrm{d}c_1}{2}\int_0^{2\pi}\frac{\mathrm{d}\phi_1}{2\pi}\int_{-1}^{0}\frac{\mathrm{d}c_2}{2}\int_0^{2\pi}\frac{\mathrm{d}\phi_2}{2\pi}\int_0^1\frac{\mathrm{d}c_3}{2}\int_0^{2\pi}\frac{\mathrm{d}\phi_3}{2\pi}\mathcal{B}_{ab}^{123}.\end{aligned} \tag{B.9}$$

For the ladder term (first term above), which was also evaluated and resummed to all orders in the main text, we have the result

$$I_1^{(3)} = \zeta_3. \tag{B.10}$$

For the second cascade term we have

$$I_2^{(3)} = -\int_{-1}^{0}\frac{\mathrm{d}c_1}{2}\int_0^{2\pi}\frac{\mathrm{d}\phi_1}{2\pi}\int_{-1}^{0}\frac{\mathrm{d}c_2}{2}\int_0^{2\pi}\frac{\mathrm{d}\phi_2}{2\pi}\int_0^1\frac{\mathrm{d}c_3}{2}\int_0^{2\pi}\frac{\mathrm{d}\phi_3}{2\pi}w_{ab}^1\left(\mathcal{A}_{a1}^{23}+\mathcal{A}_{1b}^{23}-\mathcal{A}_{ab}^{23}\right). \tag{B.11}$$

Substituting the results of integration from the previous subsection we find

$$I_2^{(3)} = \int_{-1}^{0} \frac{\mathrm{d}c_1}{2} \int_0^{2\pi} \frac{\mathrm{d}\phi_1}{2\pi} w_{ab}^1 \left(\mathcal{S}_{a1}^{(2)} + \mathcal{S}_{b1}^{(2)} - \mathcal{S}_{ab}^{(2)} \right)$$
$$= -\int_{-1}^{0} \frac{\mathrm{d}c_1}{2} \frac{2}{1-c_1^2} \left(\frac{\zeta_2}{2} - \frac{1}{2} \mathrm{Li}_2 \left[\frac{2c_1}{c_1 - 1} \right] \right). \tag{B.12}$$

Making the change of variables

$$x = \frac{1+c_1}{1-c_1} \Rightarrow c_1 = \frac{x-1}{x+1}, \tag{B.13}$$

the cascade integral then reads

$$I_2^{(3)} = -\frac{1}{4} \int_0^1 \mathrm{d} \ln x \left[\zeta_2 - \mathrm{Li}_2(1-x) \right]. \tag{B.14}$$

Before computing this integral let us first give a short review of multiple polylogarithms.

- **Multiple Polylogarithms:**

Goncharov polylogarithms (GPLs) [86] are multivalued functions, defined recursively via the iterated integral

$$G\left(a_1, a_2, \ldots, a_n; x\right) = \int_0^x \frac{\mathrm{d}t}{t - a_1} G\left(a_2, \ldots, a_n; t\right), \tag{B.15}$$

with $G(x) = 1$ and where $a_i, x \in \mathbb{C}$. Goncharov polylogarithm represented by $G\left(a_1, \ldots, a_n; x\right)$, is one variable function of say x which is called its argument, while the number of elements a_i is called the weight(transcendentality) of the GPLs.

Multiple polylogarithms defined as power series

$$\mathrm{Li}_{n_1,\ldots,n_k}\left(x_1, \ldots, x_k\right) = \sum_{1 \le p_1 < \cdots < p_k} \frac{x_1^{p_1}}{p_1^{n_1}} \cdots \frac{x_k^{p_1}}{p_k^{n_k}}. \tag{B.16}$$

These power series are convergent in a polydisc $|x_i| < 1$. These polylogarithms can be written in terms of Goncharov polylogarithms as

$$\mathrm{Li}_{n_1,\ldots,n_k}\left(x_1, \ldots, x_k\right) = (-1)^k G\left(\underbrace{0, \ldots, 0}_{n_k - 1}, \frac{1}{x_k}, \ldots, \frac{1}{x_2, \ldots, x_k}, \underbrace{0, \ldots, 0}_{n_k - 1}, \frac{1}{x_1, \ldots, x_k}; 1 \right). \tag{B.17}$$

For special values of the weight vector $(a_1, \ldots, a_n)$, GPLs reduce to special cases which are

the so-called logarithms, classical polylogarithms and harmonic polylogarithms:

$$\begin{aligned} G\left(0,\ldots,0_n;x\right) &= \frac{1}{n!}\ln^n x\,, \\ G\left(a,\ldots,a_n;x\right) &= \frac{1}{n!}\ln^n\left(1-\frac{x}{a}\right)\,, \\ G\left(0,\ldots,0_{n-1},a;x\right) &= -\mathrm{Li}_n\left(\frac{x}{a}\right)\,, \end{aligned} \tag{B.18}$$

where the classical polylogarithms are defined recursively

$$\mathrm{Li}_n(x) = \int_0^x \frac{\mathrm{d}t}{t}\,\mathrm{Li}_{n-1}(t)\,, \tag{B.19}$$

with $\mathrm{Li}_1(x) = -\ln(1-x)$. The differential relation is

$$x\,\frac{\partial}{\partial x}\,\mathrm{Li}_n(x) = \mathrm{Li}_{n-1}(x)\,. \tag{B.20}$$

We have introduced the vector notation $\vec{a}_n = (a_1,\ldots,a_n)$, Harmonic polylogarithms HPL's are defined via

$$H\left(\vec{a};x\right) = (-1)^k\,G\left(\vec{a};x\right)\,, \quad a_i \in \{-1,0,1\}\,, \tag{B.21}$$

where k is the number of elements in $\vec{a}$ equal to $(+1)$.

The Shuffle product [87]: The product of two GPLs with weights n_1 and n_2 of the same argument x is a combination of GPLs of argument x with weight $n = n_1 + n_2$

$$G\left(\vec{a}_{n_1};x\right)\,G\left(\vec{a}_{n_2};x\right) = \sum_{\vec{a}_n = \vec{a}_{n_1} \uplus \vec{a}_{n_2}} G\left(\vec{a}_n;x\right)\,, \tag{B.22}$$

where $\vec{a}_n = \vec{a}_{n_1} \uplus \vec{a}_{n_2}$ represents all different possible permutations of the sequences $\vec{a}_{n_1}$ and $\vec{a}_{n_2}$ in which the relative ordering of the elements of both sets are preserved.

Notice that unlike the two and three loops polar integrals that can easily be performed using `Mathematica`, when we move on to four loops, polar integrals involve complicated classical polylogarithms that could not be evaluated following the same method. We can instead make progress by exploiting the iterated structure of these integrals and we are able to use the technology of symbols and coproducts which paved the way to the conversion of these complicated classical polylogarithms into GPL's whose integrals can trivially be done. These classical polylogarithms are however usually not special cases of the GPL's and hence this conversion is not straightforward as it is shown in the above Eq. (B.18). In order to make this conversion possible, it is necessary to resorting to a certain tensor calculus associated to iterated integrals, are the so-called "Symbols technology" [88], i.e, the question arises as to how one can determine a class of functions that can reproduce the same symbol. We will not provide a general definition, but we will instead just mention some examples of symbols corresponding to the most

commonly used multipolylogarithms and for every non-negative integer n we have

$$\begin{aligned}
\mathcal{S}\left(\log x\right) &= x\,, \\
\mathcal{S}\left(\frac{1}{n!}\log^n x\right) &= \underbrace{x\otimes\cdots\otimes x}_{n}\,, \\
\mathcal{S}\left(\mathrm{Li}_n x\right) &= -(1-x)\otimes\underbrace{x\otimes\cdots\otimes x}_{(n-1)}\,, \\
\mathcal{S}\left[G\left(a_1,\ldots,a_n;x\right)\right] &= \left(1-\frac{x}{a_n}\right)\otimes\cdots\otimes\left(1-\frac{x}{a_1}\right)\,.
\end{aligned} \tag{B.23}$$

The symbol of the iterated integral is then given by

$$\mathcal{S}\left(\mathrm{Li}_2\left[1-x\right]\right) = -x\otimes(1-x)\,. \tag{B.24}$$

We see that

$$\mathcal{S}\left[-\mathrm{G}\left(1,0;x\right)\right] = -x\otimes(1-x) = \mathcal{S}\left(\mathrm{Li}_2\left[1-x\right]\right)\,. \tag{B.25}$$

Since the symbol is related to the differential of the transcendental function it maps all constants to zero, hence two functions with the same symbol differ by constant terms. At transcendentality (weight) 2 they differ by terms π^2 and $i\pi\times\ln$. Therefore

$$\mathrm{Li}_2[1-x] = -G(1,0;x) + \alpha\pi^2 + \beta i\pi\times\ln\,. \tag{B.26}$$

For $0<x<1$ the dilogarithm is real and thus $\beta=0$. The rational number α by computing the two sides of the equality numerically. Using the program `GiNaC` [89] we find $\alpha = 0.1666666\cdots = 1/6$. In other words

$$\mathrm{Li}_2[1-x] = -G(1,0;x) + \frac{\pi^2}{6} = -G(1,0;x) + \zeta_2. \tag{B.27}$$

Using the definition of the GPLs, we can easily carry out our original integral, then substituting back into Eq. (B.14) and using the shuffle identities we end up with

$$\begin{aligned}
I_2^{(3)}(x) &= -\frac{1}{4}G(0,1,0;x) = -\frac{1}{4}\left[G(0,1;x)G(0;x) - 2G(0,0,1;x)\right] \\
&= -\frac{1}{4}\left[-\mathrm{Li}_2[x]\ln[x] + 2\mathrm{Li}_3[x]\right].
\end{aligned} \tag{B.28}$$

Substituting the limits one immediately gets $I_2^{(3)} = -\zeta_3/2$, and thus

$$\mathcal{S}_{ab}^{(3)} = \frac{\zeta_3}{2}. \tag{B.29}$$

We have also checked this result numerically.

B.2.1 Four-loops calculations

The NGLs coefficient at this order reads:

$$\mathcal{S}_{ab}^{(4)} = \int \mathrm{d}\Omega_{1234}\,\Theta_1^{\mathrm{out}}\,\Theta_4^{\mathrm{in}}\left(-\Theta_2^{\mathrm{in}}\,\Theta_3^{\mathrm{in}}\,\mathcal{A}_{ab}^{12}\,\bar{\mathcal{A}}_{ab}^{13}\,\bar{\mathcal{A}}_{ab}^{14}+\right.$$
$$\left.+3\,\Theta_2^{\mathrm{in}}\Theta_3^{\mathrm{out}}\,\mathcal{A}_{ab}^{12}\bar{\mathcal{B}}_{ab}^{134}+\Theta_2^{\mathrm{out}}\Theta_3^{\mathrm{in}}\mathfrak{A}_{ab}^{1234}-\Theta_2^{\mathrm{out}}\Theta_3^{\mathrm{out}}\mathcal{C}_{ab}^{1234}\right)\,. \tag{B.30}$$

The ladder term is simple and yields the result

$$\begin{aligned} I_1^{(4)} &= -\int \mathrm{d}\Omega_{1234}\Theta_1^{\mathrm{out}}\Theta_2^{\mathrm{in}}\Theta_3^{\mathrm{in}}\Theta_4^{\mathrm{in}}\mathcal{A}_{ab}^{12}\bar{\mathcal{A}}_{ab}^{13}\bar{\mathcal{A}}_{ab}^{14} \\ &= -\int_{-1}^{0}\frac{\mathrm{d}c_1}{1-c_1^2}\ln^3\left[\frac{c_1-1}{2c_1}\right] \\ &= -3\zeta_4. \end{aligned} \tag{B.31}$$

The ladder-cascade term is given by

$$\begin{aligned} I_2^{(4)} &= 3\int \mathrm{d}\Omega_{1234}\Theta_1^{\mathrm{out}}\Theta_2^{\mathrm{in}}\Theta_3^{\mathrm{out}}\Theta_4^{\mathrm{in}}\mathcal{A}_{ab}^{12}\bar{\mathcal{B}}_{ab}^{134} \\ &= \frac{3}{2}\int_{-1}^{0}\frac{\mathrm{d}c_1}{1-c_1^2}\ln\left[\frac{c_1-1}{2c_1}\right]\left(\zeta_2-\mathrm{Li}_2\left[\frac{2c_1}{c_1-1}\right]\right) \\ &= \frac{21}{16}\,\zeta_4\,. \end{aligned} \tag{B.32}$$

Note that we have used the Hopf algebra of co-products to carry out the above integral. Additionally we have

$$\begin{aligned} I_3^{(4)} &= \int \mathrm{d}\Omega_{1234}\Theta_1^{\mathrm{out}}\Theta_2^{\mathrm{out}}\Theta_3^{\mathrm{in}}\Theta_4^{\mathrm{in}}\mathfrak{A}_{ab}^{1234} \\ &= \frac{1}{4}\int \mathrm{d}\Omega_{12}\Theta_1^{\mathrm{out}}\Theta_2^{\mathrm{out}}\frac{2}{1-c_1^2}\left[\frac{2(1-c_1c_2)}{(1-c_2^2)(12)}\right. \\ &\left.\left(\ln\left[\frac{c_2-1}{2c_2^2(c_1-1)}\right]+\ln[12]\right)^2-\frac{8}{1-c_2^2}\ln^2\left(\frac{c_2-1}{2c_2}\right)\right] \\ &= \frac{17}{16}\,\zeta_4\,. \end{aligned} \tag{B.33}$$

The last integral to perform at four loops is the cascade term

$$\begin{aligned} I_4^{(4)} &= -\int \mathrm{d}\Omega_{1234}\Theta_1^{\mathrm{out}}\Theta_2^{\mathrm{out}}\Theta_3^{\mathrm{out}}\Theta_4^{\mathrm{in}}\mathcal{C}_{ab}^{1234} \\ &= -\int \mathrm{d}\Omega_{1234}\Theta_1^{\mathrm{out}}\Theta_2^{\mathrm{out}}\Theta_3^{\mathrm{out}}\Theta_4^{\mathrm{in}}w_{ab}^1\left[\mathcal{B}_{a1}^{234}+\mathcal{B}_{1b}^{234}-\mathcal{B}_{ab}^{234}\right]. \end{aligned} \tag{B.34}$$

Note that the integrations over each separate term is divergent, but the overall result is finite. We can put a spurious collinear cutoff ϵ on the integration over c_1 and perform each integral

separately. The divergences cancel in the sum and ϵ disappears. The integral over the term involving $\mathcal{B}_{ab}^{123}$ is straightforward and yields the result

$$I_{4,1}^{(4)} = \int_{-1}^{0} \frac{\mathrm{d}c_1}{2} \int_0^{2\pi} \frac{\mathrm{d}\phi_1}{2\pi} w_{ab}^1 \frac{\zeta_3}{2} = -\frac{\zeta_3}{4} \lim_{\epsilon\to 0} \ln \frac{\epsilon}{2}. \tag{B.35}$$

The second integral is also easy and gives

$$\begin{aligned} I_{4,2}^{(4)} =& -\int_{-1}^{0} \frac{\mathrm{d}c_1}{2} \int_0^{2\pi} \frac{\mathrm{d}\phi_1}{2\pi} \int_{-1}^{0} \frac{\mathrm{d}c_2}{2} \int_0^{2\pi} \frac{\mathrm{d}\phi_2}{2\pi} w_{ab}^1 w_{1b}^2 \frac{1}{2} \\ &\times \left(\mathrm{Li}_2\left[\frac{2c_1}{c_1-1}\right] - \mathrm{Li}_2\left[\frac{2c_2}{c_2-1}\right]\right) \\ =& -\frac{1}{4}\int_{-1}^{0} \frac{\mathrm{d}c_1}{1-c_1^2} \int_{-1}^{0} \frac{\mathrm{d}c_2}{1-c_2^2} \frac{(1+c_1)(1-c_2)}{|c_1-c_2|} \\ &\times \left(\mathrm{Li}_2\left[\frac{2c_1}{c_1-1}\right] - \mathrm{Li}_2\left[\frac{2c_2}{c_2-1}\right]\right) . \end{aligned} \tag{B.36}$$

Thus

$$I_{4,2}^{(4)} = -\frac{\zeta_3}{4} \lim_{\epsilon\to 0} \ln \frac{\epsilon}{2} - \frac{3\zeta_4}{4}. \tag{B.37}$$

The remaining integral is the lest trivial of all. It reads

$$\begin{aligned} &I_{4,3}^{(4)} = \\ &-\int_{-1}^{0} \frac{\mathrm{d}c_1}{2} \int_0^{2\pi} \frac{\mathrm{d}\phi_1}{2\pi} \int_{-1}^{0} \frac{\mathrm{d}c_2}{2} \int_0^{2\pi} \frac{\mathrm{d}\phi_2}{2\pi} w_{ab}^1 (w_{a1}^2 + w_{1b}^2) \mathcal{A}_{12}^{\overline{34}} \\ &= -\int_{-1}^{0} \frac{\mathrm{d}c_1}{1-c_1^2} \int_{-1}^{0} \frac{\mathrm{d}c_2}{1-c_2^2} (1-c_1c_2) \int_0^{2\pi} \frac{\mathrm{d}\phi_2}{2\pi} \frac{1}{(12)} \mathcal{A}_{12}^{\overline{34}}, \end{aligned} \tag{B.38}$$

where the bar in $\mathcal{A}_{12}^{\overline{34}}$ means that both particles 3 and 4 have been integrated out with 3 being out and 4 inside the measured hemisphere. We find for this term the result

$$I_{4,3}^{(4)} = \lim_{\epsilon\to 0} \frac{\zeta_3}{2} \ln \frac{\epsilon}{2} - \frac{7\zeta_4}{16}. \tag{B.39}$$

Thus the overall cascade contribution to the non-global coefficient at four loops is given by

$$I_4^{(4)} = -\frac{19}{16}\,\zeta_4\,. \tag{B.40}$$

Finally, adding up the results of the various contributions (ladder, ladder-cascade and cascade) to the NGLs coefficient at this order we obtain the result

$$\mathcal{S}_{ab}^{(4)} = -\frac{29}{16}\,\zeta_4\,. \tag{B.41}$$

Bibliography

[1] G. Herten, "The First Year of the Large Hadron Collider: A Brief Review," Mod. Phys. Lett. A **26** (2011), 843-855.

[2] Peter W. Higgs, "Broken symmetries and the masses of gauge bosons," Phys. Rev. Lett.**13** (1964), 508–509.

[3] G. Aad *et al.* [ATLAS], "Observation of a new particle in the search for the Standard Model Higgs boson with the ATLAS detector at the LHC," Phys. Lett. B **716** (2012), 1-29.

[4] S. Chatrchyan *et al.* [CMS], "Observation of a New Boson at a Mass of 125 GeV with the CMS Experiment at the LHC," Phys. Lett. B **716** (2012), 30-61.

[5] G. Aad *et al.* [ATLAS], "Combined measurements of Higgs boson production and decay using up to 80 fb^{-1} of proton-proton collision data at $\sqrt{s} = 13$ TeV collected with the ATLAS experiment," Phys. Rev. D **101** (2020) no.1, 012002.

[6] A. M. Sirunyan *et al.* [CMS], "Combined measurements of Higgs boson couplings in proton–proton collisions at $\sqrt{s} = 13\,\text{TeV}$," Eur. Phys. J. C **79** (2019) no.5, 421.

[7] Y. Fukuda *et al.* [Super-Kamiokande], "Evidence for oscillation of atmospheric neutrinos," Phys. Rev. Lett. **81** (1998), 1562-1567.

[8] D. V. Forero, M. Tortola and J. W. F. Valle, "Global status of neutrino oscillation parameters after Neutrino-2012," Phys. Rev. D **86** (2012), 073012.

[9] A. D. Sakharov, "Violation of CP Invariance, C asymmetry, and baryon asymmetry of the universe," Pisma Zh. Eksp. Teor. Fiz. **5** (1967), 32-35.

[10] P. A. R. Ade *et al.* [Planck], "Planck 2013 results. I. Overview of products and scientific results," Astron. Astrophys. **571** (2014), A1.

[11] S. P. Martin, "A Supersymmetry primer," Adv. Ser. Direct. High Energy Phys. **18** (1998), 1-98.

[12] K. K. Kerfa, "QCD resummation for high-p_T jet shapes at hadron colliders," PhD thesis, University of Manchester, 2012.

[13] J. M. Butterworth, B. E. Cox and J. R. Forshaw, "WW scattering at the CERN LHC," Phys. Rev. D **65** (2002), 096014.

[14] A. J. Larkoski, I. Moult and B. Nachman, "Jet Substructure at the Large Hadron Collider: A Review of Recent Advances in Theory and Machine Learning," Phys. Rept. **841** (2020), 1-63.

[15] R. Kogler, B. Nachman, A. Schmidt, L. Asquith, M. Campanelli, C. Delitzsch, P. Harris, A. Hinzmann, D. Kar and C. McLean, *et al.* "Jet Substructure at the Large Hadron Collider: Experimental Review," Rev. Mod. Phys. **91** (2019) no.4, 045003.

[16] D. Krohn, J. Thaler and L. T. Wang, "Jet Trimming," JHEP **02** (2010), 084

[17] D. E. Soper and M. Spannowsky, "Combining subjet algorithms to enhance ZH detection at the LHC," JHEP **08** (2010), 029.

[18] M. Dasgupta, A. Fregoso, S. Marzani and G. P. Salam, "Towards an understanding of jet substructure," JHEP **09** (2013), 029.

[19] S. Weinzierl, "The SISCone jet algorithm optimised for low particle multiplicities," Comput. Phys. Commun. **183** (2012), 813-820.

[20] S. Catani, Y. L. Dokshitzer, M. H. Seymour and B. R. Webber, "Longitudinally invariant K_t clustering algorithms for hadron hadron collisions," Nucl. Phys. B **406** (1993), 187-224.

[21] J. Thaler and K. Van Tilburg, "Identifying Boosted Objects with N-subjettiness," JHEP **03** (2011), 015.

[22] S. Chekanov and J. Proudfoot, "Searches for TeV-scale particles at the LHC using jet shapes," Phys. Rev. D **81** (2010), 114038.

[23] J. Gallicchio and M. D. Schwartz, "Seeing in Color: Jet Superstructure," Phys. Rev. Lett. **105** (2010), 022001.

[24] A. Hook, M. Jankowiak and J. G. Wacker, "Jet Dipolarity: Top Tagging with Color Flow," JHEP **04** (2012), 007.

[25] A. J. Larkoski, I. Moult and B. Nachman, "Jet Substructure at the Large Hadron Collider: A Review of Recent Advances in Theory and Machine Learning," Phys. Rept. **841** (2020), 1-63.

[26] M. Dasgupta and G. P. Salam, "Event shapes in e^+e^- annihilation and deep inelastic scattering," J. Phys. G **30** (2004), R143.

[27] G. Abbiendi *et al.* [OPAL], "Measurement of event shape distributions and moments in $e^+e^- \to$ hadrons at 91-GeV - 209-GeV and a determination of alpha(s)," Eur. Phys. J. C **40** (2005), 287-316.

[28] S. Kluth, "Tests of Quantum Chromo Dynamics at e^+e^- Colliders," Rept. Prog. Phys. **69** (2006), 1771-1846.

[29] A. Gehrmann-De Ridder, T. Gehrmann, E. W. N. Glover and G. Heinrich, "Second-order QCD corrections to the thrust distribution," Phys. Rev. Lett. **99** (2007), 132002.

[30] S. Brandt, C. Peyrou, R. Sosnowski and A. Wroblewski, "The principal axis of jets - an attempt to analyse high-energy collisions as two-body processes," Phys. Lett. Physics Letters**12** (1964) 57.

[31] E. Farhi, "A QCD Test for Jets," Phys. Rev. Lett. **39** (1977), 1587-1588.

[32] B. Flaugher and K. Meier . To be publ. in Proc. of 1990 Summer Study on High Energy Physics, Research Directions for the Decade, Snowmass, CO, Jun 25-Jul 13, 1990.

[33] G. F. Sterman and S. Weinberg, "Jets from Quantum Chromodynamics," Phys. Rev. Lett. **39** (1977), 1436.

[34] M. Bahr, S. Gieseke, M. A. Gigg, D. Grellscheid, K. Hamilton, O. Latunde-Dada, S. Platzer, P. Richardson, M. H. Seymour and A. Sherstnev, *et al.* "Herwig++ Physics and Manual," Eur. Phys. J. C **58** (2008), 639-707.

[35] J. Bellm, G. Bewick, S. Ferrario Ravasio, S. Gieseke, D. Grellscheid, P. Kirchgaeßer, M. R. Masouminia, G. Nail, A. Papaefstathiou and S. Platzer, *et al.* "Herwig 7.2 release note," Eur. Phys. J. C **80** (2020) no.5, 452.

[36] T. Sjostrand, S. Mrenna and P. Z. Skands, "PYTHIA 6.4 Physics and Manual," JHEP **05** (2006), 026.

[37] T. Sjöstrand, S. Ask, J. R. Christiansen, R. Corke, N. Desai, P. Ilten, S. Mrenna, S. Prestel, C. O. Rasmussen and P. Z. Skands, "An introduction to PYTHIA 8.2," Comput. Phys. Commun. **191** (2015), 159-177.

[38] E. Bothmann *et al.* [Sherpa], "Event Generation with Sherpa 2.2," SciPost Phys. **7** (2019) no.3, 034.

[39] C. W. Bauer and I. W. Stewart, "Invariant operators in collinear effective theory," Phys. Lett. B **516** (2001), 134-142.

[40] C. W. Bauer, D. Pirjol and I. W. Stewart, "Soft collinear factorization in effective field theory," Phys. Rev. D **65** (2002), 054022.

[41] G. F. Sterman and S. Weinberg, "Jets from Quantum Chromodynamics," Phys. Rev. Lett. **39** (1977), 1436.

[42] S. Catani and M. H. Seymour, "A General algorithm for calculating jet cross-sections in NLO QCD," Nucl. Phys. B **485** (1997), 291-419.

[43] A. Gehrmann-De Ridder, T. Gehrmann, E. W. N. Glover and G. Heinrich, "Jet rates in electron-positron annihilation at O(alpha(s)**3) in QCD," Phys. Rev. Lett. **100** (2008), 172001.

[44] A. H. Hoang, D. W. Kolodrubetz, V. Mateu and I. W. Stewart, "C-parameter distribution at N^{3}LL' including power corrections," Phys. Rev. D **91** (2015) no.9, 094017.

[45] G. P. Salam, "Towards Jetography," Eur. Phys. J. C **67** (2010), 637-686.

[46] C. Buttar, J. D'Hondt, M. Kramer, G. Salam, M. Wobisch, N. E. Adam, V. Adler, A. Arbuzov, D. Bardin and U. Baur, *et al.* "Standard Model Handles and Candles Working Group: Tools and Jets Summary Report,"

[47] J. E. Huth, N. Wainer, K. Meier, N. Hadley, F. Aversa, M. Greco, P. Chiappetta, J. P. Guillet, S. Ellis and Z. Kunszt, *et al.* "Toward a standardization of jet definitions," FERMILAB-CONF-90-249-E.

[48] Y. L. Dokshitzer, G. D. Leder, S. Moretti and B. R. Webber, "Better jet clustering algorithms," JHEP **08** (1997), 001.

[49] A. Banfi and M. Dasgupta, "Problems in resumming interjet energy flows with k_t clustering," Phys. Lett. B **628** (2005), 49-56.

[50] Y. Delenda, R. Appleby, M. Dasgupta and A. Banfi, "On QCD resummation with k(t) clustering," JHEP **12** (2006), 044.

[51] R. B. Appleby and M. H. Seymour, "Nonglobal logarithms in interjet energy flow with kt clustering requirement," JHEP **12** (2002), 063.

[52] M. Dasgupta and G. P. Salam, "Resummation of nonglobal QCD observables," Phys. Lett. B **512** (2001), 323-330

[53] Y. Delenda and K. Khelifa-Kerfa, "On the resummation of clustering logarithms for non-global observables," JHEP **09** (2012), 109.

[54] H. Benslama, Y. Delenda, K. Khelifa-Kerfa and A. M. Ibrahim, "Eikonal Amplitudes and Nonglobal Logarithms from the BMS Equation," Phys. Part. Nucl. Lett. **18** (2021) no.1, 5-18.

[55] D. J. Griffiths, "Introduction to Elementary Particles" (John Wiley and Sons, Inc., 1987), ISBN 0-471-60386-4.

[56] J. I. Friedman and H. W. Kendall, "Deep inelastic electron scattering," Ann. Rev. Nucl. Part. Sci. **22** (1972), 203-254.

[57] J. D. Bjorken and E. A. Paschos, "Inelastic Electron Proton and gamma Proton Scattering, and the Structure of the Nucleon," Phys. Rev. **185** (1969), 1975-1982.

[58] R. P. Feynman, "Very high-energy collisions of hadrons," Phys. Rev. Lett. **23** (1969), 1415-1417.

[59] J. Iliopoulos, "Symmetries and the Weak Interactions,"

[60] L. D. Faddeev, "Faddeev-Popov ghosts," Int. J. Mod. Phys. A **25** (2010), 1079-1089.

[61] G. 't Hooft and M. J. G. Veltman, "Regularization and Renormalization of Gauge Fields," Nucl. Phys. B **44** (1972), 189-213.

[62] R. K. Ellis, W. J. Stirling and B. R. Webber, "QCD and collider physics" (Cambridge: Cambridge University Press, 1996).

[63] I. J. R. Aitchison and A. J. G. Hey, "Gauge theories in particle physics: A practical introduction. Vol. 1: From relativistic quantum mechanics to QED", . Bristol, UK: IOP (2003) 406 p.

[64] I. J. R. Aitchison and A. J. G. Hey "Gauge theories in particle physics: A practical introduction. Vol. 2: Non-Abelian gauge theories: QCD and the electroweak theory", . Bristol, UK: IOP (2004) 454 p.

[65] M. Peskin and D. Schroeder, "An Introduction To Quantum Field Theor". Advanced Book Program. Addison-Wesley Publishing Company, 1995.

[66] F. Mandl and G. Shaw, "Quantum field theory" (Chichester: John Wiley and Sons, 1984).

[67] B. R. Martin, G. Shaw, "Particle Physics" (Chichester: John Wiley and Sons, 1992).

[68] G. Sterman, "An Introduction to Quantum Field Theory". Cambridge University Press, 1993.

[69] G. Sterman et al, "Handbook of perturbative QCD", Rev. Mod. Phys. 67 (Jan, 1995) 157-248.

[70] S. Bethke, "The 2009 World Average of alpha(s)," Eur. Phys. J. C **64** (2009), 689-703.

[71] J. P. Kneller and G. C. McLaughlin, "BBN and Lambda(QCD)," Phys. Rev. D **68** (2003), 103508.

[72] J. C. Collins, D. E. Soper and G. F. Sterman, "Factorization of Hard Processes in QCD," Adv. Ser. Direct. High Energy Phys. **5** (1989), 1-91.

[73] G. T. Bodwin, "Factorization of the Drell-Yan Cross-Section in Perturbation Theory," Phys. Rev. D **31** (1985), 2616.

[74] H. Jones, Groups, " Representations And Physics". Insitute of Physics Pub.,1998.

[75] H. Georgi, " Lie Algebras in Particle Physics. Frontiers in Physics". Perseus Books, Advanced Book Program, 1999.

[76] S. A. Larin and J. A. M. Vermaseren, "The alpha-s**3 corrections to the Bjorken sum rule for polarized electroproduction and to the Gross-Llewellyn Smith sum rule," Phys. Lett. B **259** (1991), 345-352.

[77] L. D. Faddeev and V. N. Popov, "Feynman Diagrams for the Yang-Mills Field," Phys. Lett. B **25** (1967), 29-30.

[78] G. 't Hooft and M. J. G. Veltman, "Regularization and Renormalization of Gauge Fields," Nucl. Phys. B **44** (1972), 189-213.

[79] C. G. Bollini and J. J. Giambiagi, "Dimensional Renormalization: The Number of Dimensions as a Regularizing Parameter," Nuovo Cim. B **12** (1972), 20-26.

[80] J. F. Ashmore, "A Method of Gauge Invariant Regularization," Lett. Nuovo Cim. **4** (1972), 289-290.

[81] W. A. Bardeen, A. J. Buras, D. W. Duke, and T. Muta, " Deep Inelastic Scattering Beyond the Leading Order in Asymptotically Free Gauge Theories", Phys. Rev. **D18** (1978) 3998.

[82] F. Bloch and A. Nordsieck, "Note on the radiation field of the electron," Phys. Rev., vol. 52,p. 54, 1937.

[83] T. Kinoshita, "Mass singularities of Feynman amplitudes," J. Math. Phys. **3** (1962), 650-677.

[84] T. Lee and M. Nauenberg, "Degenerate systems and mass singularities," Phys. Rev., vol. B133,p. 1549, 1964.

[85] J. Zinn-Justin, "Quantum Field Theory and Critical Phenomena". International Series of Monographs on Physics. Clarendon Press, 2002.

[86] A. B. Goncharov, Math. Res. Lett. "Multiple polylogarithms, cyclotomy and modular complexes" 5, 497 (1998)

[87] R. Ree, "The Annals of Mathematics" (1958) **68**, No. 2, pp. 210-220.

[88] A. B. Goncharov, "Galois symmetries of fundamental groupoids and noncommutative geometry," Duke Math. J. **128**, 209 (2005).

[89] C. W. Bauer, A. Frink and R. Kreckel, "Introduction to the GiNaC framework for symbolic computation within the C++ programming language," J. Symb. Comput. **33** (2002), 1-12.

[90] L. N. Lipatov, "The parton model and perturbation theory," Yad. Fiz. **20** (1974), 181-198.

[91] G. Altarelli and G. Parisi, "Asymptotic Freedom in Parton Language," Nucl. Phys. B **126** (1977), 298-318.

[92] Y. L. Dokshitzer, "Calculation of the Structure Functions for Deep Inelastic Scattering and e+ e- Annihilation by Perturbation Theory in Quantum Chromodynamics.," Sov. Phys. JETP **46** (1977), 641-653.

[93] Y. Delenda and K. Khelifa-Kerfa, "Eikonal gluon bremsstrahlung at finite N_c beyond two loops," Phys. Rev. D, **93** (5): 054027 (2016).

[94] M. Dasgupta and G. P. Salam, "Accounting for coherence in interjet E(t) flow: A Case study," JHEP, **03**: 017 (2002).

[95] A. Banfi, G. Marchesini, and G. Smye, "Away from jet energy flow," JHEP, **08**: 006 (2002).

[96] M. D. Schwartz and H. X. Zhu, "Nonglobal logarithms at three loops, four loops, five loops, and beyond," Phys. Rev. D, **90** (6): 065004 (2014).

[97] H. Weigert, "Nonglobal jet evolution at finite N(c)," Nucl. Phys. B, **685**: 321 (2004).

[98] Y. Hatta and T. Ueda, "Resummation of non-global logarithms at finite N_c," Nucl. Phys. B, **874**: 808 (2013).

[99] Y. Hagiwara, Y. Hatta, and T. Ueda, "Hemisphere jet mass distribution at finite N_c," Phys. Lett. B, **756**: 254 (2016).

[100] R. Ángeles Martínez, M. De Angelis, J. R. Forshaw, S. Plätzer, and M. H. Seymour, "Soft gluon evolution and non-global logarithms," JHEP, **05**: 044 (2018).

[101] J. R. Forshaw, J. Holguin, and S. Plätzer, "Parton branching at amplitude level," JHEP, **08**: 145 (2019).

[102] K. Khelifa-Kerfa and Y. Delenda, "Non-global logarithms at finite N_c beyond leading order," JHEP, **03**: 094 (2015).

[103] D. Neill, "Non-Global and Clustering Effects for Groomed Multi-Prong Jet Shapes," JHEP, **02**: 114 (2019).

[104] M. Dasgupta and G. P. Salam, "Resummed event shape variables in DIS," JHEP, **08**: 032 (2002).

[105] M. Dasgupta and G. P. Salam, "Event shapes in e^+e^- annihilation and deep inelastic scattering," J. Phys. G, **30**: R143 (2004).

[106] S. Catani, L. Trentadue, G. Turnock and B. Webber, Nucl. Phys. B, **407**: 3 (1993).

[107] F. Hautmann and H. Jung, "Angular correlations in multi-jet final states from k-perpendicular - dependent parton showers," JHEP **10** (2008), 113.

[108] A. Aktas *et al.* [H1], "Inclusive dijet production at low Bjorken x in deep inelastic scattering," Eur. Phys. J. C **33** (2004), 477-493.

[109] M. Aaboud *et al.* [ATLAS], "Measurement of dijet azimuthal decorrelations in *pp* collisions at $\sqrt{s} = 8$ TeV with the ATLAS detector and determination of the strong coupling," Phys. Rev. D **98** (2018) no.9, 092004.

[110] G. Aad *et al.* [ATLAS], "Measurement of Dijet Azimuthal Decorrelations in *pp* Collisions at $\sqrt{s} = 7$ TeV," Phys. Rev. Lett. **106** (2011), 172002.

[111] A. M. Sirunyan *et al.* [CMS], "Azimuthal correlations for inclusive 2-jet, 3-jet, and 4-jet events in pp collisions at $\sqrt{s} = 13$ TeV," Eur. Phys. J. C **78** (2018) no.7, 566.

[112] V. M. Abazov *et al.* [D0], "Measurement of dijet azimuthal decorrelations at central rapidities in $p\bar{p}$ collisions at $\sqrt{s} = 1.96$ TeV," Phys. Rev. Lett. **94** (2005), 221801.

[113] M. Aaboud *et al.* [ATLAS], "Dijet azimuthal correlations and conditional yields in pp and p+Pb collisions at sNN=5.02TeV with the ATLAS detector," Phys. Rev. C **100** (2019) no.3, 034903.

[114] A. Banfi, M. Dasgupta and Y. Delenda, "Azimuthal decorrelations between QCD jets at all orders," Phys. Lett. B **665** (2008), 86-91.

[115] Serguei Chatrchyan et al. "Event Shapes and Azimuthal Correlations in Z + Jets Events in pp Collisions at $\sqrt{s} = 7$ TeV".Phys. Lett. B, 722:238-261, 2013.

[116] X. Liu, F. Ringer, W. Vogelsang and F. Yuan, "Lepton-jet Correlation in Deep Inelastic Scattering," Phys. Rev. D **102** (2020) no.9, 094022.

[117] H. Abramowicz *et al.* [ZEUS], "Further studies of isolated photon production with a jet in deep inelastic scattering at HERA," JHEP **01** (2018), 032.

[118] S. Catani, Y. L. Dokshitzer, M. H. Seymour and B. R. Webber, "Longitudinally invariant K_t clustering algorithms for hadron hadron collisions," Nucl. Phys. B **406** (1993), 187-224.

[119] S. D. Ellis and D. E. Soper, "Successive combination jet algorithm for hadron collisions," Phys. Rev. D **48** (1993), 3160-3166.

[120] M. Cacciari, G. P. Salam and G. Soyez, "FastJet User Manual," Eur. Phys. J. C **72** (2012), 1896.

[121] M. Cacciari, G. P. Salam and G. Soyez, "The anti-k_t jet clustering algorithm," JHEP **04** (2008), 063.

[122] Y. L. Dokshitzer, G. D. Leder, S. Moretti and B. R. Webber, "Better jet clustering algorithms," JHEP **08** (1997), 001.

[123] M. Wobisch and T. Wengler, "Hadronization corrections to jet cross-sections in deep inelastic scattering".

[124] S. Catani and M. H. Seymour, "A General algorithm for calculating jet cross-sections in NLO QCD," Nucl. Phys. B **485** (1997), 291-419.

[125] S. Catani and M. H. Seymour, "The Dipole formalism for the calculation of QCD jet cross-sections at next-to-leading order," Phys. Lett. B **378** (1996), 287-301.

[126] A. Banfi, F. A. Dreyer and P. F. Monni, "Next-to-leading non-global logarithms in QCD," JHEP **10** (2021), 006.

[127] A. Banfi, F. A. Dreyer and P. F. Monni, "Higher-order non-global logarithms from jet calculus," JHEP **03** (2022), 135.

[128] K. Khelifa-Kerfa, "Non-global logs and clustering impact on jet mass with a jet veto distribution," JHEP **02** (2012), 072.

[129] A. Banfi, M. Dasgupta, K. Khelifa-Kerfa and S. Marzani, "Non-global logarithms and jet algorithms in high-pT jet shapes," JHEP **08** (2010), 064.

[130] R. Alemany-Fernandez et al., "The Large Hadron Collider: Harvest of Run 1". Springer, Berlin, Germany, 1st edition, May, 2015.

Abstract

The study of jet observables is of great importance for current and future collider phenomenology, including hunting for new physics as well as making precision measurements. In this thesis we perform perturbative calculations for some relevant non global event and jet shapes observables where the jets are produced in e^+e^- colliders, such as the FCC-ee.

We start by specifically examining the non-global and clustering logarithms in the azimuthal decorrelation between two jets in e^+e^- dijet events, where the jets are defined with the generalised k_t or anti-k_t algorithm with E-scheme recombination. We calculate at one loop and to all orders the leading global single logarithms of the distribution of the said observable. We also compute at fixed order up to four loops the non-global and clustering logarithms, and numerically resum them to all orders in the large-N_c approximation. We compare our results at $\mathcal{O}(\alpha_s)$ and $\mathcal{O}(\alpha_s^2)$ with those of the `EVENT2` fixed-order Monte Carlo program and find agreement of the leading singular behavior of the azimuthal decorrelation distribution. Finally, we use the program `Gnole` to calculate the resummed distribution at NLL accuracy, thus achieving state-of-the-art accuracy for the resummation of this quantity.

Then we address the Banfi-Marchesini-Smye (BMS) equation which accounts for non-global logarithms to all orders in perturbation theory in the large N_c approximation. We show that the squared amplitudes for the emission of soft energy-ordered gluons are correctly embedded in this equation, and explicitly verify that they coincide with those derived in previous works in the large-N_c limit up to sixth order in the strong coupling. We perform analytical calculations for the non-global logarithms up to fourth order for the specific event shape hemisphere mass distribution in e^+e^- collisions, thus confirming previous semi-numerical results. We show that the solution to the BMS equation may be cast into a product of an infinite number of exponentials each of which resums a class of Feynman diagrams that manifest a symmetry pattern, and explicitly carry out the computation of the first of these exponentials. Our results exhibit full agreement with those reported in the literature.

Résumé

L'étude des observables des jets est d'une grande importance pour la phénoménologie actuelle et future des collisionneurs, y compris la recherche de nouvelles physiques ainsi que la réalisation de mesures de précision. Dans cette thèse, nous effectuons des calculs perturbatifs pour certaines observables de jet pertinentes et non globaux où les jets sont produits dans des collisionneurs e^+e^-, comme le FCC-ee.

Nous commençons par examiner spécifiquement les logarithmes non globaux et de clustering dans la décorrélation azimutale entre deux jets dans des événements e^+e^- dijet, où les jets sont définis avec l'algorithme généralisé k_t ou anti-k_t avec recombinaison E-scheme. On calcule à une boucle et à tous les ordres les principaux logarithmes simples globaux de la distribution de ladite observable. Nous calculons également à ordre fixe jusqu'à quatre boucles les logarithmes non globaux et de clustering, et les résommons numériquement à tous les ordres dans l'approximation à grand $\mathrm{N_c}$. Nous comparons nos résultats à $\mathcal{O}(\alpha_s)$ et $\mathcal{O}(\alpha_s^2)$ avec ceux du programme Monte Carlo à ordre fixe EVENT2 et trouvons un accord sur le comportement singulier principal de la distribution de décorrélation azimutale. Enfin, nous utilisons le programme Gnole pour calculer la distribution resommée avec une précision NLL, et donc obtenant létat de l'art pour la resommation de cette quantité.

Ensuite, nous abordons l'équation de Banfi-Marchesini-Smye (BMS) qui tient compte des logarithmes non globaux à tous les ordres dans la théorie des perturbations dans la grande approximation $\mathrm{N_c}$. Nous montrons que les amplitudes au carré pour l'émission de gluons à énergie douce sont correctement intégrées dans cette équation, et vérifions explicitement qu'elles coincident avec celles obtenues dans des travaux antérieurs dans la limite des grands $\mathrm{N_c}$ jusqu'au sixiéme ordre dans le couplage fort. Nous effectuons des calculs analytiques pour les logarithmes non globaux jusqu'au quatrième ordre pour la distribution de la specific event shape hémisphére mass dans les collisions e^+e^-, confirmant ainsi les résultats semi-numériques précédents. Nous montrons que la solution de l'équation BMS peut être convertie en un produit d'un nombre infini d'exponentielles dont chacune résomme une classe de diagrammes de Feynman qui manifestent un motif de symétrie, et effectuons explicitement le calcul de la première de ces exponentielles. Nos résultats sont en parfait accord avec ceux rapportés dans la littérature.

ملخص

تعتبر دراسة النفاثة ذات أهمية كبيرة لظواهر المصادمات الحالية و المستقبلية، بما في ذلك البحث عن فيزياء جديدة بالإضافة إلى إجراء قياسات دقيقة. في هذحه الأطروحة، نجري حسابات مضطربة لنفاثات QCD لتوزيعات أشكال الحدث و النفاثة غير العالمية حيث يتم إنشاء النفاثات في مصادمات e^+e^-، مثل FCC-ee.

نبدأ على وجه التحديد بفحص اللوغاريتمات غير العالمية و التجميعية في علاقة الديكور السمتي بين نفاثتين في أحداث e^+e^- حيث يتم تحديد النفاثات باستخدام خوارزمية k_t أو anti-k_t المعممة و باستخدام مخطط إعادة التركيب E-scheme. نقوم بحساب الحلقة الأولى ثم جميع درجات اللوغاريتمات العالمية الفردية الاولية لتوزيع الملحوظة المدروسة. نحسب أيضا اللوغاريتمات غير العالمية و التجميعية إلى الدرجة الرابعة، ونعيد تجميعها إلى جميع الدرجات عدديا باستخدام تقريب N_c الكبير. عند مقارنة النتائج التي تحصلنا عليها في الدرجة الأولى $\mathcal{O}(\alpha_s)$ وفي الدرجة الثانية $\mathcal{O}(\alpha_s^2)$ مع نتائج برنامج مونت كارلو EVENT2 ذي الترتيب الثابت نجد إتفاق لسلوك التفرق الأولي لتوزيع الديكور السمتي. أخيرا نستخدم برنامج Gnole لحساب إعادة تجميع التوزيع بدقة NLL، و بالتالي تحقيق أحدث دقة لإعادة تجميع هذه الكمية.

ثم نتناول معادلة Banfi-Marchesini-Smye (BMS) التي تقوم بإعادة تجميع كل درجات اللوغاريتمات غير العالمية في نظرية الإضطراب باستخدام تقريب N_c الكبير. نوضح أن السعات التربيعية لانبعاث الغلوونات ذات الطاقة الضعيفة مدمجة بشكل صحيح في هذه المعادلة، ونتحقق بشكل صريح أنها تتطابق مع تلك المشتقة في الاعمال السابقة حتى المرتبة السادسة في الإقتران القوي. نقوم بإجراء حسابات تحليلية للوغاريتمات غير العالمية لتوزيع شكل الحدث المسمى بنصف الكرة في تصادمات e^+e^-، وبالتالي تأكيد النتائج شبه العددية السابقة. نبين أن حل معادلة (BMS) يمكن اعتباره كجداء لعدد لا حصر له من الأسيات، كل منها يعيد تجميع فئة من مخططات فاينمان التي تظهر نمط تناظر، ونقوم بحساب الأسية الأولى بشكل مبسط. النتائج المتحصل عليها تبدي إتفاق كامل مع تلك الموجودة سابقا.